

QED Radiative Processes in Deep Inelastic Scattering at HERA^{*}

Harald Anlauf

Abstract

High energy scattering processes of charged particles are accompanied by radiation of hard photons. Emission collinear to the incident particles, which leads to a reduction of the effective beam energy, and the possibility to directly measure these photons at the HERA electron-proton collider provides important physics opportunities. For deep inelastic scattering, the measurement of radiative processes extends the kinematic range accessible to the HERA experiments to lower Q^2 , as well as helps in separating the proton structure functions without the need to run at different collider energies. QED corrections to these radiative processes are discussed, and the calculation of the model-independent leptonic corrections is described in some detail for the complete one-loop contributions as well as for the higher order leading logarithms.

^{*}Habilitationsschrift, Universität Siegen, Germany, February 2002

Contents

1	Introduction	3
2	Deep Inelastic Scattering	7
2.1	Kinematics	7
2.2	Determination of kinematic variables	9
2.3	The Born cross section for $ep \rightarrow eX$	11
2.4	The Born cross section at high energies	13
2.5	Structure functions	14
2.5.1	Structure functions from perturbative QCD	14
2.5.2	Structure functions in the region of low Q^2	17
2.5.3	Structure functions at high Q^2	21
3	QED Radiative Corrections and Radiative Processes	23
3.1	Classification of radiative corrections	24
3.2	Radiative DIS	26
3.2.1	The QED Compton tensor	27
3.2.2	The cross section for single photon emission	28
3.2.3	Kinematic effects of photon radiation	38
3.3	Collinear radiation and tagged photon processes	42
3.4	The general radiative DIS process	47
3.5	Tagged photons in charged current reactions	48
3.6	Radiation from the hadron	50
4	QED Corrections to Radiative Scattering	52
4.1	Radiative corrections in the leading logarithmic approximation	53
4.1.1	Structure function formalism	53
4.1.2	Leading logarithms at the next order	54
4.1.3	The radiatively corrected cross section	57
4.1.4	Numerical results	58
4.2	Complete leptonic corrections	61
4.2.1	Compton tensor	61

4.2.2	Virtual and soft corrections	62
4.2.3	Double hard bremsstrahlung: ISR	63
4.2.4	Final state collinear radiation	68
4.2.5	Semi-collinear emission	71
4.3	Corrections to radiative DIS	72
5	Estimates of Higher Order QED Corrections	81
5.1	Exclusive photons in the leading logarithmic approximation	82
5.2	Leading radiative corrections to DIS with tagged ISR	86
5.3	The non-singlet structure function	90
5.4	Numerical results for higher order corrections	93
6	Concluding Remarks and Outlook	96
A	Auxiliary Calculations	103
A.1	Integrals for virtual corrections	104
A.2	Integrals for double collinear emission	107
A.2.1	Integrals over photon angles	109
A.2.2	Integrals over relative photon energy	118
B	The Semi-Collinear Contribution	121

Chapter 1

Introduction

In our quest for the understanding of the structure of matter, scattering experiments have always played an outstanding rôle. Important landmarks are the classic experiments by Rutherford [1] leading to the discovery of the atomic nucleus, the determination of the size of nucleons and atomic nuclei from their electromagnetic form factors by Hofstadter and McAllister [2], and the establishing of the parton model of the nucleon in deep inelastic lepton-proton scattering at SLAC [3].

Supported by an increasing amount of data from high precision scattering experiments at high energy electron-positron, proton-antiproton, and electron-proton colliders, the electroweak Standard Model (SM) including Quantum Chromodynamics (QCD) is currently accepted as the simplest quantum field theory describing the observed phenomena of elementary particle physics. The fundamental particles of the SM, the leptons, quarks, gauge fields and the (experimentally not yet established) Higgs are point-like. The very good agreement of many theoretical predictions and present experimental results from LEP, Tevatron and HERA indicates that any substructure of these particles must be smaller than 10^{-19} m, corresponding to a compositeness scale above several TeV [4, 5, 6].

On the theoretical side, still one of the major challenges is a complete understanding of hadronic interactions and hadron structure. The startup of the lepton-proton collider HERA at DESY with a center of mass energy of $\sqrt{s} \approx 300$ GeV (27.5 GeV electrons/positrons on initially 820 GeV, currently 920 GeV protons) marked the beginning of a new era of deep inelastic scattering (DIS) experiments, extending the kinematic domain for structure function measurements covered by earlier fixed-target experiments in the Bjorken variable x and momentum transfer Q^2 by several orders of magnitude. Besides the inclusive (w.r.t. the hadronic final state) electroproduction structure functions, HERA also provides increasingly precise data for the

study of hadronic final states in DIS, in particular multi-jet events and event shapes.

The large accessible kinematic region at HERA allows the investigation of different aspects of strong interaction dynamics. In the perturbative regime of QCD, much interest is devoted to the study of the transition from the traditional Altarelli-Parisi (DGLAP) evolution of structure functions at large x to the Balitsky-Fadin-Kuraev-Lipatov (BFKL) [7, 8] behavior at small x , and to a determination of the gluon density which is expected to be strongly rising for $x \rightarrow 0$. Unitarity requires that the rapid rise predicted by the perturbative evolution must eventually be damped. There are indications from the DIS data at low x that this unitarization manifests itself in a phenomenon called *geometric scaling* [9], where the cross section is not a function of two independent variables x and Q^2 but rather a function of a single variable $\tau = Q^2/Q_s^2(x)$. The function $Q_s(x)$ is interpreted as a saturation scale in a description of non-linear QCD evolution [10, 11].

Of the structure functions of the proton, $F_2(x, Q^2)$ and $F_L(x, Q^2)$, the longitudinal one, F_L , is much more difficult to access. The measurement of F_L at low x is particularly interesting due to its tight connection to the gluon distribution in the proton. There exist several ways to separately extract F_2 and F_L from the experimental data. One possibility is to run the collider at different —usually lower— center-of-mass energies, which may not be desirable from the point of view of other parts of the physics program looking for possible hints of physics beyond the SM at the highest accessible scales [12].

Indirect methods for the determination of F_L can be used at fixed collision energy but usually require substantial input from theory or other assumptions, and they depend more or less on the modeling of the hadronic final state, like extrapolations or QCD fits (see e.g., [13, 14, 15, 16]), or the measurement of the azimuthal angle distribution of final state hadrons [17].

Krasny et al. [18] suggested a direct method that utilizes radiative events with an exclusive hard photon registered (tagged) in a forward photon detector (PD). Such a device is actually a central part of the luminosity monitoring system of the H1 and ZEUS experiments [19, 20] that measures the radiative elastic process $ep \rightarrow ep + \gamma$ [21]; it was further improved during the HERA luminosity upgrade [22]. The idea of this method is that emission of photons in a direction close to the incident electron corresponds to a reduction in the effective beam energy. The effective electron energy for each radiative event is determined from the energy of the photon observed in the PD.

Besides measuring F_L , radiative events extend the accessible kinematic range to lower values of Q^2 . This is important for a closing of the gap between the fixed-target experiments and HERA. The potential of this method is sup-

ported by preliminary results from the H1 collaboration of an analysis at low Q^2 for F_2 [23, 24, 25, 26] (for earlier analyses that did not take into account QED radiative corrections see [19, 27]). The feasibility of the corresponding determination of F_L was studied in [28]. However, with currently analyzed data sets it is not yet possible to compete with F_L from extrapolations or QCD fits [24].

A precise analysis of experimental data requires the inclusion of radiative corrections. In the case of the exclusive radiative events, even at HERA energies only the kinematic region of momentum transfers far below the masses of the W and Z bosons has a significant cross section. As a consequence only the QED subset of the electroweak interaction is relevant, so that we can safely restrict ourselves to the calculation of the QED corrections. A minor complication is the well known fact that the full theoretical control of the radiative corrections in non-radiative deep inelastic scattering is aggravated by the dependence of the corrections on the knowledge of the proton structure functions even in kinematic regions which may be difficult to access. However, this is almost precisely where a measurement of the radiative process can help, and why it is important that this measurement is performed.

From the calculation of radiative corrections to deep inelastic scattering it is well known that the model independent QED corrections on the lepton side are most important. For the tagged photon reaction in the HERA kinematic regime, the leptonic QED corrections have been discussed at the leading logarithmic level [29, 30] and taking into account next-to-leading logarithms [31, 32, 33]. Since the leading logarithmic corrections lead to compact and transparent expressions, we use them for a qualitative study of the dependence of the QED radiation effects on the kinematic reconstruction method.

A central part of the present work deals with the complete leptonic $\mathcal{O}(\alpha)$ corrections¹ to this process which were outlined in [34]. We will present here all essential details of this calculation. Since it is well known that also higher-order corrections are very important in a quantitative description of deep-inelastic scattering, we shall describe in some length a systematic method to obtain the leading logarithms to the tagged photon process to all orders.

The organization of this report is as follows. Section 2 introduces our notation in the context of deep inelastic scattering to lowest order. We recapitulate some basic knowledge of the proton structure functions and their connection to QCD. After providing a brief review of the general features of QED radiative corrections to deep inelastic scattering, section 3 emphasizes

¹In this work corrections are always counted *relative* to the leading contribution for a given final state, which is already proportional to α^3 for radiative deep inelastic scattering.

the importance of the exclusive radiative processes that are the main subject of this work. In section 4 we calculate the QED radiative corrections to the tagged photon process, beginning with the leading logarithmic approximation and extending to the complete leptonic corrections. Section 5 considers the leading logarithmic contributions at higher orders. We conclude with a short summary, recent experimental results on the structure function F_2 obtained with the tagged photon method and an outlook on the application of photon tagging to e^+e^- collisions. Finally, the appendices explain several details of the more involved parts of the analytic calculations and collect several formulae that are needed for a numerical implementation.

Chapter 2

Deep Inelastic Scattering

2.1 Kinematics

We start by considering the general deep inelastic electron proton scattering process

$$e(p) + p(P) \rightarrow l(p') + X(P_X) , \quad (2.1)$$

where e and p represent the incoming electron and proton, and l and X the scattered lepton and the final hadronic system, while the respective four-momenta are given in parentheses. Although the HERA ep collider is designed to also run with positron beams instead of electrons and even collected more integrated luminosity with the former, we use the latter as the generic denotation of the lepton beam below, but we shall explicitly indicate the dependence on the lepton charge where needed.

Equation (2.1) describes the so-called neutral current (NC) processes, where the scattered lepton equals the incoming one, $l = e$, as well as charged-

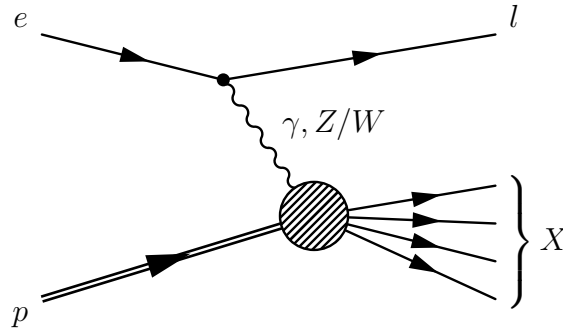


Figure 2.1: Deep inelastic lepton-proton scattering

current (CC) processes, where the outgoing lepton is an electron neutrino ν_e for electron beams and an electron anti-neutrino $\bar{\nu}_e$ for positron beams, respectively.

Let us introduce the notation used in this report. We choose coordinates in the HERA laboratory system in which the incoming electrons move in the positive z -direction,¹ whereas the protons move in the negative z -direction. Furthermore, the direction of the x -axis is chosen such that the momentum of the scattered lepton lies in the x - z plane:

$$\begin{aligned} p &= (E_e, 0, 0, p_e) , \\ P &= (E_p, 0, 0, -p_p) , \\ p' &= (E'_l, p'_l \sin \theta, 0, p'_l \cos \theta) . \end{aligned} \quad (2.2)$$

The HERA ep collider is typically run at an energy of 27.5 GeV for the electron beam, while the nominal energy of the proton ring, initially 820 GeV, now reaches up to 920 GeV.

The kinematics of the scattering process (2.1) is described by several Lorentz invariants. The square of the total center of mass energy available is given by

$$s = (p + P)^2 = m^2 + M^2 + S \simeq 4E_e E_p , \quad (2.3)$$

where we introduced the related invariant

$$S = 2P \cdot p . \quad (2.4)$$

At high energies, the electron mass m and the proton mass M can be mostly neglected, and $s \simeq S$. We shall therefore use them almost synonymously below. For the HERA beam energies mentioned above, $\sqrt{S} \simeq 300$ GeV and $\sqrt{S} \simeq 318$ GeV, resp.

The invariant momentum transfer from the lepton to the hadronic system reads

$$Q^2 \equiv -q^2 = -(p - p')^2 \simeq 4E_e E'_l \sin^2 \frac{\theta}{2} , \quad (2.5)$$

assuming that the energy and angle of the outgoing lepton can be measured.

Further commonly used invariants are the dimensionless Bjorken variables

$$x = \frac{Q^2}{2P \cdot q} \simeq \frac{E_e E'_l \sin^2 \frac{\theta}{2}}{E_p (E_e - E'_l \cos^2 \frac{\theta}{2})} , \quad (2.6)$$

$$y = \frac{P \cdot q}{P \cdot p} = \frac{Q^2}{xS} \simeq 1 - \frac{E'_l}{E_e} \cos^2 \frac{\theta}{2} . \quad (2.7)$$

¹As a consequence, one should always keep in mind our definition of the *forward direction* being along the positive z -axis as the *initial lepton direction*, in contrast to the historical decision of the HERA experiments to use the direction of the incoming proton beam for that purpose.

The quantity y corresponds to the relative energy loss of the lepton in the rest frame of the incoming hadron. It is easy to show that x and y are restricted to the range

$$0 \leq x, y \leq 1 . \quad (2.8)$$

Finally, the total mass of the hadronic final state X is obtained as

$$W^2 \equiv M_X^2 = (P + q)^2 = M^2 + \frac{1-x}{x} Q^2 = M^2 + (1-x)yS . \quad (2.9)$$

Elastic ep scattering corresponds to $x = 1$.

2.2 Determination of kinematic variables

Because of four-momentum conservation, the kinematic invariants x , y and $Q^2 = xyS$ can in principle be determined in different ways from the measured final state. Instead of using only the information from the scattered lepton, one can also take into account the measured hadronic final state. In the case of charged current scattering, where the final state neutrino escapes detection, this is actually necessary.

In the description of deep inelastic scattering in the language of the naive quark-parton model (QPM), the lepton scatters elastically with a quasi-free quark within the proton. The two-body final state of this subprocess is completely determined by two variables, which can be taken to be e.g., the energy E'_e and the polar angle θ of the electron in the lab frame, or quantities constructed from the hadronic final state.

Assuming local parton-hadron duality, one identifies the energy and direction of the hadron jet with the energy and direction of the scattered quark. Thus, denoting the four-momenta of the produced hadrons by $p_h = (E_h; \vec{p}_{\perp,h}, p_{z,h})$, one can construct the following quantities:²

$$\Sigma_h = \sum_h (E_h + p_{z,h}) , \quad p_{T,h} = \sqrt{\left(\sum_h \vec{p}_{\perp,h} \right)^2} , \quad (2.10)$$

the latter being the total transverse momentum of the hadronic final state. Neglecting masses, one can define an inclusive angle γ of the hadronic system which then corresponds to the angle of the scattered quark in the QPM,

$$\tan \frac{\gamma}{2} = \frac{\Sigma_h}{p_{T,h}} . \quad (2.11)$$

²Remember that the initial proton moves in the negative z direction.

Obviously one can define similar quantities for the scattered electron,

$$\Sigma_e = E'_e(1 + \cos \theta) , \quad p_{T,e} = E'_e \sin \theta , \quad \Rightarrow \quad \tan \frac{\theta}{2} = \frac{\Sigma_e}{p_{T,e}} . \quad (2.12)$$

Starting from these four variables $[E'_e, \theta, \Sigma_h, \gamma]$, among which only two are independent, one derives the following “basic methods”, that use only two variables:

- For neutral current events, the electron method (*e*), which uses E'_e and θ , see eqs. (2.5)–(2.7), and
- the double angle method (DA), which uses θ and γ [35], whereas
- for charged current events only the “hadrons only” method (*h*), also known as Jacquet-Blondel method (JB) [36], is available.

The Jacquet-Blondel method defines:

$$y_{\text{JB}} = \frac{\Sigma_h}{2E_e} , \quad Q_{\text{JB}}^2 = \frac{p_{T,h}^2}{1 - y_{\text{JB}}} , \quad x_{\text{JB}} = \frac{Q_{\text{JB}}^2}{y_{\text{JB}} S} . \quad (2.13)$$

For neutral current processes, there are possibilities and reasons to also consider methods that employ more than two of the measured variables to determine the kinematics, either analytically or using the full event information for kinematic fits. Real detectors are not perfect; they possess finite energy and angle resolution, and they usually do not cover the full solid angle, so that particles may escape in the beam pipe. Therefore e.g. the energy of the incoming electron may not be well known as it might emit a collinear photon before the hard collision.

As an example for an analytic method using three variables we mention here the Σ method, which basically uses (2.13), but replaces $2E_e$ with the help of four-momentum conservation by the combination $\Sigma_e + \Sigma_h$, thereby making the determination of the variable y independent of collinear photon emission in the initial state, and replaces the hadronic transverse momentum $p_{T,h}$ by the leptonic $p_{T,e}$,

$$y_{\Sigma} = \frac{\Sigma_h}{\Sigma_e + \Sigma_h} , \quad Q_{\Sigma}^2 = \frac{p_{T,e}^2}{1 - y_{\Sigma}} , \quad x_{\Sigma} = \frac{Q_{\Sigma}^2}{y_{\Sigma} S} . \quad (2.14)$$

For a thorough discussion of the essential features of these methods and some extensions we refer the reader to [37, 38], and references cited therein.

2.3 The Born cross section for $ep \rightarrow eX$

Let us now turn to the model-independent description of the cross section for semi-inclusive deep inelastic scattering, where only the final state electron is measured (electroproduction). For the time being, we shall restrict to the case where the momentum transfer Q^2 is far below the electroweak scale, i. e., $Q^2 \ll M_Z^2$. The Born contribution to the scattering amplitude taking into account only one-photon exchange reads:

$$S_{fi} = i(2\pi)^4 \delta^4(P_X + p' - P - p) \bar{u}(p') \gamma^\mu u(p) \frac{Q_e e^2}{q^2} \langle P_X | J_\mu^{\text{em}}(0) | P \rangle . \quad (2.15)$$

where Q_e is the charge of the lepton in units of the proton charge ($Q_e = +1$ for the positron), and $J_\mu^{\text{em}}(x)$ is the electromagnetic current operator.

The differential cross section for the scattering of unpolarized particles reads ($q = p - p'$):

$$d\sigma = \frac{1}{2\sqrt{\lambda_S}} \left(\frac{e^2}{q^2} \right)^2 L^{\mu\nu} H_{\mu\nu}(P, q) \frac{d^3 \vec{p}'}{(2\pi)^3 2E'_e} \quad (2.16)$$

with the lepton tensor:

$$\begin{aligned} L^{\mu\nu} &= \frac{1}{2} \sum_{\text{spins}} [\bar{u}(p') \gamma^\mu u(p)]^* \bar{u}(p') \gamma^\nu u(p) \\ &= \tilde{g}^{\mu\nu} q^2 + 4\tilde{p}^\mu \tilde{p}^\nu , \\ \tilde{g}^{\mu\nu} &= g^{\mu\nu} - \frac{q^\mu q^\nu}{q^2} , \quad \tilde{p}^\mu = p^\mu - q^\mu \frac{p \cdot q}{q^2} . \end{aligned} \quad (2.17)$$

We normalize the hadron tensor $H_{\mu\nu}$ as follows:

$$\begin{aligned} H_{\mu\nu}(P, q) &= \frac{1}{2} \sum_{\text{pol}} \sum_X \langle P | J_\mu^{\text{em}}(0) | P_X \rangle \langle P_X | J_\nu^{\text{em}}(0) | P \rangle \\ &= \frac{1}{2} \sum_{\text{pol}} \int d^4 x e^{iq \cdot x} \langle P | [J_\mu^{\text{em}}(x), J_\nu^{\text{em}}(0)] | P \rangle . \end{aligned} \quad (2.18)$$

Using current conservation, charge conjugation and parity symmetry, we decompose this tensor as:

$$\begin{aligned} H_{\mu\nu}(P, q) &= 4\pi \left(-\tilde{g}_{\mu\nu} F_1(x, Q^2) + \tilde{P}_\mu \tilde{P}_\nu \frac{1}{P \cdot q} F_2(x, Q^2) \right) \\ &= 4\pi \left(-\tilde{g}_{\mu\nu} F_1(x, Q^2) + \tilde{P}_\mu \tilde{P}_\nu \frac{2x}{Q^2} F_2(x, Q^2) \right) , \\ \tilde{P}_\nu &= P_\nu - q_\nu \frac{P \cdot q}{q^2} , \quad x = \frac{Q^2}{2P \cdot q} , \quad Q^2 = -q^2 . \end{aligned} \quad (2.19)$$

The functions $F_1(x, Q^2)$ and $F_2(x, Q^2)$ are the (electromagnetic) structure functions of the hadron.

The quantity λ_S appearing in the flux factor reads:

$$\lambda_S = S^2 - 4m^2 M^2 . \quad (2.20)$$

Expressing the final electron momentum via the invariants (y, Q^2) yields:

$$\frac{d^3 \vec{p}'}{(2\pi)^3 2E'_e} = \frac{1}{(4\pi)^2} \frac{S}{\sqrt{\lambda_S}} dy dQ^2 . \quad (2.21)$$

Inserting into (2.16), we obtain for the differential cross section:

$$\begin{aligned} \frac{d^2 \sigma}{dy dQ^2} &= \frac{\alpha^2}{Q^4} \frac{S}{2\lambda_S} L^{\mu\nu} H_{\mu\nu}(P, q) \\ &= \frac{2\pi\alpha^2}{Q^2 xy^2} \frac{S}{\lambda_S} \left[\left(2(1-y) - 2x^2 y^2 \frac{M^2}{Q^2} \right) F_2(x, Q^2) \right. \\ &\quad \left. + 2 \left(1 - \frac{2m^2}{Q^2} \right) xy^2 F_1(x, Q^2) \right] \end{aligned} \quad (2.22)$$

It is convenient to introduce the ratio R ,

$$R(x, Q^2) \equiv \frac{F_L(x, Q^2)}{F_T(x, Q^2)} = \left(1 + 4x^2 \frac{M^2}{Q^2} \right) \frac{F_2(x, Q^2)}{2xF_1(x, Q^2)} - 1 , \quad (2.23)$$

of the longitudinal and transverse structure functions,

$$\begin{aligned} F_L(x, Q^2) &\equiv \left(1 + 4x^2 \frac{M^2}{Q^2} \right) F_2(x, Q^2) - 2xF_1(x, Q^2) , \\ F_T(x, Q^2) &\equiv 2xF_1(x, Q^2) . \end{aligned} \quad (2.24)$$

Neglecting the small mass of the electron, and changing the kinematic variables from (y, Q^2) to (x, y) , we finally obtain for the Born cross section:

$$\begin{aligned} \frac{d^2 \sigma}{dx dy} &= \frac{2\pi\alpha^2}{Q^2 xy} \left[\left(1 + (1-y)^2 + 2x^2 y^2 \frac{M^2}{Q^2} \right) F_2(x, Q^2) - y^2 F_L(x, Q^2) \right] \\ &= \frac{2\pi\alpha^2}{Q^2 xy} \left[2(1-y) - 2x^2 y^2 \frac{M^2}{Q^2} \right. \\ &\quad \left. + \left(1 + 4x^2 \frac{M^2}{Q^2} \right) \frac{y^2}{1 + R(x, Q^2)} \right] F_2(x, Q^2) . \end{aligned} \quad (2.25)$$

The r.h.s. of the cross section (2.25) depends on the two proton structure functions to be measured, $F_2(x, Q^2)$ and $F_L(x, Q^2)$. For fixed center of mass

energy, only two of the three invariants x , y and Q^2 can be varied independently. The separate determination of the structure functions at fixed x and Q^2 requires the variation of y and therefore the variation of the center of mass energy. For the HERA collider, this means running with different beam energies [39].

2.4 The Born cross section at high energies

The HERA ep collider was designed to reach center of mass energies at the same order of magnitude as the masses of the electroweak gauge bosons, $\sqrt{S} \simeq 3 \cdot 10^2 \text{ GeV} \gtrsim M_Z, M_W$, so that both neutral and charged current reactions can be observed in the same experiments. For the neutral current process, $ep \rightarrow eX$, this means that we have to take into account not only photon but also Z-exchange.

The generalization of the cross section (2.25) that takes into account both γ - and Z-exchange and their interference can be written as (see e.g., [40]):

$$\frac{d^2\sigma_{\text{NC}}^\mp}{dx dy} = \frac{2\pi\alpha^2}{Q^2 xy} \{Y_+ \mathcal{F}_2(x, Q^2) \pm Y_- x \mathcal{F}_3(x, Q^2) - y^2 \mathcal{F}_L(x, Q^2)\} , \quad (2.26)$$

with

$$Y_\pm(y) = 1 \pm (1 - y)^2 . \quad (2.27)$$

In (2.26) we have used the ultrarelativistic limit, $S \gg m^2, M^2$, which is applicable at HERA energies. Upper and lower signs correspond to electron and positron scattering, respectively.

The structure functions \mathcal{F}_2 and \mathcal{F}_L are generalizations of the structure functions F_2 and F_L of the previous section where only photon exchange was taken into account. The additional structure function \mathcal{F}_3 is due to the parity violating contributions from Z-exchange to the scattering amplitude.

At HERA energies also the charged current reaction $ep \rightarrow \nu_e X$ has an appreciable cross section, which reads:

$$\begin{aligned} \frac{d^2\sigma_{\text{CC}}^\mp}{dx dy} &= \frac{G_\mu^2 S}{4\pi} \left(\frac{M_W^2}{M_W^2 + Q^2} \right)^2 \\ &\times \{Y_+ \mathcal{W}_2^\mp(x, Q^2) \pm Y_- x \mathcal{W}_3^\mp(x, Q^2) - y^2 \mathcal{W}_L^\mp(x, Q^2)\} , \end{aligned} \quad (2.28)$$

with G_μ being the muon decay constant, and the charged current structure functions denoted by \mathcal{W}_2 , \mathcal{W}_3 and \mathcal{W}_L .

2.5 Structure functions

In the naive quark parton model, the deep inelastic scattering cross section is calculated as an incoherent superposition of the electron scattering on free partons. The electroproduction structure functions are expressed in terms of probability distributions of massless quarks and antiquarks in the proton,

$$F_2^{\text{QPM}}(x) = 2xF_1^{\text{QPM}}(x) = x \sum_l |Q_l|^2 [q_{0l}(x) + \bar{q}_{0l}(x)] . \quad (2.29)$$

Here the sum runs over all quark flavors, Q_l is the charge of the quark q_l in units of the elementary charge, and $q_{0l}(x)$ and $\bar{q}_{0l}(x)$ denote the ‘bare’ quark and antiquark distributions. Bjorken scaling is implemented by assuming Q^2 -independence of the bare distributions. As the Callan-Gross relation, $F_2 = 2xF_1$, holds in the naive quark parton model, the longitudinal structure function vanishes, $F_L^{\text{QPM}}(x) = 0$.

2.5.1 Structure functions from perturbative QCD

The calculation of radiative corrections to scattering processes involving hadrons in QCD requires the renormalization of the parton densities. This results in a logarithmic violation of Bjorken scaling³ and parton densities $q_l(x, Q^2)$ that will weakly depend on the scale Q^2 .

In the leading order of QCD, the structure functions $F_{1,2}(x, Q^2)$ are given in terms of the renormalized parton distributions by

$$F_2^{\text{LO}}(x, Q^2) = x \sum_l |Q_l|^2 [q_l(x, Q^2) + \bar{q}_l(x, Q^2)] , \quad (2.30)$$

$$F_1^{\text{LO}}(x, Q^2) = \frac{1}{2} \sum_l |Q_l|^2 [q_l(x, Q^2) + \bar{q}_l(x, Q^2)] , \quad (2.31)$$

where the $q_l(x, Q^2)$ and $\bar{q}_l(x, Q^2)$ now denote the Q^2 -dependent quark and antiquark distributions. At this order there is no contribution from the gluon distribution $g(x, Q^2)$, and the longitudinal structure function still vanishes, $F_L^{\text{LO}}(x, Q^2) = 0$.

Beyond the leading order, these simple relations between the quark and gluon distributions and the physical structure functions are modified. From

³For an introduction to QCD and hadron structure we refer the reader to the many excellent reviews and textbooks, e.g., [41, 42, 43, 44] and [45, 46, 47].

the operator product expansion it follows that they may be written as [48]:

$$F(x, Q^2) = \int_x^1 \frac{dy}{y} \left\{ \sum_l C_l \left(\frac{x}{y}, \alpha_S \right) q_l(y, Q^2) + C_g \left(\frac{x}{y}, \alpha_S \right) g(y, Q^2) \right\} , \quad (2.32)$$

where the sum runs over all quarks and antiquarks. The coefficient functions C_l and C_g , the quark and gluon distributions $q_l(x, Q^2)$, $g(x, Q^2)$, and the QCD coupling $\alpha_S = \alpha_S(Q^2)$ depend on the chosen renormalization scheme, and they may also become gauge dependent at higher orders. However, it is still useful to write structure functions at next-to-leading order as

$$F^{\text{NLO}}(x, Q^2) = F^{\text{LO}}(x, Q^2) + \Delta F(x, Q^2) , \quad (2.33)$$

with $\Delta F(x, Q^2)$ formally being $\mathcal{O}(\alpha_S)$.

Common renormalization schemes used in deep inelastic scattering are the $\overline{\text{MS}}$ scheme and the so-called DIS scheme. In the DIS scheme the parton densities are redefined such that relation (2.30) for F_2 also holds beyond the leading order [49, 50, 51]. The QCD corrections to F_2 are completely absorbed into the redefinition of the parton distributions, so that

$$\begin{aligned} F_2^{\text{DIS}}(x, Q^2) &= x \sum_l |Q_l|^2 [q_l(x, Q^2) + \bar{q}_l(x, Q^2)]_{\text{DIS}} , \\ \Delta F_2^{\text{DIS}}(x, Q^2) &\equiv 0 . \end{aligned} \quad (2.34)$$

The renormalized quark and gluon densities satisfy the Altarelli-Parisi evolution equations [52]:⁴

$$\begin{aligned} \frac{dq_l(x, Q^2)}{d \ln Q^2} &= \frac{\alpha_S(Q^2)}{2\pi} \int_x^1 \frac{dy}{y} \left[P_{qq} \left(\frac{x}{y} \right) q_l(y, Q^2) + P_{qG} \left(\frac{x}{y} \right) g(y, Q^2) \right] , \\ \frac{dg(x, Q^2)}{d \ln Q^2} &= \frac{\alpha_S(Q^2)}{2\pi} \int_x^1 \frac{dy}{y} \left[\sum_l P_{Gq} \left(\frac{x}{y} \right) q_l(y, Q^2) \right. \\ &\quad \left. + P_{GG} \left(\frac{x}{y} \right) g(y, Q^2) \right] , \end{aligned} \quad (2.35)$$

with the splitting functions P being given e.g., in [41].

⁴Nowadays it has become customary to denote these integro-differential equations as Dokshitzer[53] - Gribov-Lipatov[54, 55] - Altarelli-Parisi, or DGLAP equations.

The NLO correction to the structure function F_1 in the DIS scheme reads:

$$\begin{aligned} \Delta F_1^{\text{DIS}}(x, Q^2) = & \frac{1}{2} \int_x^1 \frac{dy}{y} \left\{ \sum_l |Q_l|^2 \alpha_S(Q^2) \Delta f_q \left(\frac{x}{y} \right) [q_l(y, Q^2) + \bar{q}_l(y, Q^2)] \right. \\ & \left. + 2 \left(\sum_l |Q_l|^2 \right) \alpha_S(Q^2) \Delta f_g \left(\frac{x}{y} \right) g(y, Q^2) \right\}, \quad (2.36) \end{aligned}$$

where the sum runs over all active quark flavors.

At next-to-leading order, the correction terms in (2.36) are gauge independent, ultraviolet- and infrared-finite; they read [49]:

$$\begin{aligned} \alpha_S \Delta f_q(z) &= \alpha_S [f_{q,1}(z) - f_{q,2}(z)] = -\frac{\alpha_S}{2\pi} \frac{4}{3} 2z, \\ \alpha_S \Delta f_g(z) &= \alpha_S [f_{g,1}(z) - f_{g,2}(z)] = -\frac{\alpha_S}{2\pi} \frac{1}{2} 4z(1-z). \quad (2.37) \end{aligned}$$

The QCD corrections to the structure functions lead to a violation of the Callan-Gross relation and to a QCD prediction of the leading twist term of the longitudinal structure at next-to-leading order,

$$\begin{aligned} F_L(x, Q^2) = & \frac{\alpha_S(Q^2)}{2\pi} \int_x^1 \frac{dy}{y} \left(\frac{x}{y} \right)^2 \left\{ \frac{8}{3} F_2(y, Q^2) \right. \\ & \left. + 4 \left(\sum_l |Q_l|^2 \right) \left(1 - \frac{x}{y} \right) yg(y, Q^2) \right\}, \quad (2.38) \end{aligned}$$

showing that the ratio $R = F_L/(F_2 - F_L) \sim \mathcal{O}(\alpha_S)$ vanishes for $Q^2 \rightarrow \infty$ because of asymptotic freedom. Expression (2.38) is also interesting as it predicts a strong variation of F_L at low x where the gluon distribution is expected to be strongly rising. For a discussion of the gluon distribution and further details regarding the DIS scheme we refer the reader to [51].

The calculation of the QCD corrections in the $\overline{\text{MS}}$ scheme is extensively covered in the literature. The analogous expressions for the electroproduction structure functions in terms of renormalized parton densities will not be reproduced here, they can be found e.g., in [48].

Since the Altarelli-Parisi equations predict only the evolution of the parton distributions in Q^2 , the initial conditions have to be fixed otherwise. Using certain assumptions about the shape of the parton distribution at some low initial scale Q_0^2 , which is typically of the order $(2 \dots 5) \text{ GeV}^2$, several groups provide parameterizations of the evolved distributions that are selected by comparison with experimental data. A large collection of parton distributions is available in the program library PDFLIB [56].

2.5.2 Structure functions in the region of low Q^2

Exact Bjorken scaling is a built-in property of the naive parton model. Because of asymptotic freedom it also holds approximately true within QCD in the region of large momentum transfers, where it receives perturbatively calculable corrections. However, one should expect that a naive extrapolation of perturbative results valid for $Q^2 \gg 1 \text{ GeV}^2$ down to the photoproduction region $Q^2 \approx 0$ will fail sooner or later for several reasons.

Physically, the spatial resolution power of the virtual photon on the proton is given by $\sim \hbar/\sqrt{Q^2}$, and therefore a photon of virtuality $Q^2 \lesssim (\hbar/r_p)^2 \approx (0.2 \text{ GeV})^2$, with $r_p \sim 1 \text{ fm}$ being a typical hadron radius, is not able to resolve the individual partons. Therefore, the probabilistic, partonic description of the proton structure must break down at that scale.

On the technical side, in a systematic analysis of the structure functions in the Bjorken limit using the operator product expansion (see e.g., [47]), one obtains an asymptotic expansion of the structure functions in inverse powers of Q^2 , e.g.,

$$F_2(x, Q^2) = \sum_{n=0}^{\infty} \frac{C_n(x, Q^2)}{(Q^2)^n} . \quad (2.39)$$

The coefficient functions $C_n(x, Q^2)$ depend only weakly, i.e., logarithmically on Q^2 . The terms with $n = 0$ and $n \geq 1$ are usually referred to as leading and higher twists, respectively. For approximate Bjorken scaling, the contribution of the higher twists in (2.39) must be negligible, which is the case only for Q^2 of the order of or above a few GeV^2 . Furthermore, a perturbative evaluation of the coefficient functions becomes doubtful at small momentum transfers $Q^2 \lesssim 1 \text{ GeV}^2$ where the running QCD coupling $\alpha_S(Q^2)$ approaches unity.

And finally, as we shall see below, electromagnetic gauge invariance actually requires that the structure functions F_2 and F_1 vanish in the limit $Q^2 \rightarrow 0$. This clearly forbids Bjorken scaling at very low Q^2 and calls for a formal resummation of the series (2.39) in that region.

Constraints for $Q^2 \rightarrow 0$

To investigate the general behavior and to obtain constraints on the structure functions for small Q^2 , let us rewrite the hadronic tensor (2.19) in order to exhibit potential kinematic singularities as follows [57]:

$$\begin{aligned} H_{\mu\nu}(P, q) = & 4\pi \left[-g_{\mu\nu} F_1 + \frac{P_\mu P_\nu}{P \cdot q} F_2 + \frac{q_\mu q_\nu}{q^2} \left(F_1 + \frac{P \cdot q}{q^2} F_2 \right) \right. \\ & \left. - \frac{P_\mu q_\nu + P_\nu q_\mu}{q^2} F_2 \right] . \end{aligned} \quad (2.40)$$

As the total cross section for real photons on a proton is finite, these singularities can only be artifacts of the tensor decomposition of $H_{\mu\nu}$ into a sum of manifestly gauge-invariant terms. The limit $q^2 \rightarrow 0$ of this expression clearly must exist. This allows to impose the conditions

$$F_2 = \mathcal{O}(Q^2) , \quad (2.41)$$

$$F_1 + \frac{P \cdot q}{q^2} F_2 = \mathcal{O}(Q^2) , \quad (2.42)$$

on the structure functions in the limit $Q^2 \rightarrow 0$.

One can go further and relate the structure functions F_2 and F_L to the total photoproduction cross section for transverse and longitudinal photons,

$$\begin{aligned} F_2 &= \frac{Q^2}{4\pi^2\alpha} (\sigma_T + \sigma_L) , \\ F_L &= \frac{Q^2}{4\pi^2\alpha} \sigma_L . \end{aligned} \quad (2.43)$$

The cross sections on the r.h.s. are functions $\sigma_{T,L} = \sigma_{T,L}(Q^2, W^2)$, where $W^2 = M^2 + 2P \cdot q - Q^2$ is the invariant mass of the hadronic final state. The Bjorken variable x appearing in the structure functions on the l.h.s. reads:

$$x = \frac{Q^2}{W^2 - M^2 + Q^2} . \quad (2.44)$$

Invoking conservation of the electromagnetic current, which guarantees the decoupling of the longitudinal degrees of freedom of the photon, the cross section $\sigma_L \rightarrow 0$ for $Q^2 \rightarrow 0$ and at fixed $P \cdot q$. We therefore expect [57, 58]

$$F_L = \mathcal{O}(Q^4) , \quad (2.45)$$

so that the ratio R should also vanish in this limit,

$$R(x, Q^2) = \frac{\sigma_L}{\sigma_T} = \mathcal{O}(Q^2) . \quad (2.46)$$

Obviously it is a crucial requirement for reasonable phenomenological parameterizations of the structure functions in the region of low Q^2 that they incorporate the above constraints.

Models for low Q^2

There exist several models for the description of high-energy photon-hadron interactions that automatically provide the proper behavior for $Q^2 \rightarrow 0$. A

complete overview is far beyond the scope of this report, so we will only name a few popular ones, and suggest the interested reader to consult the reviews [59, 60] for more detailed descriptions of several phenomenological approaches and dynamical models of the F_2 .

In the Vector Meson Dominance (VMD) model (see e.g., [61] and references cited therein), the interaction of a photon with a hadron is described by assuming that the photon can fluctuate into a vector meson which then interacts with the hadron.

A qualitative description of the low x behavior of cross sections is motivated by the parameterization of the high energy behavior of total cross sections in hadron-hadron interactions in Regge theory [62]. In this approach, the amplitude for hadronic elastic scattering processes at center of mass energy $\sqrt{s} = W$ and momentum transfer t is written as a sum of terms of the form $T(s, t) \sim \beta_i(t) s^{\alpha_i(t)}$, with $\alpha(t)$ being a so-called Regge trajectory. Appealing to the optical theorem and the similarity of hadron-hadron and photon-hadron total cross sections, the high energy behavior of the total photoproduction cross section is written as

$$\sigma_{\text{tot}} = \sum_i \beta_i (W^2)^{\alpha_i - 1}, \quad (2.47)$$

where the $\alpha_i = \alpha_i(0)$ and $\beta_i = \beta_i(0)$ denote the intercept and the coupling of the corresponding Regge trajectory, respectively. Phenomenologically, the energy dependence of the total hadronic and photoproduction cross sections are fairly well described by taking into account two terms in (2.47): the (soft) pomeron with intercept $\alpha_{\mathbb{P}} \simeq 1.08$, which is identified with an exchange of vacuum quantum numbers, and the Reggeon with intercept $\alpha_{\mathbb{R}} \sim 0.5$ [63], corresponding to an exchange which is odd under charge conjugation.

Using the relation between the total photoproduction cross section and the structure functions (2.43), the Regge parameterization (2.47) then implies the following ansatz for a parameterization of the structure function $F_2(x, Q^2)$,

$$F_2(x, Q^2) = \sum_i \tilde{\beta}_i(Q^2) (W^2)^{\alpha_i - 1}, \quad (2.48)$$

which is expected to be valid for high energies and for $W^2 \gg Q^2$. In this case, $x = Q^2/(W^2 - M^2 + Q^2) \simeq Q^2/W^2 \ll 1$. Therefore, the parameterization (2.48) implies a powerlike small x behavior of $F_2(x, Q^2)$,

$$F_2(x, Q^2) = \sum_i \tilde{\beta}_i(Q^2) (Q^2)^{\alpha_i - 1} x^{1 - \alpha_i}. \quad (2.49)$$

Furthermore, from (2.48) and (2.43) we find that the functions $\tilde{\beta}_i(Q^2)$ have to satisfy the conditions $\tilde{\beta}_i(Q^2) = \mathcal{O}(Q^2)$ for $Q^2 \rightarrow 0$.

The H1 collaboration has extracted the derivative [64]

$$\lambda(x, Q^2) \equiv - \left. \frac{\partial \ln F_2(x, Q^2)}{\partial \ln x} \right|_{Q^2}, \quad (2.50)$$

and found $\lambda(x, Q^2)$ to be independent of x for $x < 0.01$ within the experimental accuracy. This implies that the leading x -dependence of F_2 at low x is consistent with the power-law behavior $F_2 \propto x^{-\lambda}$ for fixed Q^2 .

However, experimental data from HERA on J/ψ photoproduction and the charm structure function of the proton show a steeper rise at low x , providing evidence for a deviation from the simple Pomeron behavior described above. A good description of all available data requires to take into account an additional contribution from a “hard” pomeron with intercept ≈ 1.4 [65, 66].

A power-like behavior of structure functions for $x \rightarrow 0$ compatible with the hard pomeron can be obtained from perturbative QCD. Performing an all-order resummation of large $\alpha_S \ln(1/x)$ terms leads to the Balitsky-Fadin-Kuraev-Lipatov (BFKL) [7] evolution equation,⁵ whose solution in the leading logarithmic approximation is interpreted as a pomeron with intercept

$$\alpha_{\text{BFKL}} = 1 + \frac{12\alpha_S}{\pi} \ln 2. \quad (2.51)$$

For this reason the hard pomeron is identified with the perturbative BFKL pomeron, while the soft pomeron that dominates in the total cross section is associated with non-perturbative effects.

Recently the color dipole picture has attracted a lot attention. This approach considers the fluctuation of the virtual photon into a quark-antiquark system as an effective color dipole, which then interacts with the proton through pomeron exchange. The proper low Q^2 behavior is implemented by suitably parameterized wave functions for transversely and longitudinally polarized photons. Some model variants also consider the proton as a quark-diquark system, i.e., as a color dipole. For an overview see e.g., [68, 69] and references cited therein.

Parameterizations of the structure function F_2 for phenomenological applications based on the Regge behavior described above and fit to the HERA data have been provided by Abramowicz-Levin-Levy-Maor (ALLM) [70, 71], Donnachie and Landshoff [65, 66], Adel et al. [72], Capella et al. [73], and Desgrolard et al. [74].

⁵See e.g., ref. [8] for a recent review on BFKL, or the textbook by Forshaw and Ross [67] for a modern introduction to QCD and Regge theory.

2.5.3 Structure functions at high Q^2

For neutral current scattering processes at high Q^2 one has to take into account both γ - and Z-exchange and their interference. The generalized structure functions $\mathcal{F}_i(x, Q^2)$ describing the interaction of leptons with charge Q_l and lepton beam polarization ξ may be decomposed (using the notation of [75]) as:

$$\begin{aligned}\mathcal{F}_{1,2}(x, Q^2) &= F_{1,2}(x, Q^2) + 2|Q_e|(v_e + \lambda a_e)\kappa(Q^2)G_{1,2}(x, Q^2) \\ &\quad + 4(v_e^2 + a_e^2 + 2\lambda v_e a_e)\kappa^2(Q^2)H_{1,2}(x, Q^2), \\ x\mathcal{F}_3(x, Q^2) &= -2\text{sign}(Q_l)\left\{|Q_e|(a_e + \lambda v_e)\kappa(Q^2)xG_3(x, Q^2) \right. \\ &\quad \left. + [2v_e a_e + \lambda(v_e^2 + a_e^2)]\kappa^2(Q^2)xH_3(x, Q^2)\right\},\end{aligned}\quad (2.52)$$

with $Q_e = -1$ and

$$\begin{aligned}\lambda &= \xi \text{sign}(Q_l), \\ v_e &= 1 - 4\sin^2\theta_W^{\text{eff}}, \\ a_e &= 1,\end{aligned}\quad (2.53)$$

and

$$\kappa(Q^2) = \frac{G_\mu M_Z^2}{8\sqrt{2}\pi\alpha(Q^2)} \frac{Q^2}{Q^2 + M_Z^2}. \quad (2.54)$$

The quantity $\sin^2\theta_W^{\text{eff}}$ refers to an effective mixing angle for the renormalized fermion-Z boson couplings.

The leading order expressions of the structure functions read:

$$\begin{aligned}F_2(x, Q^2) &= x \sum_q |Q_q|^2 [q(x, Q^2) + \bar{q}(x, Q^2)], \\ G_2(x, Q^2) &= x \sum_q |Q_q| v_q [q(x, Q^2) + \bar{q}(x, Q^2)], \\ H_2(x, Q^2) &= x \sum_q \frac{v_q^2 + a_q^2}{4} [q(x, Q^2) + \bar{q}(x, Q^2)], \\ xG_3(x, Q^2) &= x \sum_q |Q_q| a_q [q(x, Q^2) - \bar{q}(x, Q^2)], \\ xH_3(x, Q^2) &= x \sum_q \frac{v_q a_q}{2} [q(x, Q^2) - \bar{q}(x, Q^2)],\end{aligned}\quad (2.55)$$

where $q(x, Q^2)$ and $\bar{q}(x, Q^2)$ denote the quark and antiquark distributions. The neutral current couplings of the quarks are:

$$v_q = 1 - 4|Q_q|\sin^2\theta_W^{\text{eff}},$$

$$a_q = 1 . \quad (2.56)$$

The charged current generalized structure functions,

$$\begin{aligned} \mathcal{W}_2(x, Q^2) &= \frac{1+\lambda}{2} W_2^{Q_l}(x, Q^2) , \\ x\mathcal{W}_3(x, Q^2) &= -\text{sign}(Q_l) \frac{1+\lambda}{2} xW_3^{Q_l}(x, Q^2) , \end{aligned} \quad (2.57)$$

are obtained from the parton distributions by:

$$\begin{aligned} W_2^+(x, Q^2) &= 2x \sum_i [d_i(x, Q^2) + \bar{u}_i(x, Q^2)] , \\ W_2^-(x, Q^2) &= 2x \sum_i [u_i(x, Q^2) + \bar{d}_i(x, Q^2)] , \\ xW_3^+(x, Q^2) &= 2x \sum_i [d_i(x, Q^2) - \bar{u}_i(x, Q^2)] , \\ xW_3^-(x, Q^2) &= 2x \sum_i [u_i(x, Q^2) - \bar{d}_i(x, Q^2)] , \end{aligned} \quad (2.58)$$

with u_i and d_i denoting the densities of the up-type (u, c, t) and down-type (d, s, b) quarks.

At leading order, the longitudinal structure functions vanish. We will not discuss here the QCD corrections to the generalized structure functions above but refer the reader to the review [76].

Chapter 3

QED Radiative Corrections and Radiative Processes

The cross sections given in the previous chapter correspond to the Born approximation in perturbation theory and have to be improved to include higher order contributions, i.e., radiative corrections. At HERA energies, the radiative corrections in general need to be treated within the Standard Model of the electroweak interaction.

The electroweak radiative corrections to deep inelastic scattering have already been extensively discussed in the literature (for a review see [40, 77] and references cited therein). It is well known that the numerically most important parts of the corrections arise from virtual photon corrections, photon emission and light fermion loops. Furthermore, in the kinematic region of low to moderate momentum transfers, $Q^2 \ll M_W^2, M_Z^2$, only the QED part of the electroweak corrections is relevant. In this work we will be concerned only with QED radiative corrections to scattering processes.

This chapter starts by briefly reviewing the most important features of the $\mathcal{O}(\alpha)$ electroweak radiative corrections, but refer the reader who is interested in details to the literature. We will then focus on exclusive radiative processes at this order where the emitted photon is measured. As we shall argue, these radiative processes are of particular interest by themselves. Not only do they constitute an important part of the complete radiative corrections, but their measurement gives access to physical information that may be difficult to obtain otherwise. The treatment of QED corrections to these radiative processes, which are a subset of the higher order corrections to deep inelastic scattering, will follow in the next chapters.

3.1 Classification of radiative corrections

The basic process in deep inelastic scattering is lepton-quark scattering. It is well known that the $\mathcal{O}(\alpha)$ radiative corrections to the neutral current cross section can be classified in the following way [40]:

- (1) the *leptonic corrections* are described by Feynman diagrams containing an additional photon attached to the lepton line, i.e., the virtual corrections from the purely photonic correction to the lepton vertex, the photon loop contribution to the self-energies of the external leptons, and the photon emission from the lepton line,
- (2) the *quarkonic corrections* are represented by diagrams with an additional photon connected to the quark line, analogous to (1),
- (3) the *lepton-quark interference* part, consisting of box diagrams with at least one photon, and the interference part of the bremsstrahlung off leptons and off quarks,
- (4) and the *purely weak corrections*, that are given by all other diagrams that do not contain an additional photon.

Each of the above classes can easily be seen to form a gauge-invariant (w.r.t. QED gauge transformations) subset of the full set of corrections.^{1,2} The infrared-singularities of individual contributions therefore cancel within each of the classes (1–3), while each correction in subset (4) is infrared-finite.

The contribution of each loop correction diagram i to the cross section can be expressed by a correction factor δ_i , defined via:

$$\frac{d^2\sigma_i}{dx dy} = \frac{d^2\sigma_{\text{Born}}}{dx dy} \cdot \delta_i(x, y) . \quad (3.1)$$

The total correction from virtual corrections can in principle be obtained by summing over the individual contributions (3.1). However, there are some contributions which are known to be universal and large and which should be treated in a special way.

The vector boson self energies are dominated by fermion loops. Their contribution is large because the momentum transfers Q^2 attained at HERA

¹For non-abelian gauge theories there exists an algorithm for the construction of the minimal gauge-invariant subsets of the tree amplitudes at a given order [78].

²Class (4) is not irreducible. For example, one may treat the fermion-loop contributions to the vector-boson self energies separately.

are much larger than the masses of the light fermions, leading to large logarithms $\sim \ln Q^2/m_f^2$. The fermion loops of the photon self energy (the vacuum polarization) can be taken into account by use of the running QED coupling $\alpha(Q^2)$, thereby summing these leading logarithms to all orders:

$$\alpha(Q^2) = \frac{\alpha(0)}{1 - \Pi_f^\gamma(Q^2)} . \quad (3.2)$$

Here $\Pi_f^\gamma(Q^2) = \hat{\Sigma}_f^\gamma(Q^2)/Q^2$ denotes the fermionic part of the vacuum polarization derived from the renormalized photon self-energy $\hat{\Sigma}^\gamma$, and $\alpha(0) \simeq 1/137.036$. Since the hadronic part is notoriously difficult to calculate for small Q^2 , it is preferably evaluated instead via a dispersion relation and parameterized for practical applications, see e.g., Burkhardt and Pietrzyk [79].

Another set of contributions to the corrections containing large logarithms arises from the infrared-divergent virtual corrections and from photon bremsstrahlung. This part in general does depend on details of the experimental setup, i.e., whether the radiated photons can be resolved in the detector or not. We shall address this issue later.

According to the above classification of the Feynman diagrams, one distinguishes the bremsstrahlung contributions into the classes (1–3). The radiation from the lepton line, which belongs to class (1), is completely independent of the modeling of the hadron side.³ The approach of radiative corrections that restricts to the *leptonic corrections* and to the vacuum polarization will be referred to as the *model independent approach*. The model independent framework has first been used in deep inelastic scattering in [80]. A very detailed account with application to a large set of experimental determinations of kinematic variables can be found in [81]. In this chapter we shall outline the essentials.

In the quark-parton model, there are also contributions from radiation off the quark line and from lepton-quark interference. While we shall comment on the former later on, the latter is in general rather small. For details and references we refer the reader again to [40].

In the case of charged-current processes, there is no gauge-invariant separation of the Feynman diagrams as in the NC case. A similar decomposition can only be performed in a given physical gauge. However, the attribution of the leading logarithmic terms of the corrections to the lepton and quark lines is still gauge invariant [82, 83]. Thus, while the leading logarithms of the leptonic corrections are model-independent according to the above defini-

³It nevertheless depends on the *shape* of the proton structure functions, i.e., their dependence on x and Q^2 .

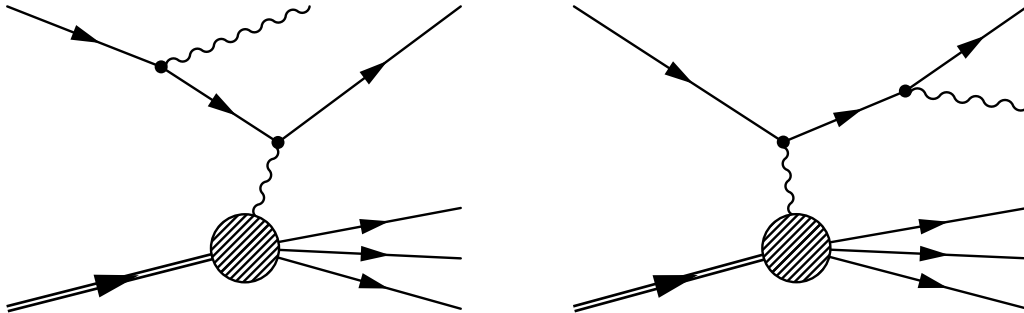


Figure 3.1: Model-independent contributions to radiative deep inelastic electron-proton scattering

tion, the complete set of radiative corrections to CC scattering is necessarily model-dependent.

The main target of this chapter will be bremsstrahlung in NC processes, which we shall treat in the model-independent approach. We will comment only briefly on radiation in charged-current processes which has a much smaller cross section, and close with a discussion of emission off the hadron.

In calculations of cross sections below we always take into account the large fermionic contributions to the vector boson self energies in the form of running couplings. For the neutral current cross section (2.25) or (2.26), this implies replacing the prefactor α^2 by $\alpha^2(Q^2)$. In the charged current case, however, we shall continue to use eq. (2.28), which is accurate enough for our purposes.

3.2 Radiative DIS

In the following we shall be interested in the model-independent calculation of the cross section for the radiative deep inelastic scattering reaction

$$e(p) + p(P) \rightarrow e(p') + \gamma(k) + X(P_X), \quad (3.3)$$

taking into account only photon exchange⁴ and emission of the radiated photon off the electron. This bremsstrahlung contribution is often called the Bethe-Heitler (BH) process. The contributing Feynman diagrams are shown in figure 3.1. The scattering amplitude for this reaction can be factorized into the Born amplitude for the process of scattering of a virtual photon on

⁴The cross section for this process taking into account both photon and Z-exchange is given in detail in [81, 29].

the lepton and the matrix element of the electromagnetic current between the proton and the hadronic final state,

$$\mathcal{M}^{\text{rad}} = M_{\mu}^{e\gamma^* \rightarrow e'\gamma} \frac{g^{\mu\lambda}}{q^2} e \langle P_X | J_{\lambda}^{\text{em}}(0) | P \rangle , \quad (3.4)$$

where $q = p - p' - k$. The differential cross section for the scattering of unpolarized particles can then be expressed as a contraction of the hadron tensor with a tensor describing the QED Compton process:

$$\begin{aligned} d\sigma &= \frac{1}{2\sqrt{\lambda_S}} \cdot \frac{1}{2} \sum_{\text{spins}} \frac{1}{2} \sum_X |\mathcal{M}^{\text{rad}}|^2 \widetilde{dp'} \widetilde{dk} \\ &= \frac{1}{2\sqrt{\lambda_S}} H^{\mu\nu}(P, q) \cdot \left[\frac{1}{2} \sum_{\text{spins}} M_{\mu}^{e\gamma^* \rightarrow e'\gamma} (M_{\nu}^{e\gamma^* \rightarrow e'\gamma})^* \right] \widetilde{dp'} \widetilde{dk} . \end{aligned} \quad (3.5)$$

We shall first discuss the expression in square brackets and turn to the treatment of phase space later.

3.2.1 The QED Compton tensor

Consider the (sub-)process of Compton scattering of a virtual photon on an electron,

$$e(p_1) + \gamma^*(-q) \rightarrow e(p_2) + \gamma(k) , \quad (3.6)$$

and let M_{μ} be the matrix element of this process with the index μ describing the polarization state of the virtual photon. Adopting the notation and normalization of [84], we define the unpolarized Compton tensor

$$K_{\mu\nu}(p_1, p_2, k) = \frac{1}{(2e^2)^2} \sum_{\text{spins}} M_{\mu}^{e\gamma^* \rightarrow e'\gamma} (M_{\nu}^{e\gamma^* \rightarrow e'\gamma})^* . \quad (3.7)$$

With the help of current and momentum conservation, this tensor is conveniently decomposed as follows:

$$K_{\mu\nu} = \tilde{g}_{\mu\nu} B_g + \sum_{i,j=1,2} \tilde{p}_{i\mu} \tilde{p}_{j\nu} B_{ij} , \quad (3.8)$$

where

$$\tilde{g}_{\mu\nu} = g_{\mu\nu} - \frac{q_{\mu} q_{\nu}}{q^2} , \quad \tilde{p}_{i\mu} = p_{i\mu} - q_{\mu} \frac{p_i \cdot q}{q^2} , \quad i = 1, 2 . \quad (3.9)$$

We introduce the following invariants for this subprocess,

$$\hat{s} = 2p_2 \cdot k , \quad \hat{t} = -2p_1 \cdot k , \quad \hat{u} = (p_1 - p_2)^2 , \quad (3.10)$$

so that, using $p_1^2 = p_2^2 = m^2$, $k^2 = 0$, we have

$$\hat{s} + \hat{t} + \hat{u} = q^2 . \quad (3.11)$$

The expressions for the quantities B_{ij} in the Born approximation read:

$$\begin{aligned} B_g &= \frac{1}{\hat{s}\hat{t}} [(\hat{s} + \hat{u})^2 + (\hat{t} + \hat{u})^2] - 2m^2 q^2 \left(\frac{1}{\hat{s}} + \frac{1}{\hat{t}} \right)^2 , \\ B_{11} &= \frac{4q^2}{\hat{s}\hat{t}} - \frac{8m^2}{\hat{s}^2} , \quad B_{22} = \frac{4q^2}{\hat{s}\hat{t}} - \frac{8m^2}{\hat{t}^2} , \\ B_{12} &= B_{21} = -\frac{8m^2}{\hat{s}\hat{t}} . \end{aligned} \quad (3.12)$$

In the high-energy limit, when at least two of the variables $\hat{s}, \hat{t}, \hat{u}, q^2$ are large compared to m^2 , one can drop the terms proportional to $m^2/\hat{s}\hat{t}$, as their contribution is suppressed when integrating over any finite part of phase space for the real photon. Therefore in the high-energy limit of (3.12) we can set

$$\begin{aligned} B_g &\rightarrow \frac{1}{\hat{s}\hat{t}} [(\hat{s} + \hat{u})^2 + (\hat{t} + \hat{u})^2] - 2m^2 q^2 \left(\frac{1}{\hat{s}^2} + \frac{1}{\hat{t}^2} \right) , \\ B_{12} &= B_{21} \rightarrow 0 . \end{aligned} \quad (3.13)$$

3.2.2 The cross section for single photon emission

With the expression for the lowest order Compton tensor of the previous section we can now write the unpolarized cross section (3.5) for the radiative process as:

$$d\sigma = \frac{(4\pi\alpha)^3}{\sqrt{\lambda_S} Q_h^4} K_{\mu\nu}(p, p', k) H^{\mu\nu}(P, q_h) \widetilde{dp'} \widetilde{dk} \Big|_{q_h=p-p'-k} . \quad (3.14)$$

Here we have introduced the hadronic momentum transfer

$$Q_h^2 \equiv -q_h^2 , \quad q_h \equiv P_X - P = p - p' - k , \quad (3.15)$$

to distinguish it from the leptonic momentum transfer

$$Q_l^2 \equiv -q_l^2 , \quad q_l \equiv p - p' . \quad (3.16)$$

Note that hadronic and leptonic momentum transfer are related via

$$Q_h^2 = Q_l^2 + 2p \cdot k - 2p' \cdot k . \quad (3.17)$$

In the following we shall need kinematic invariants which are the “hadronic” and “leptonic” generalizations of the Bjorken variables,

$$\begin{aligned} y_h &= \frac{P \cdot q_h}{P \cdot p} = \frac{P \cdot (P_X - P)}{P \cdot p}, & x_h &= \frac{Q_h^2}{y_h S} = \frac{Q_h^2}{2P \cdot q_h}, \\ y_l &= \frac{P \cdot q_l}{P \cdot p} = \frac{P \cdot (p - p')}{P \cdot p}, & x_l &= \frac{Q_l^2}{y_l S} = \frac{Q_l^2}{2P \cdot q_l}. \end{aligned} \quad (3.18)$$

The contraction of the Compton tensor with the hadron tensor can be decomposed as:

$$K_{\mu\nu} H^{\mu\nu} = 8\pi [S_1 F_1(x_h, Q_h^2) + S_2 F_2(x_h, Q_h^2)] . \quad (3.19)$$

Retaining only those terms that survive in the limit $S \gg m^2$, but keeping all terms of order M^2 , the coefficient functions $S_{1,2}$ can be expressed as follows:

$$\begin{aligned} S_1 &= -\frac{1}{\hat{s}\hat{t}} [(\hat{s} + \hat{u})^2 + (\hat{t} + \hat{u})^2] + 2m^2 q^2 \left(\frac{1}{\hat{s}^2} + \frac{1}{\hat{t}^2} \right) = -B_g, \\ S_2 &= -\frac{S}{q^2} \left[[x_h S + (\hat{t} + \hat{u})] \frac{B_{11}}{4} + (1 - y_l) [x_h (1 - y_l) S - (\hat{s} + \hat{u})] \frac{B_{22}}{4} \right] \\ &\quad + \frac{x_h M^2}{q^2} S_1. \end{aligned} \quad (3.20)$$

where

$$\hat{s} = 2p' \cdot k, \quad \hat{t} = -2p \cdot k, \quad \hat{u} = q_l^2, \quad q^2 = q_h^2.$$

The functions S_1 and S_2 agree with those given in [29].

Let us assume that the kinematics of the scattering process is determined by a measurement of the scattered lepton and the radiated photon. We can express the phase space integral for the scattered electron in terms of y_l and Q_l^2 , see (2.21):

$$\widetilde{dp'} = \frac{1}{(4\pi)^2} dy_l dQ_l^2. \quad (3.21)$$

The differential cross section (3.14) then reads:

$$\begin{aligned} d\sigma &= \frac{32\pi^2 \alpha^3}{Q_h^4 S} [S_1 F_1 + S_2 F_2] dy_l dQ_l^2 \widetilde{dk} \\ &= \frac{2\alpha^3}{\pi Q_h^4 S} [S_1 F_1 + S_2 F_2] dy_l dQ_l^2 E_\gamma dE_\gamma d\Omega_\gamma \\ &= \frac{2\alpha^3}{\pi} \frac{y_l}{Q_h^4} [S_1 F_1 + S_2 F_2] dx_l dy_l E_\gamma dE_\gamma d\Omega_\gamma. \end{aligned} \quad (3.22)$$

In the last line we have change from the set (y_l, Q_l^2) to the set (x_l, y_l) . Note that the cross section (3.22) may be generalized to also take into account Z-boson exchange by replacing $[S_1 F_1 + S_2 F_2]$ by $\sum_{i=1}^3 S_i \mathcal{F}_i$, with the \mathcal{F}_i being the generalized structure functions, and S_3 given e. g., in [29]. We will return to it in section 3.4.

Parameterizations of the photon phase space

In the radiative cross section (3.22), we have chosen to express the phase space of the photon in terms of variables $E_\gamma, \vartheta, \phi$ that are measured in the HERA frame. Although Lorentz invariance is not obvious, this representation is useful for practical applications, as it allows an easy implementation of experimental cuts and constraints given by the detector. We will therefore only sketch the relation to the manifestly Lorentz covariant approach, which is described in great detail in [81].⁵

Let us choose a coordinate system for the HERA frame such that the unit three-vectors in the direction of the incoming and outgoing lepton and the radiated photon are as follows:

$$\begin{aligned}\vec{e}_1 &= \vec{e}_z = (0, 0, 1) , \\ \vec{e}_2 &= (\sin \theta, 0, \cos \theta) , \\ \vec{e} &= (\sin \vartheta \cos \phi, \sin \vartheta \sin \phi, \cos \vartheta) .\end{aligned}\tag{3.23}$$

We then have

$$\begin{aligned}c &\equiv \vec{e}_1 \cdot \vec{e}_2 = \cos \theta , \\ c_1 &\equiv \vec{e} \cdot \vec{e}_1 = \cos \vartheta , \\ c_2 &\equiv \vec{e} \cdot \vec{e}_2 = c \cos \vartheta + s \sin \vartheta \cos \phi ,\end{aligned}\tag{3.24}$$

with $s = \sin \theta = \sqrt{1 - c^2}$. The integral over the solid angle of the photon may be alternatively expressed in terms of c_1, c_2 as

$$d\Omega_\gamma \equiv d(\cos \vartheta) d\phi = J(c_1, c_2) dc_1 dc_2 ,\tag{3.25}$$

with the Jacobian

$$J(c_1, c_2) = \frac{2}{|ss_1 \sin \phi|} = \frac{2}{\sqrt{1 - c^2 - c_1^2 - c_2^2 + 2cc_1c_2}} =: \frac{1}{\sqrt{\mathcal{D}}} ,\tag{3.26}$$

⁵For a classic textbook on particle kinematics and the treatment of multi-particle phase space see [85].

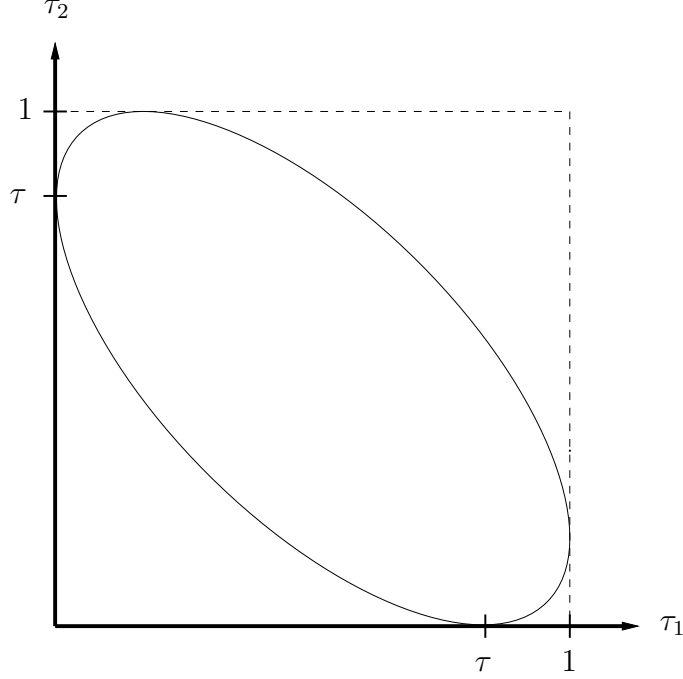


Figure 3.2: Schematic view of the kinematic range for the integration over the angles τ_1 and τ_2 for fixed τ . The allowed range corresponding to $\mathcal{D} \geq 0$ is given by the interior of the ellipse.

where $s_1 = \sqrt{1 - c_1^2}$. The allowed region for (c_1, c_2) is given by the requirement that $\mathcal{D} \geq 0$. This representation is obviously symmetric w.r.t. incoming and scattered lepton, i.e., $c_1 \leftrightarrow c_2$.

Furthermore, it is convenient to change variables to

$$\tau_{1,2} = \frac{1 - c_{1,2}}{2}, \quad \tau = \frac{1 - c_{1,2}}{2}, \quad (3.27)$$

so that

$$d\Omega_\gamma = \frac{4}{\sqrt{\mathcal{D}}} d\tau_1 d\tau_2. \quad (3.28)$$

Expressing \mathcal{D} in terms of $\tau_{1,2}$, we find:

$$\mathcal{D} = -4\tau\tau_1\tau_2 - [\tau^2 + \tau_1^2 + \tau_2^2 - 2\tau\tau_1 - 2\tau\tau_2 - 2\tau_1\tau_2]. \quad (3.29)$$

The domain $\mathcal{D} \geq 0$ corresponds to the interior of the ellipse shown in fig. 3.2, which can be parameterized as follows:

$$0 \leq \tau_1 \leq 1, \quad \tau_2^-(\tau_1) \leq \tau_2 \leq \tau_2^+(\tau_1), \quad (3.30)$$

which is derived from the factorization

$$\mathcal{D} = (\tau^+(\tau_1) - \tau_2) (\tau_2 - \tau^-(\tau_1)) , \quad (3.31)$$

with

$$\tau_2^\pm(\tau_1) = \tau(1 - \tau_1) + \tau_1(1 - \tau) \pm 2\sqrt{\tau(1 - \tau)\tau_1(1 - \tau_1)} . \quad (3.32)$$

Similar expressions are obtained under the exchange $\tau_1 \leftrightarrow \tau_2$.

We assume now the leptonic determination of the kinematic variables, i.e., we keep x_l, y_l fixed. The upper limit on the energy of the radiated photon is calculated as follows. The true invariant mass of the hadronic final state reads:

$$\begin{aligned} W^2 &= M_X^2 = (P + p - p' - k)^2 \\ &= M^2 + (1 - x_l)y_l S - 2k \cdot (P + p - p') \\ &= W_{\text{rec}}^2 - 2k \cdot (P + p - p') , \end{aligned} \quad (3.33)$$

where W_{rec}^2 is the reconstructed (apparent) hadronic mass if only the scattered lepton is measured. The true hadronic mass in inelastic scattering must be higher than the threshold for pion production,

$$M_X^2 \geq \bar{M}^2 \equiv (M + m_\pi)^2 . \quad (3.34)$$

This leads to

$$\begin{aligned} 2k \cdot (P + p - p') &\leq [M^2 + (1 - x_l)y_l S] - \bar{M}^2 \\ &\leq [M^2 + 2P \cdot (p - p') - Q_l^2] - \bar{M}^2 . \end{aligned} \quad (3.35)$$

Expressing this kinematic limit in the HERA frame we obtain, assuming $E_p \gg M, E_e \gg m$:

$$E_\gamma^{\text{max}}(\tau_1, \tau_2) = \frac{S[1 - Y(1 - \tau)] - 4E_e^2 Y \tau - (\bar{M}^2 - M^2)}{4[E_p(1 - \tau_1) + E_e \tau_1 - Y E_e \tau_2]} , \quad (3.36)$$

with

$$\begin{aligned} Y &\equiv \frac{E'_e}{E_e} = 1 - y_l + x_l y_l \frac{E_p}{E_e} , \\ \tau &= \frac{Q_l^2}{4E_e^2 Y} = \frac{x_l y_l E_p}{(1 - y_l)E_e + x_l y_l E_p} . \end{aligned} \quad (3.37)$$

Using the above parameterization for the photon angles, we can calculate the kinematic variables occurring in the Compton tensor (3.12) and in the coefficient functions $S_{1,2}$ in the cross section (3.22):

$$\begin{aligned}
\hat{s} &= 2p' \cdot k = 2E'_e E_\gamma (1 - \beta'_e c_2) \simeq 4E'_e E_\gamma \left(\tau_2 + \frac{m^2}{4E_e'^2} \right), \\
\hat{t} &= -2p \cdot k = -2E_e E_\gamma (1 - \beta_e c_1) \simeq -4E_e E_\gamma \left(\tau_1 + \frac{m^2}{4E_e^2} \right), \\
\hat{u} &= -Q_l^2, \\
Q_h^2 &= -q^2 = -(\hat{s} + \hat{t} + \hat{u}) \simeq Q_l^2 + 4E_e E_\gamma \tau_1 - 4E'_e E_\gamma \tau_2, \\
x_h &= \frac{Q_h^2}{y_l S - 2P \cdot k} \simeq \frac{Q_h^2}{y_l S - 4E_p E_\gamma (1 - \tau_1)}.
\end{aligned} \tag{3.38}$$

Note that we explicitly kept the leading lepton mass terms in \hat{s} and \hat{t} . It is necessary to retain them when they occur as denominator factors and we want to integrate over the regions $\tau_1 \rightarrow 0$ or $\tau_2 \rightarrow 0$, where the emitted photon is collinear to either the incoming or the outgoing lepton.

Inspecting (3.38) and remembering (3.28) one easily sees with a little algebra that we can express the integration over photon phase space in terms of invariants,

$$\widetilde{dk} = \mathcal{J}' d\hat{s} d|\hat{t}| dx_h, \tag{3.39}$$

with the Jacobian \mathcal{J}' being given in [81]. With the help of relations like $Q_h^2 = Q_l^2 - \hat{s} - \hat{t}$ one may switch to other equivalent sets of kinematic invariants as integration variables.

For a fixed energy of the radiated photon, the cross section (3.22) obviously exhibits a strong dependence on the integration variables in three domains of phase space: (1) $\tau_1 \rightarrow 0$, (2) $\tau_2 \rightarrow 0$, (3) $Q_h^2 \rightarrow 0$. One can decompose the cross section so that each contribution peaks in only one of these regions (the peaks were called “s-peak”, “p-peak” and “t-peak” in [80]). We shall now investigate this peaking behavior in a simplified fashion.

Emission collinear to the incoming electron

In the region $\tau_1 \rightarrow 0$, where the photon is almost collinear to the incoming electron (“initial state radiation”, ISR), the kinematic variable \hat{t} of the Compton subprocess becomes very small; it approaches $|\hat{t}| \simeq \mathcal{O}(m^2)$ rather than being of order Q_l^2 . As a consequence, the expression for the differential cross section simplifies significantly. Defining the variable

$$z = \frac{E_e - E_\gamma}{E_e}, \tag{3.40}$$

which describes the relative energy fraction of the incoming electron after emission of the photon, we obtain the relations

$$Q_h^2 = zQ_l^2, \quad y_h = y_l - (1 - z), \quad x_h = \frac{Q_h^2}{y_h S} = \frac{x_l y_l z}{y_l + z - 1}. \quad (3.41)$$

This implies $0 \leq y_h \leq z$ and $(1 - z) \leq y_l \leq 1$.

The coefficient functions $S_{1,2}$ reduce to:

$$\begin{aligned} S_1 &\simeq \frac{Q_h^2}{z} \left(\frac{1 + z^2}{1 - z} \frac{1}{(-\hat{t})} - 2z \frac{m^2}{\hat{t}^2} \right), \\ S_2 &\simeq \frac{S}{Q_h^2} \left[x_h z S \left(1 - \frac{M^2 Q_h^2}{(zS)^2} \right) - Q_h^2 \right] \left(\frac{1 + z^2}{1 - z} \frac{1}{(-\hat{t})} - 2z \frac{m^2}{\hat{t}^2} \right). \end{aligned} \quad (3.42)$$

Obviously, these functions factorize into the respective Born expressions S_1^B , S_2^B (see [81, 29]) and a universal function given in parentheses.

For initial state radiation and at high electron energy it is convenient to write the photon phase space as

$$\widetilde{dk} = \frac{1}{(4\pi)^2} dz d|\hat{t}| \frac{d\phi}{2\pi}. \quad (3.43)$$

The radiative cross section (3.22) schematically simplifies to:

$$d\sigma \sim d\sigma^{\text{Born}}(x_h, y_h/z, Q_h^2) \cdot \frac{\alpha}{2\pi} \left(\frac{1 + z^2}{1 - z} \frac{1}{(-\hat{t})} - 2z \frac{m^2}{\hat{t}^2} \right) dz d|\hat{t}| \frac{d\phi}{2\pi}. \quad (3.44)$$

When the radiated photon is not observed, we have to integrate over all available phase space as discussed above. The integral over \hat{t} leads to large logarithm in the electron mass, of the order $\ln(E_e^2/m^2)$ resp. $\ln(Q_l^2/m^2)$:

$$d\sigma^{\text{ISR}} \approx \left[\frac{\alpha}{2\pi} \left(\frac{1 + z^2}{1 - z} \ln \frac{Q_l^2}{m^2} - \frac{2z}{1 - z} \right) \right] \cdot d\sigma^{\text{Born}}(x_h, y_h/z, Q_h^2) dz. \quad (3.45)$$

The soft photon singularity encountered in the integration over z for $z \rightarrow 1$ is canceled by matching infrared singular terms in the virtual corrections.

Emission collinear to the outgoing electron

For $\tau_2 \rightarrow 0$, the photon becomes collinear to the scattered electron (“final state radiation”, FSR). In this case we have $\hat{s} \simeq \mathcal{O}(m^2)$. Defining analogously

$$z_f = \frac{E'_e + E_\gamma}{E'_e}, \quad (3.46)$$

we obtain

$$Q_h^2 = z_f Q_l^2, \quad y_h = 1 - z_f(1 - y_l), \quad x_h = \frac{x_l y_l z_f}{1 - z_f(1 - y_l)}. \quad (3.47)$$

The coefficient functions again exhibit factorization,

$$\begin{aligned} S_1 &\simeq \frac{Q_h^2}{z_f} \left(\frac{1 + z_f^2}{z_f - 1} \frac{1}{\hat{s}} - 2z_f \frac{m^2}{\hat{s}^2} \right), \\ S_2 &\simeq \frac{S}{z_f Q_h^2} \left[x_h S \left(1 - \frac{M^2 Q_h^2}{S^2} \right) - Q_h^2 \right] \left(\frac{1 + z_f^2}{z_f - 1} \frac{1}{\hat{s}} - 2z_f \frac{m^2}{\hat{s}^2} \right). \end{aligned} \quad (3.48)$$

We write the photon phase for final state radiation as

$$\widetilde{dk} = \frac{1}{(4\pi)^2} dz_f d\hat{s} \frac{d\phi'}{2\pi}, \quad (3.49)$$

with the azimuthal angle ϕ' measured w.r.t. the outgoing electron. The radiative cross section (3.22) now reads:

$$d\sigma \sim d\sigma^{\text{Born}}(x_h, y_h, Q_h^2) \cdot \frac{\alpha}{2\pi} \left(\frac{1 + z_f^2}{z_f - 1} \frac{1}{\hat{s}} - 2z_f \frac{m^2}{\hat{s}^2} \right) \frac{dz_f}{z_f^3} d\hat{s} \frac{d\phi'}{2\pi}. \quad (3.50)$$

The integration over the photon solid angle again leads to a large logarithm in the electron mass, $\ln(E_e'/m)^2$. The soft photon singularity for $z_f \rightarrow 1$ cancels against the remaining infrared divergent parts of the virtual correction. The sum of virtual corrections at relative order $\mathcal{O}(\alpha)$ and the contributions from initial and final state radiation at the same order is infrared finite, as required by the Bloch-Nordsieck theorem.

The above discussion assumes that the detector is able to distinguish the scattered electron from an almost collinear photon. This is the case if the detector determines the momentum of the electron directly, e.g., by the bending of its trajectory in a magnetic field. We will refer to such a measurement as an *exclusive* one.

On the other hand, electromagnetic calorimeters essentially provide information about the deposited electromagnetic energy and the location and profile of the generated showers. When the showers of nearby hits overlap, it may no longer be possible to distinguish the particles that initiated these showers, and only the sum of their energies can be determined accurately. For the present work we will assume for simplicity that a minimum angle exists, below which electrons and photons cannot be separated anymore, and denote this type of measurement as a *calorimetric* one.

In the calorimetric case, collinear final state radiation therefore does not change the measured kinematic variables if the momenta of final electron and photon are combined, $p'_{\text{cal}} = p' + k$, since

$$Q_{\text{cal}}^2 = -(p - p'_{\text{cal}})^2 = Q_h^2, \quad x_{\text{cal}} = \frac{Q_{\text{cal}}^2}{2P \cdot (p - p'_{\text{cal}})} = x_h. \quad (3.51)$$

and similarly $y_{\text{cal}} = y_h$. Using $p' \simeq p'_{\text{cal}}/z_f$, we can rewrite eq. (3.21) as

$$\widetilde{dp'} \rightarrow \frac{1}{z_f^2} \widetilde{dp'_{\text{cal}}} = \frac{1}{z_f^2} \cdot \frac{1}{(4\pi)^2} dy_{\text{cal}} dQ_{\text{cal}}^2, \quad (3.52)$$

and we identify the leptonic kinematic variables with the measured ones. After the appropriate variable transformation in the Born cross section, the radiative cross section becomes proportional to the non-radiative one:

$$d\sigma \sim d\sigma^{\text{Born}}(x_l, y_l, Q_l^2) \cdot \frac{\alpha}{2\pi} \left(\frac{1+z_f^2}{z_f-1} \frac{1}{\hat{s}} - 2z_f \frac{m^2}{\hat{s}^2} \right) \frac{dz_f}{z_f^3} d\hat{s} \frac{d\phi'}{2\pi}. \quad (3.53)$$

Performing the integration over the photon solid angle, integrating over z_f and combining with the virtual corrections, one can show that – besides the cancellation of infrared singularities as in the exclusive case – the large logarithm in the electron mass cancels for final state radiation, and only a logarithm in the resolution parameter remains, in accordance with the Kinoshita-Lee-Nauenberg theorem [86].

The QED Compton peak

A moderately strong peaking behavior of the cross section is also found for $Q_h^2 \rightarrow 0$. In this case the exchanged photon between the hadron and the electron becomes almost real; its momentum is almost collinear to the incoming proton. The contributing region in phase space lies in the vicinity of the upper boundary in figure 3.2, $\tau_2 \rightarrow \tau_2^+(\tau_1)$, corresponding to the outgoing electron and photon having opposite azimuthal angles and compensating transverse momenta in the HERA frame. The hard scattering process with large momentum transfer occurs between this photon and the electron, leading to its denomination as the QED Compton process in deep inelastic scattering. Approximating the four-momentum of the exchanged photon as

$$q_h \simeq -\xi P + q_{\perp,h}, \quad (3.54)$$

such that ξ represents the momentum fraction of the proton taken by this photon, and $q_{\perp,h}$ being a small transverse momentum, we find for the invariants of the electron-photon scattering process:

$$\hat{s} \simeq \xi S, \quad \hat{t} \simeq -\xi(1-y_l)S, \quad \hat{u} \simeq -\xi y_l S, \quad q^2 \approx 0. \quad (3.55)$$

Assuming that we determine the kinematic variables from a measurement of the scattered electron, $x_l \simeq \xi$. The coefficient functions factorize into one piece proportional to the differential cross section for Compton scattering,

$$\begin{aligned} S_1 &\simeq \frac{1 + (1 - y_l)^2}{1 - y_l}, \\ S_2 &\simeq \frac{1 + (1 - y_l)^2}{1 - y_l} \cdot \left[\frac{x_h - x_l}{x_l^2} - \frac{x_h M^2}{Q_h^2} \right], \end{aligned} \quad (3.56)$$

and one can express the differential cross section in the form [87, 88]

$$d\sigma \simeq \frac{2\pi\alpha^2}{S} \frac{1 + (1 - y_l)^2}{x_l(1 - y_l)} \cdot \gamma(x_l, Q_l^2) dx_l dy_l, \quad (3.57)$$

with $\gamma(x_l, Q_l^2)$ being the inelastic contribution to the photon distribution within the proton [89, 75],

$$\begin{aligned} \gamma(x_l, Q_l^2) &= \frac{\alpha}{2\pi} \int_{x_l}^1 \frac{dz}{x_l z} \int_{(Q_h^2)^{\min}}^{(Q_h^2)^{\max}} \frac{dQ_h^2}{Q_h^2} \left[\left(1 + (1 - z)^2 + 2x_l^2 \frac{M^2}{Q_h^2} \right) F_2\left(\frac{x_l}{z}, Q_h^2\right) \right. \\ &\quad \left. - z^2 F_L\left(\frac{x_l}{z}, Q_h^2\right) \right]. \end{aligned} \quad (3.58)$$

With the integration limits $(Q_h^2)^{\min, \max}$ given below in (3.61), it is evident that the logarithm obtained from the Q_h^2 -integration, $\ln(Q_l^2/M^2)$, does not depend on a small mass. It therefore is much smaller than the corresponding logarithms in the electron mass for ISR and FSR. Nevertheless, the QED Compton contribution is significant in the region of large y_l .

An accurate calculation of the photon distribution, $\gamma(x, Q^2)$, requires a detailed modeling of the contributions to the proton structure functions from low mass hadronic final states. However, it should be noted that also elastic proton scattering contributes to the QED Compton process at HERA, and it even dominates the inelastic contribution [90]. A separation of elastic and inelastic contributions may be difficult but possible via the residual transverse momentum of the hadronic system. On the other hand, the elastic contribution is essentially independent of Q^2 . Provided sufficient statistics, the QED Compton process could also be used as a test of QCD, as the Q^2 evolution of the photon distribution within the proton differs from that of the colored partons [91]. No separation of elastic and inelastic contributions would be required for that purpose.

3.2.3 Kinematic effects of photon radiation

It was already mentioned in the introduction to this chapter that the radiative corrections are sensitive to the shape of the structure functions. Following Krasny [92] we shall illuminate the connection of this shape dependence to the contributions with emission of hard photons. We assume that only the scattered electron is measured.

Kinematic limits

If we are only interested in the differential cross section in the lepton variables, $d^2\sigma/dx_l dy_l$, we may integrate over the phase space of the photon. When no experimental cuts are to be applied it is convenient to express this phase space integral in terms of kinematic invariants, e.g., x_h , Q_h^2 , and \hat{s} or \hat{t} , see (3.39). Then the integration over \hat{s} (resp. \hat{t}) may be performed analytically. The domain of integration for the other two variables is constrained by the inequality (ref. [81], eq. B.4):

$$[y_l^2 Q_h^2 + y_h^2 Q_l^2 - y_l y_h (Q_l^2 + Q_h^2)] S^2 - M^2 (Q_l^2 - Q_h^2)^2 \leq 0 . \quad (3.59)$$

Taking (x_h, Q_h^2) as remaining integration variables, the boundary of the domain described by (3.59) reads:

$$\begin{aligned} x_h^{\min} &= x_l , \\ (Q_h^2)^{\max(\min)} &= x_h \frac{(x_h y_l S - Q_l^2) (y_l S \pm \sqrt{\lambda_q}) + 2x_h M^2 Q_l^2}{2[x_h y_l S - Q_l^2 + x_h^2 M^2]} , \end{aligned} \quad (3.60)$$

where

$$\lambda_q = y_l^2 S^2 + 4M^2 Q_l^2 .$$

In the high-energy limit, $S \gg M^2$, the boundaries for Q_h^2 following from (3.60) are

$$\begin{aligned} (Q_h^2)^{\min} &\simeq \frac{x_h x_l^2 M^2}{x_h - x_l (1 - x_h^2 M^2 / Q_l^2)} , \\ (Q_h^2)^{\max} &\simeq x_h y_l S = \frac{x_h Q_l^2}{x_l} . \end{aligned} \quad (3.61)$$

The upper limit on x_h and a further restriction on Q_h^2 is obtained from the inelastic threshold:

$$M_X^2 = M^2 + \frac{1 - x_h}{x_h} Q_h^2 \geq \bar{M}^2 . \quad (3.62)$$

Obviously, $x_h = 1$ corresponds to elastic scattering of the proton. For $x_h \rightarrow 1$, the upper limit (3.61) then implies

$$x_h^{\max} \simeq 1 - \frac{x_l (\bar{M}^2 - M^2)}{Q_l^2} , \quad (3.63)$$

and the actual lower limit on Q_h^2 reads

$$(Q_h^2)^{\min} \simeq \max \left(\frac{x_h x_l^2 M^2}{x_h - x_l (1 - x_h^2 M^2 / Q_l^2)}, \frac{x_h}{1 - x_h} (\bar{M}^2 - M^2) \right) . \quad (3.64)$$

Alternatively, one can switch to (x_h, y_h) as integration variables. In that case,

$$\begin{aligned} y_h^{\min} &\simeq \frac{x_l^2 y_l M^2 / S}{(x_h - x_l) y_l + x_h^2 M^2 / S} , \\ y_h^{\max} &= y_l . \end{aligned} \quad (3.65)$$

Neglecting the proton mass, the above conditions simplify to:

$$x_l \leq x_h \leq 1 , \quad 0 \leq y_h \leq y_l . \quad (3.66)$$

The radiatively corrected cross section

As discussed above, the measured differential cross section depends on the structure functions in the whole domain $x_h \geq x_l$ and $y_h \leq y_l$. At leading order this dependence can be written in the form of a convolution,

$$\frac{d^2 \sigma^{\text{meas}}}{dx_l dy_l} \simeq \int_{x_l}^{x_h^{\max}} dx_h \int_{y_h^{\min}}^{y_l} dy_h K(x_l, y_l; x_h, y_h) \frac{d\sigma^{\text{Born}}(x_h, y_h)}{dx_h dy_h} . \quad (3.67)$$

The analytic form of the kernel $K(x_l, y_l; x_h, y_h)$ can be found e.g., in [93]. We do not need its precise form here, but the relevant approximations have been given in section 3.2.2.

The implications of hard photon radiation are most easily understood by considering the following simple examples [92]. The boundaries of the integration region contributing to the inclusive cross section at $x_l = 10^{-3}$, $Q_l^2 = 95$ GeV and at $x_l = 9 \cdot 10^{-3}$, $Q_l^2 = 95$ GeV are shown as dashed lines in fig. 3.3a and fig. 3.3b, respectively. The shaded areas roughly correspond to the kinematic domains accessible to fixed-target experiments (upper left corner) and the HERA experiments. The HERA band is essentially limited

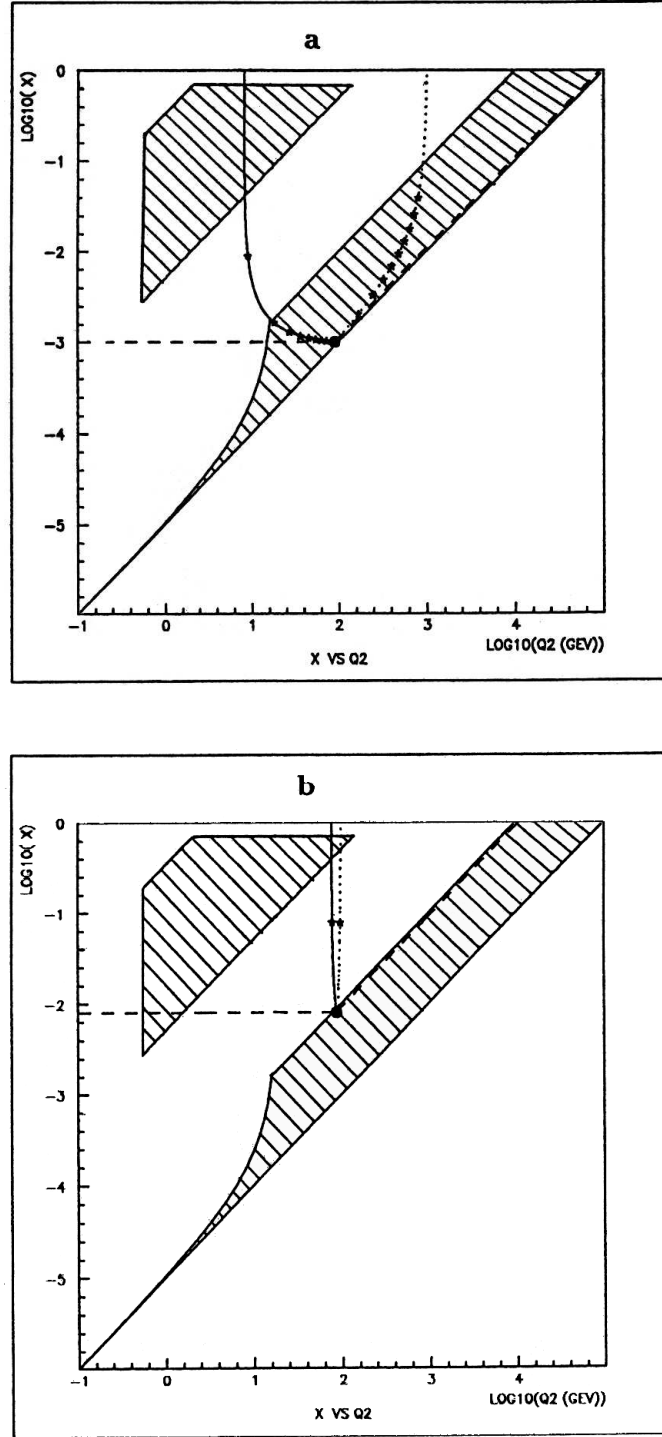


Figure 3.3: The topology of the (x, Q^2) domains contributing to the radiative cross section at HERA. (a) $x_l = 10^{-3}$, $Q_l^2 = 95 \text{ GeV}$; (b) $x_l = 9 \cdot 10^{-3}$, $Q_l^2 = 95 \text{ GeV}$. (Taken from [92])

by the measurement of the scattered electron energy and the geometrical acceptance of the detectors [94].⁶ The solid curve on the left side of each point (x_l, y_l) corresponds to the integration region contributing in the case when the photon is collinear to the incoming electron; it is described by the parameterization (see eq. (3.41)):

$$x_h = \frac{x_l y_l z}{y_l + z - 1}, \quad Q_h^2 = z Q_l^2, \quad (3.68)$$

with $y_l = Q_l^2/x_l S$ and $z = (E_e - E_\gamma)/E_e$. Each asterisk on the curve represents a $z(E_\gamma)$, with $E_{\gamma,j} = 3j$ GeV. The asterisk closest to the full circle corresponds to $j = 1$, i.e., $E_\gamma = 3$ GeV. The upper limit on the photon energy in this case follows from the condition $(1 - y_l)/(1 - x_l y_l) \leq z \leq 1$.

Similarly, the dotted curve on the right side of the (x_l, y_l) point corresponds to the case where the photon is emitted collinear to the scattered electron. Here,

$$x_h = \frac{x_l y_l z_f}{1 - z_f(1 - y_l)}, \quad Q_h^2 = z_f Q_l^2, \quad (3.69)$$

with y_l as above and $z_f = (E'_e + E_\gamma)/E'_e$. The kinematically allowed range is $1 \leq z_f \leq 1/(1 - y_l(1 - x_l))$. The symbols on the curve correspond to the same choice of photon energies as above, $E_{\gamma,j} = 3j$ GeV.

The dominant contributions to the measured cross section (3.67) originate from small bands centered around the curves discussed above; they correspond to the domain where the kernel K is large. The scale of width of these bands can be estimated using the approximations (3.44) and (3.53); for the photon solid angle they correspond to cones of half opening angle $\sim m/E_e$ and $\sim m/E'_e$ around initial and final electron, respectively. Another significant contribution to the cross section is the region where the Born differential cross section in the integrand is large, i.e., where Q_h^2 is close to its lower limit (3.64). In this region the photon exchanged between the electron and the hadronic system is almost real, and the hard scattering process is interpreted as QED Compton scattering, $e\gamma \rightarrow e\gamma$, between the electron and the photon emitted from a quark or proton.

As can be seen from fig. 3.3, moving the point (x_l, y_l) around within the HERA kinematic domain, one can easily find regions where the dominant contributions to the convolution integral (3.67) involve mostly “uncharted territory”. This is especially the case for small $x \lesssim 10^{-4}$ and $Q^2 \lesssim 10$ GeV.

⁶The kinematic domain covered by the HERA experiments has been extended over time, mostly towards lower values of x and Q^2 , by successive upgrades of the detectors (e.g., small angle taggers) or using a longitudinally shifted position of the interaction vertex. However, an ‘unexplored gap’ between the shaded domains still remains.

At this point uncertainties enter the radiatively corrected cross section. While one might expect reliable predictions for the structure functions from perturbative QCD already for moderate momentum transfers, say, above 4 GeV^2 , this appears questionable when the non-perturbative regime $Q^2 \lesssim 1 \text{ GeV}^2$ is approached. Therefore, extrapolations of the structure functions such as those mentioned in section 2.5.2 will be needed, leading to a model-dependence and uncertainty in the predictions of the radiative corrections.

We would like to point out that in the case of HERA this strong model-dependence concerns mainly initial state radiation and the Compton process. The Compton contribution to the structure function measurement can however be suppressed by imposing some minimum experimental cut on the transverse momentum or invariant mass of the outgoing hadronic system. For final state radiation, the calorimetric measurement of electrons and photons leads to a cancellation of the large logarithmic contribution as discussed above. It also does not shift the kinematic variables.

The uncertainties related to the model-dependence can be brought under control if one can experimentally detect events with emitted hard photons and either rejects them (see e.g., the discussion in [95] for using tagged ISR at HERA), or if one turns necessity into a virtue and actually accepts these events and recalculates the kinematic variables of the hard subprocess taking into account the four-momentum of the emitted photon. This way one can actually extend the kinematic region in which the structure functions of the proton can be measured. Furthermore, we shall see another virtue of the measurement of radiative events in the next section in that it helps in the determination of the longitudinal structure function F_L .

The above reasoning in principle also applies to other methods of determination of the kinematic variables, although the relations between the measured kinematic variables and those of the hard scattering process differ.

Finally we would like to mention that the neglect of photon emission off the hadrons in the above discussion is not a problem. We shall argue in section 3.6 that initial state radiation can be absorbed into the evolution of the parton distributions, while final state radiation off hadrons does not shift the kinematic variables at all.

3.3 Collinear radiation and tagged photon processes

The measurement of deep inelastic scattering with an exclusive photon can be expected to be a challenging task, as the radiative cross section (3.22) is

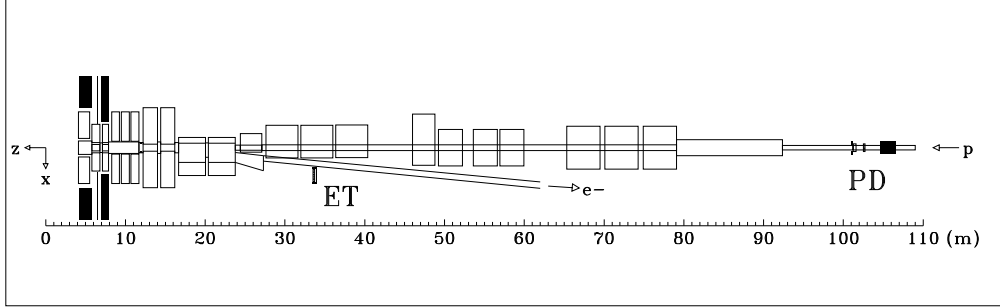


Figure 3.4: Schematic view of the H1 luminosity system. (Taken from [23])

formally suppressed by a factor α/π relative to the non-radiative cross section. We mentioned three regions of photon phase space where the radiative cross section is enhanced and can partially compensate the large suppression. However, only the emission collinear to the incoming electron appears to have been exploited yet.

The main reaction used for the determination of the luminosity at the H1 and ZEUS experiments at the HERA collider is the radiative elastic scattering process $ep \rightarrow ep + \gamma$. For the identification of the emitted photon, both experiments possess a small photon detector (PD) in the very forward direction, see fig. 3.4 for H1 and see fig. 3.5 for ZEUS. The solid angle covered by these photon detectors is roughly described by $0 \leq \vartheta_\gamma \leq \vartheta_0$ about the direction of the initial electron beam, with the maximum angle ϑ_0 being of the order of $(0.45 \dots 0.5)$ mrad for both experiments.

This forward photon detector is an ideal device for tagging radiative deep inelastic scattering events. Since the maximum angle ϑ_0 is small compared to the scattering angle of the electron θ that is measured in the main detector, the differential cross section for these radiative events factorizes exactly. Assuming azimuthal symmetry, integrating the Compton tensor over the solid angle covered by the photon detector yields:

$$\begin{aligned} \frac{E_e^2}{\pi} \int_{\text{PD}} d\Omega_\gamma K_{\mu\nu} &= \left[\frac{1+z^2}{1-z} \ln \left(1 + \frac{E_e^2 \vartheta_0^2}{m^2} \right) - \frac{2z}{1-z} \left(1 + \frac{m^2}{E_e^2 \vartheta_0^2} \right)^{-1} \right] \\ &\times \frac{1}{z} \left(-Q_l^2 \tilde{g}_{\mu\nu} + 4z \tilde{p}_\mu \tilde{p}_\nu \right) + \mathcal{O}(\vartheta_0^2) . \end{aligned} \quad (3.70)$$

The tensor structure in the last line is proportional to the non-radiative lepton tensor (2.17):

$$\frac{1}{z(1-z)} L_{\mu\nu}(zp, p') . \quad (3.71)$$

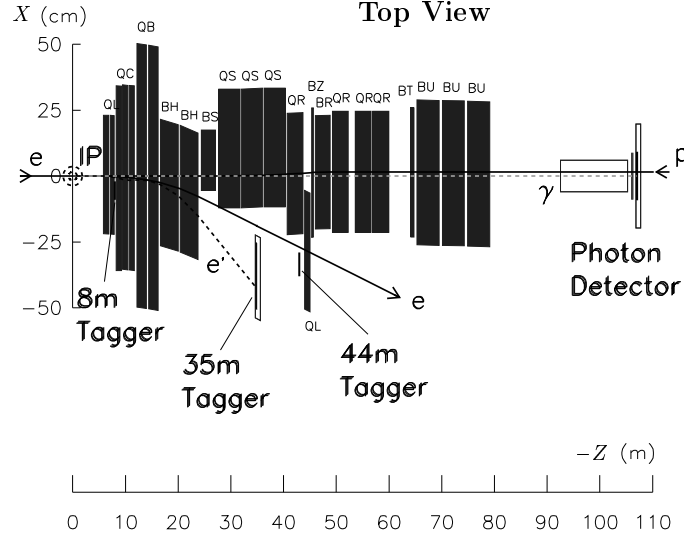


Figure 3.5: General layout of the ZEUS luminosity monitor. (From [20])

We therefore find:

$$\begin{aligned} \frac{d^3\sigma}{dx_l dy_l dz} &= \frac{1}{z} d\sigma^{\text{Born}}(x_h, y_h, Q_h^2) \\ &\times \frac{\alpha}{2\pi} \left[\frac{1+z^2}{1-z} \ln \left(1 + \frac{E_e^2 \vartheta_0^2}{m^2} \right) - \frac{2z}{1-z} \left(1 + \frac{m^2}{E_e^2 \vartheta_0^2} \right)^{-1} \right]. \end{aligned} \quad (3.72)$$

Inserting the conditions at HERA, we find for $E_e = 27.5$ GeV and $\vartheta_0 = (0.45 \dots 0.5)$ mrad:

$$\zeta_0 := \frac{E_e^2 \vartheta_0^2}{m^2} \simeq (6 - 7) \cdot 10^2 \gg 1, \quad (3.73)$$

thus $\zeta_0 \gg 1$ even if $\vartheta_0 \ll 1$. Neglecting terms of order $\mathcal{O}(\zeta_0^{-1})$ and $\mathcal{O}(\vartheta_0)$, the cross section (3.72) simplifies to:

$$\frac{d^3\sigma}{dx_l dy_l dz} = \frac{\alpha}{2\pi} P(z, L_0) \cdot \frac{d^2\sigma^{\text{Born}}(x_h, y_h/z, Q_h^2)}{dx_h d(y_h/z)}, \quad (3.74)$$

where we have introduced

$$P(z, L_0) = \frac{1+z^2}{1-z} L_0 - \frac{2z}{1-z}, \quad L_0 = \ln \zeta_0. \quad (3.75)$$

Evaluating the “large logarithm” L_0 for the HERA forward photon detectors we obtain:

$$L_0 \approx 6.5. \quad (3.76)$$

The cross section (3.74) becomes even simpler when we interpret the emission of the photon as a reduction of the electron energy, $E_e^{\text{eff}} = zE_e$. The energy fraction z can be invariantly written as:

$$z = \frac{2P \cdot (p - k)}{S} . \quad (3.77)$$

Furthermore we choose the following set of invariant kinematic variables that use the scattered electron and take into account the energy loss due to photon emission [18]:

$$\hat{Q}^2 = -(p - p' - k)^2 , \quad \hat{x} = \frac{\hat{Q}^2}{2P \cdot (p - p' - k)} , \quad \hat{y} = \frac{P \cdot (p - p' - k)}{P \cdot (p - k)} . \quad (3.78)$$

Obviously,

$$\hat{Q}^2 = \hat{x}\hat{y}zS . \quad (3.79)$$

The physical range of the shifted Bjorken variables reads:

$$0 \leq \hat{x}, \hat{y} \leq 1 . \quad (3.80)$$

The shifted variables (3.78) are related to the standard Bjorken variables via:

$$\hat{Q}^2 = zQ_l^2 , \quad \hat{x} = \frac{x_l y_l z}{y_l + z - 1} , \quad \hat{y} = \frac{y_l + z - 1}{z} , \quad (3.81)$$

and with the Jacobian for the variable transformation:

$$\left| \frac{\partial(\hat{x}, \hat{y})}{\partial(x_l, y_l)} \right| = \frac{y_l}{y_l + z - 1} = \frac{y_l}{z\hat{y}} . \quad (3.82)$$

In terms of shifted variables, the radiative cross section (3.74) assumes a very simple, suggestive form,

$$\frac{d^3\sigma}{d\hat{x} d\hat{y} dz} = \frac{\alpha}{2\pi} P(z, L_0) \frac{d^2\sigma_{\text{Born}}}{d\hat{x} d\hat{y}} . \quad (3.83)$$

The differential Born cross section on the r.h.s. is a function of the shifted variables (3.81) only. For S , \hat{x} and \hat{Q}^2 fixed, the variable $\hat{y} = \hat{Q}^2/(\hat{x}zS)$ can still be varied through its dependence (3.77) on the tagged photon energy. Thus a measurement of cross section (3.83) for different z can be used to separate F_2 and F_L at fixed center of mass energy [18], see also (2.25). Furthermore, from (3.81) it is obvious that smaller values of \hat{Q}^2 can be attained for fixed energy and angle of the scattered electron than for the non-radiative measurement.

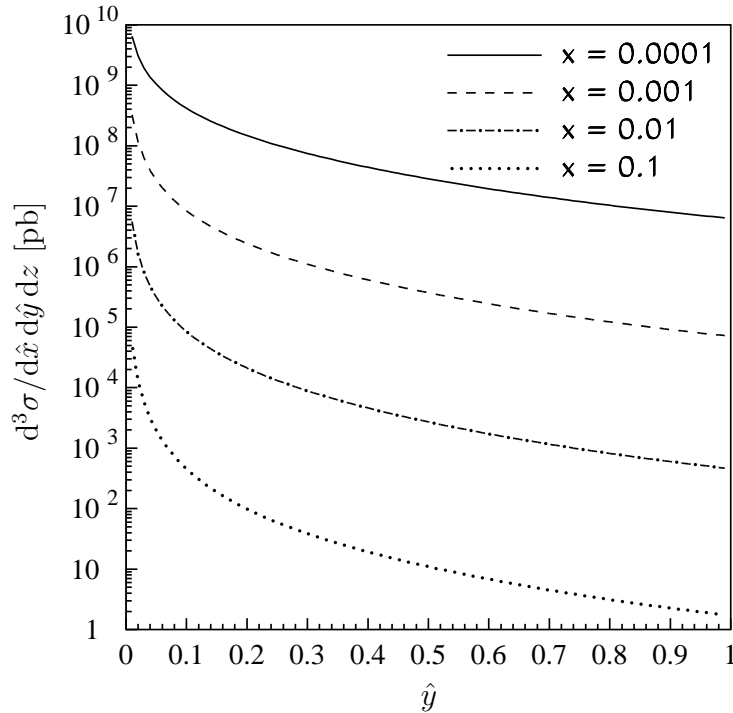


Figure 3.6: The lowest order radiative cross section (3.83) for $E_\gamma = 10$ GeV.

To give an impression of the radiative cross section, we show in figure 3.6 the differential cross section (3.83) for a tagged photon energy of $E_\gamma = 10$ GeV. As parameters we used

$$E_e = 27.5 \text{ GeV} , \quad E_p = 820 \text{ GeV} , \quad \vartheta_0 = 0.5 \text{ mrad} , \quad (3.84)$$

the ALLM97 [71] parameterization of the proton structure function F_2 , and for simplicity a fixed value $R = 0.3$. Similar results are obtained using modern structure functions from PDFLIB [56]. However, varying R in the range allowed by experimental data (see e.g., [96]) or suggested by models (see e.g., [58]) can lead to a sizable variation of the cross section for large \hat{y} .

For later convenience we shall also introduce here the quantity $\tilde{\Sigma}$ which is related to the lowest order cross section as follows:

$$\tilde{\Sigma}(\hat{x}, \hat{y}, \hat{Q}^2) = \frac{1}{\hat{y}} \frac{d^2 \sigma_{\text{Born}}}{d\hat{x} d\hat{y}} . \quad (3.85)$$

so that, together with (3.82):

$$\frac{z}{y_l} \frac{d^3\sigma}{dx_l dy_l dz} = \frac{1}{\hat{y}} \frac{d^3\sigma}{d\hat{x} d\hat{y} dz} = \frac{\alpha}{2\pi} P(z, L_0) \tilde{\Sigma}(\hat{x}, \hat{y}, \hat{Q}^2) . \quad (3.86)$$

3.4 The general radiative DIS process

In the kinematic region of high momentum transfers $Q^2 \gtrsim M_Z^2$, which are attainable at HERA, not only photon but also Z exchange have to be taken into account. The calculations of section 3.2 can be generalized by reconsidering the Compton tensor (3.7) and replacing the virtual photon by a left-handed vector current and contracting it with the generalized hadron tensor. The result is simply a replacement of (3.19):

$$K_{\mu\nu} H^{\mu\nu} \rightarrow 8\pi [S_1 \mathcal{F}_1(x_h, Q_h^2) + S_2 \mathcal{F}_2(x_h, Q_h^2) + S_3 \mathcal{F}_3(x_h, Q_h^2)] . \quad (3.87)$$

The \mathcal{F}_i are the generalized structure functions (2.52), $S_{1,2}$ are identical with (3.20), and [29]:

$$\begin{aligned} S_3 &= \frac{x_h S}{\hat{s}\hat{t}} (q^2 + \hat{u} - y_l(q^2 - \hat{t})) + \frac{q^2 + \hat{u}}{2} \left(\frac{1}{\hat{t}} - \frac{1}{\hat{s}} \right) \\ &+ \frac{m^2}{\hat{t}^2} (q^2 - 2(1 - y_l)x_h S) - \frac{m^2}{\hat{s}^2} (q^2 + 2x_h S) . \end{aligned} \quad (3.88)$$

Taking over the derivation of the differential cross section (3.14), we obtain:

$$d^5\sigma = \frac{2\alpha^3}{\pi} \frac{y_l}{Q_h^4} \left(\sum_i S_i \mathcal{F}_i \right) dx_l dy_l E_\gamma dE_\gamma d\Omega_\gamma . \quad (3.89)$$

This cross section exhibits the same peaking behavior as discussed above. For example, in the region of collinear initial state radiation we use the approximations (3.42) for $S_{1,2}$, along with

$$S_3 \simeq \left[x_h S - \frac{Q_h^2}{2z} \right] \left(\frac{1 + z^2}{1 - z} \frac{1}{(-\hat{t})} - 2z \frac{m^2}{\hat{t}^2} \right) .$$

Consequently, the tagged photon cross section at high momentum transfers factorizes:

$$\frac{d^3\sigma_{\text{NC}}}{d\hat{x} d\hat{y} dz} = \frac{\alpha}{2\pi} P(z, L_0) \cdot \frac{d^2\sigma_{\text{NC}}^{\text{Born}}}{d\hat{x} d\hat{y}} (\hat{x}, \hat{y}, \hat{Q}^2) , \quad (3.90)$$

with the neutral current Born cross section (2.26) appearing on the r.h.s.

For $Q^2 \ll M_Z^2$, eq. (3.90) agrees well with (3.83). At large momentum transfers $Q^2 \gtrsim M_Z^2$, where also Z exchange plays a significant rôle, the cross section is rather small, as it is roughly suppressed by a factor α/π relative to the non-radiative cross section, leading to a rather small number of events. Besides, in this region the QCD prediction of \mathcal{F}_L should be reliable, and it is more important to measure \mathcal{F}_3 . This, however, is better achieved by using different lepton charges rather than photon tagging.

The radiative neutral current process can in principle also be used to test the validity of the Standard Model. In [97] the possibility of a measurement of possible anomalous triple gauge boson couplings ($Z\gamma\gamma$, $ZZ\gamma$) was studied. However it was found that the sensitivity achieved at HERA is too small.

3.5 Tagged photons in charged current reactions

Radiative processes with hard photon emission do also occur in charged current reactions. However, the cross section for the non-radiative process $ep \rightarrow \nu X$ is already quite small, and “paying” another factor α/π further reduces it, making it difficult if not impossible to gather sufficient statistics even after the HERA luminosity upgrade. Nevertheless, we shall briefly discuss it here for the sake of completeness. It is worth to mention that in contrast to neutral current processes the doubly differential cross section $d^2\sigma_{CC}/dx dy$ is still a rather flat distribution in y at HERA energies, as the denominator of the W propagator is:

$$Q^2 + M_W^2 = xyS + M_W^2 \sim \mathcal{O}(S) \sim \mathcal{O}(M_W^2) .$$

In the charged current case there are no leptonic variables at our disposal. The only option to determine the kinematics is thus the measurement of the hadron variables Σ_h and $p_{T,h}$, and the energy of the tagged photon. In analogy to the non-radiative Jacquet-Blondel method (2.13) we define shifted hadron variables:

$$\hat{y}_{JB} = \frac{\Sigma_h}{2zE_e} , \quad \hat{Q}_{JB}^2 = \frac{p_{T,h}^2}{1 - \hat{y}_{JB}} , \quad \hat{x}_{JB} = \frac{\hat{Q}_{JB}^2}{\hat{y}_{JB}zS} . \quad (3.91)$$

Their relation to the unshifted variables is:

$$\hat{y}_{JB} = \frac{y_{JB}}{z} , \quad \hat{Q}_{JB}^2 = Q_{JB}^2 \frac{1 - y_{JB}}{1 - y_{JB}/z} , \quad \hat{x}_{JB} = x_{JB} \frac{1 - y_{JB}}{1 - y_{JB}/z} . \quad (3.92)$$

This apparently implies $\hat{Q}_{JB}^2 \geq Q_{JB}^2$, in contrast to $\hat{Q}^2 = zQ_l^2 \leq Q_l^2$ for the lepton method. However, it should be mentioned that this does *not* mean

that one can really access events at higher Q^2 than in the non-radiative case. It only tells us that the kinematic effect of collinear radiation makes radiative events (with untagged photons) *appear* at even lower measured values of Q^2 .

As we have argued at the beginning of the chapter, there is no gauge invariant subset of the Feynman diagrams for single photon emission in the case of charged current processes, and one cannot define leptonic or hadronic corrections. Nevertheless, the leading contribution to the radiative cross section for emission in the forward direction has the same universal structure as in the neutral current case. This may easily be verified by performing an explicit calculation, using a physical gauge for the emitted photon. As we intend to drop all terms at $\mathcal{O}(\vartheta_0^2)$ from the integrated cross section, the only relevant Feynman diagram that needs to be taken into account is the one with emission from the incoming lepton.

Let us choose an axial gauge, defined with the help of an arbitrary light-like four vector c ($c \neq k$, $c^2 = 0$). The sum over photon polarizations then reads

$$\sum_{\lambda=\pm} \epsilon_\mu^*(k, \lambda) \epsilon_\nu(k, \lambda) = -g_{\mu\nu} + \frac{k_\mu c_\nu + k_\nu c_\mu}{k \cdot c} . \quad (3.93)$$

The choice of the vector c is not important as long as we make sure that its direction is far outside the cone around the incoming electron. In the present case it is convenient to take it proportional to the momentum of the outgoing (massless) neutrino, $c = p_\nu$.

An explicit calculation confirms the tagged photon cross section, integrated over the photon polar angle in the range $0 \leq \vartheta \leq \vartheta_0$ and expressed in terms of the shifted variables (3.91):

$$\frac{d^3 \sigma_{CC}}{d\hat{x}_{JB} d\hat{y}_{JB} dz} = \frac{\alpha}{2\pi} P(z, L_0) \cdot \frac{d^2 \sigma_{CC}^{\text{Born}}}{d\hat{x}_{JB} d\hat{y}_{JB}} \left(\hat{x}_{JB}, \hat{y}_{JB}, \hat{Q}_{JB}^2 \right) . \quad (3.94)$$

with $\hat{Q}_{JB}^2 = \hat{x}_{JB} \hat{y}_{JB} z S$. At HERA energies, we may assume that the longitudinal structure function \mathcal{W}_L is small and calculable, being proportional to $\alpha_S(\hat{Q}_{JB}^2)$. A possible benefit of using radiative charged current events, more important than extending the accessible kinematic region, may be an improvement in the separation of the structure functions \mathcal{W}_2 and $x\mathcal{W}_3$, which also depend on the lepton charge, see (2.58). However, considering the small variation of the relative size of the respective coefficients Y_+ and Y_- and the projected integrated luminosity of HERA this appears very difficult.

Non-collinear emission of photons in charged current reactions can also be used to check the $WW\gamma$ vertex of the Standard Model. Helbig and Spiesberger [98] have compared the sensitivity of the reaction $ep \rightarrow \nu\gamma X$ to the W production process at HERA and concluded that it is too small to be

competitive to other determinations. (For constraints from e^+e^- colliders see e.g., [99] but also the comment in [4]).

3.6 Radiation from the hadron

In the above discussions we have put aside the QED corrections from the hadron side. These correction are in practice quite small, despite the small masses of the light quarks, and may be treated perturbatively. We will follow here the reasoning of Kripfganz and Perlt [100].

In calculating the radiative corrections to high energy processes we generally encounter mass singular terms of the type

$$\left[\frac{\alpha}{2\pi} \ln \frac{Q^2}{m^2} \right]^n ,$$

where Q^2 is a typical large invariant and m a mass of any of the external particles. In the case of QCD it has been shown that the mass singularities of this type can be factorized and absorbed into the hadronic structure or fragmentation functions [101]. Performing the factorization at some reference scale Q_0^2 then shifts all logarithms in the small masses into the distributions, and one may expect that the resulting net correction will be typically of order $\alpha/(2\pi) \cdot \ln(Q^2/Q_0^2)$. Therefore, the final result of a perturbative QCD calculation does not involve any large logarithm of a small quark mass.

This procedure can be extended to take into account the inclusive QED corrections to structure functions. Starting from the evolution equations for the parton distributions (2.35), we replace the quark splitting function

$$\begin{aligned} \frac{\alpha_S}{2\pi} P_{qq}(x) &\rightarrow \frac{\alpha_S}{2\pi} P_{qq}^{(1,0)}(x) + \left(\frac{\alpha_S}{2\pi} \right)^2 P_{qq}^{(2,0)}(x) + \dots \\ &+ \frac{\alpha}{2\pi} P_{qq}^{(0,1)}(x) + \frac{\alpha\alpha_S}{(2\pi)^2} P_{qq}^{(1,1)}(x) + \dots \\ &+ \mathcal{O}(\alpha^2) . \end{aligned} \tag{3.95}$$

The first line in (3.95) represents the usual expansion of the splitting function in QCD. The results for the $P_{qq}^{(0,m)}$ can be obtained from the $P_{qq}^{(n,0)}$ by replacing the gluons by photons, i.e., substitution of the group theoretical factors of $SU(3)$ by the corresponding ones of the $U(1)$,

$$C_F \rightarrow 1 , \quad C_A \rightarrow 0 ,$$

and taking into account the quark electric charges. Note that the leading logarithmic contributions $P_{qq}^{(1,0)}$ and $P_{qq}^{(0,1)}$ are proportional,

$$P_{qq}^{(0,1)} = \frac{3Q_q^2}{4} P_{qq}^{(1,0)} .$$

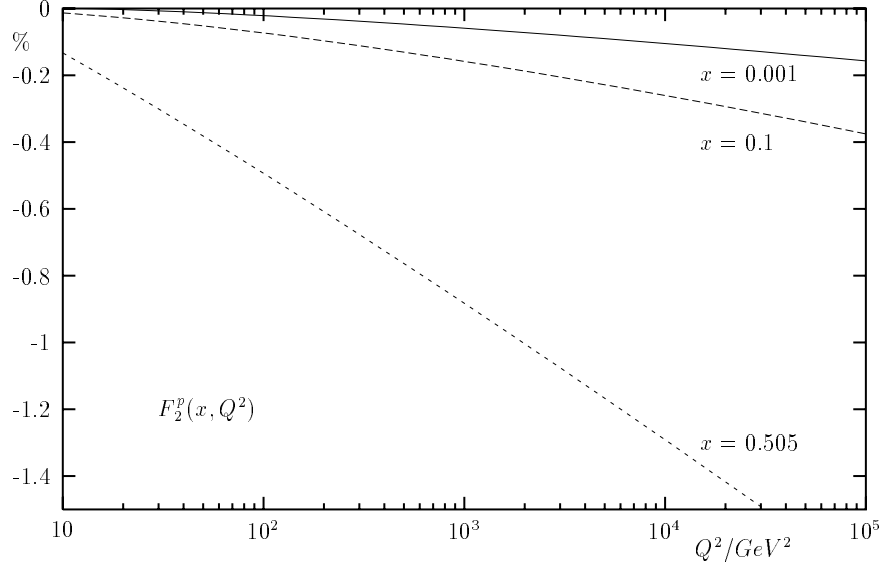


Figure 3.7: Q^2 dependence of the QED corrections to the structure function F_2^p for deep inelastic lepton-proton scattering at $x = 0.001$, $x = 0.1$ and $x = 0.505$ in percent. (Taken from [102]).

As long as we are only interested in the leading order QED correction to the quark distributions, we expand them in powers of α ,

$$q(x, Q^2) = q^{(0)}(x, Q^2) + \frac{\alpha}{2\pi} q^{(1)}(x, Q^2) + \dots, \quad (3.96)$$

$$g(x, Q^2) = g^{(0)}(x, Q^2) + \frac{\alpha}{2\pi} g^{(1)}(x, Q^2) + \dots, \quad (3.97)$$

where the upper index (0) denotes the pure QCD evolved parton distributions, and (1) the $\mathcal{O}(\alpha)$ correction. To this order we may take α fixed; any Q^2 -dependence is then shifted to order α^2 . Kripfganz and Perl explicitly demonstrate in [100] that the $\mathcal{O}(\alpha)$ correction $q^{(1)}, g^{(1)}$ obtained from the solution to the generalized DGLAP equations with (3.95) do not contain logarithms in the fermion mass.

The QED corrections to parton distributions have also been studied in [102]. Although depending on the input parton distributions, the corrections to structure functions in general stay at the per mille level, except for $x \rightarrow 1$ where they may reach of the order of 1 percent. A typical result for the structure function F_2 is shown in fig. 3.7

Photon radiation from hadrons at large angles w.r.t. the hadron is small and calculable within perturbative QCD. For the tagged photon process discussed above, its contribution is $\mathcal{O}(\vartheta_0^2)$ and thus negligible.

Chapter 4

QED Corrections to Radiative Scattering

From the viewpoint of perturbation theory, the radiative cross sections discussed in the previous chapter are interesting hybrids. On one hand, these radiative processes are already contained in the radiative corrections to the deep inelastic scattering process as part of the hard photon corrections. On the other hand, they correspond to the Born approximation for the scattering process with the given number of detected particles which is “DIS plus one exclusive photon”. For a precise description of the cross sections, radiative corrections to these processes need to be considered. Due to the abovementioned relation the corrections to radiative processes are necessarily part of the higher order corrections to non-radiative processes.

This chapter is devoted to a calculation of the QED corrections to the tagged photon process at the next order in perturbation theory. Note that they are of order $\mathcal{O}(\alpha)$ relative to the radiative process, but of order $\mathcal{O}(\alpha^2)$ relative to the non-radiative DIS process. Since the QED corrections are dominated by large logarithms in the electron mass, we start with a discussion of these corrections in a simplified framework by focusing just on the leading logarithmic terms [30]. We then illustrate the influence of the choice of reconstruction method of the kinematic variables on the size of the corrections. The qualitative features of the corrections turn out to be similar to those in the case of non-radiative DIS.

We will not repeat here the calculation of the subset of next-to-leading logarithms which were presented in [31, 32] for leptonic variables and in [33] for the Σ variables, but explain in some detail the full calculation of the model-independent $\mathcal{O}(\alpha)$ corrections by the present author [34]. A systematic approach to QED corrections taking into account the leading logarithms at all orders follows in the next chapter. Our restriction to the corrections

to the tagged photon process excludes the consideration of e^+e^- pair production corrections in DIS ([103], but see also [104] and references) which at this order do not contribute. Furthermore, we will not discuss here the QED corrections to the QED Compton process but refer the reader to [88, 89, 90].

4.1 Radiative corrections in the leading logarithmic approximation

As discussed in the previous chapter, there are two potential sources of large corrections to the cross section that contribute terms of the order of $\alpha/\pi \cdot \ln(Q^2/m_f^2)$, with m_f being the mass of a light fermion. The first one are the vacuum polarization corrections to the propagator of the exchanged boson between the electron and the hadronic system, which we assume to be taken into account and resummed using renormalized (running) couplings. The other source of large corrections is the radiation of photons off light fermions.

Following [30], we shall suppose a calorimetric experimental setup, where a hard photon radiated collinearly to the outgoing electron line cannot be distinguished from a bare outgoing electron, so that final state radiation can be neglected to the desired accuracy. We also assume some minimum lower cut on the transverse momentum of the outgoing hadronic system, in order to suppress the contribution from QED Compton events for a leptonic measurement of the kinematic variables. Therefore, the only large corrections we explicitly need to consider below originate from the radiation of photons off the incoming electron. We will treat these in the so-called structure function formalism.

4.1.1 Structure function formalism

In the structure function formalism for QED [105, 106, 107], a radiatively corrected inclusive cross section is written as a convolution of the electron non-singlet structure function $D^{\text{NS}}(z, Q^2)$ with the Born cross section σ_0 for the hard scattering process taken at reduced center of mass energy. Schematically,

$$\sigma_{\text{RC}}(s) = \int dz D^{\text{NS}}(z, Q^2) \sigma_0(zs; Q^2) , \quad (4.1)$$

with Q^2 being some typical large scale of the hard process. The electron non-singlet structure function,

$$D^{\text{NS}}(z, Q^2) = \delta(1-z) + \frac{\alpha L}{2\pi} P^{(1)}(z) + \frac{1}{2!} \left(\frac{\alpha L}{2\pi} \right)^2 P^{(2)}(z) + \mathcal{O}((\alpha L)^3) , \quad (4.2)$$

which is a QED analog of the parton distributions in QCD, depends on the large scale Q^2 only via the large logarithm $L = \ln(Q^2/m_e^2)$. It is known to properly sum the leading logarithmic contributions $(\alpha L)^n$ to all orders in perturbation theory [107].

For our purposes we need here the first two coefficients of the power series expansion (4.2) of D^{NS} . Introducing a small auxiliary parameter ϵ that serves as an infrared (IR) regulator to separate virtual and soft from hard photon contributions, these two coefficients read:

$$P^{(1,2)}(z) = P_\delta^{(1,2)} \cdot \delta(1-z) + P_\Theta^{(1,2)}(z) \cdot \Theta(1-\epsilon-z),$$

with

$$P_\Theta^{(1)}(z) = \frac{1+z^2}{1-z}, \quad P_\delta^{(1)} = 2 \ln \epsilon + \frac{3}{2}, \quad (4.3)$$

and similarly (see e.g. [107]),

$$\begin{aligned} P_\Theta^{(2)}(z) &= \int_{z/(1-\epsilon)}^{1-\epsilon} \frac{dt}{t} P_\Theta^{(1)}(t) P_\Theta^{(1)}\left(\frac{z}{t}\right) + 2P_\delta^{(1)} P_\Theta^{(1)}(z) \\ &= 2 \left[\frac{1+z^2}{1-z} \left(2 \ln(1-z) - \ln z + \frac{3}{2} \right) + \frac{1+z}{2} \ln z - 1 + z \right]. \end{aligned} \quad (4.4)$$

Inspecting the lowest order tagged photon cross section (3.83),

$$\frac{d^3\sigma_{\text{lo}}}{d\hat{x} d\hat{y} dz} = \frac{\alpha}{2\pi} P(z, L_0) \frac{d^2\sigma_{\text{Born}}}{d\hat{x} d\hat{y}},$$

and comparing with the $\mathcal{O}(\alpha)$ contribution in the integrand to the inclusive cross section (4.1), we conclude that the logarithmic piece of $P(z, L_0)$ is indeed contained in the first order correction; the difference in the logarithms $(L - L_0)$ is accounted for by the cross section for photons emitted at angles larger than ϑ_0 .

4.1.2 Leading logarithms at the next order

Let us now turn to the contributions to the cross section at order $\mathcal{O}(\alpha^2)$ [30]. The typical maximum emission angle ϑ_0 is about $(0.45 \dots 0.5)$ mrad for the HERA photon detectors. The logarithm L_0 appearing in (3.83) is moderately large, $L_0 \simeq 6.5$, see (3.76). The complement

$$L_1 \equiv L - L_0 \approx 6 \dots 16 \gg 1 \quad (\text{for e.g., } Q^2 = 0.1 \dots 1000 \text{ GeV}^2)$$

is of similar magnitude or even larger than L_0 . Starting at this order we thus have two competing large logarithms L_0, L_1 . As a consequence, in the leading

logarithmic approach at $\mathcal{O}(\alpha^2)$ we need to consider all double logarithms of the type $\alpha^2 L_0^2$, $\alpha^2 L_0 L_1$. There cannot be terms $\alpha^2 L_1^2$ since we require at least one tagged photon.

The corrections receive contributions from virtual corrections to collinear emission, one collinear plus one soft photon, two collinear photons, and one collinear plus one non-collinear photon. Since the logarithmic contribution from the non-collinear photon arises mainly from emission at small angles outside the photon detector, we shall also denote it as a semi-collinear one.

The sum of the contributions of virtual and soft corrections to collinear photon emission, with the emission angle of the soft photon being integrated over the full solid angle, but the hard photon only over the solid angle of the PD, can be obtained from the expression for the one-loop Compton tensor. The logarithmic part reads [84]:

$$\left(\frac{\alpha}{2\pi}\right)^2 L_0 \left[(L_0 + L_1) P_\delta^{(1)} - (L_0 + 2L_1) \ln z \right] P_\Theta^{(1)}(z) \cdot \sigma_0(\hat{x}, \hat{y}, z) . \quad (4.5)$$

For the double collinear contribution we assume that only the sum of the energies of photons in the PD is measured. In this case $z = 1 - (\sum_i E_\gamma^{(i)})/E_e$. The contribution from two hard photons in the PD, with the energy fraction of each being larger than ϵ , then yields [108]:

$$\left(\frac{\alpha}{2\pi}\right)^2 \frac{L_0^2}{2} \left[P_\Theta^{(2)}(z) - 2P_\Theta^{(1)}(z) \left(P_\delta^{(1)} - \ln z \right) \right] \cdot \sigma_0(\hat{x}, \hat{y}, z) , \quad (4.6)$$

see also (4.4).

The final contribution is associated with one collinear photon hitting the PD and the other one being emitted at an angle larger than ϑ_0 . Let us try to understand the origin of the large logarithms in this case. For the hard photon that hits the PD, the major contribution comes from the region of polar angles $\vartheta_\gamma^{(1)} \approx m_e/E_e \ll \vartheta_0$. Similarly, for the other photon the biggest contribution comes from polar angles close to the lower limit, $\vartheta_\gamma^{(2)} \gtrsim \vartheta_0$. Thus, the leading contributions come essentially from the region where we have strong ordering in angles, $(\vartheta_\gamma^{(2)}/\vartheta_\gamma^{(1)})^2 \approx \zeta_0 \gg 1$. One can easily see by an explicit calculation that one obtains the double logarithms entirely from the contribution where the photon hitting the PD is emitted first and the “lost” photon is emitted second, while the reversed case is suppressed as long as the following condition is satisfied:

$$x_2 \cdot \zeta_0 \gg 1 , \quad \text{where } x_2 = \frac{E_\gamma^{(2)}}{E_e} . \quad (4.7)$$

The contributions from regions where condition (4.7) is not met are subleading. Thus we shall assume in the following $\epsilon \ll 1$, but $\epsilon \cdot \zeta_0 \gg 1$.

Taking the ordering of photon emissions into account, we calculate the contribution from one tagged plus one undetected photon using the quasireal electron method [109],

$$\left(\frac{\alpha}{2\pi}\right)^2 L_0 L_1 \cdot P_\Theta^{(1)}(z) \int_\epsilon^{x_2^{\max}} \frac{dx_2}{z} P_\Theta^{(1)}\left(1 - \frac{x_2}{z}\right) \tilde{\sigma}_0(\hat{x}, \hat{y}; z - x_2), \quad (4.8)$$

where $\tilde{\sigma}_0$ is understood to be expressed in terms of the “true” kinematic variables x_t, y_t of the hard subprocess,

$$\tilde{\sigma}_0(\hat{x}, \hat{y}; z - x_2) \equiv \sigma_0(x_t, y_t, z - x_2) \cdot \mathcal{J}(\hat{x}, \hat{y}; 1 - x_2/z). \quad (4.9)$$

Note that this contribution explicitly depends on the experimental determination of the kinematic variables \hat{x} and \hat{y} , since the almost collinear emission of the second photon shifts the “true” kinematic variables (x_t, y_t) with respect to the measured ones (\hat{x}, \hat{y}) . The Jacobian

$$\mathcal{J} = \det \left(\frac{\partial(x_t, y_t)}{\partial(\hat{x}, \hat{y})} \right) \quad (4.10)$$

accounts for scaling properties of the chosen kinematic variables under radiation of the second photon. The upper limit of the x_2 -integration in (4.8) is given by either some experimental cut on the maximum energy of the second photon, or by the kinematic limit, which also depends on the choice of the reconstruction method.

After a change of variables, $x_2 = zu$, $u_0 = x_2^{\max}/z$, the integral in (4.8) may be conveniently decomposed into IR divergent (ϵ dependent) and IR convergent contributions as (suppressing the arguments \hat{x}, \hat{y}):

$$\begin{aligned} & \int_\epsilon^{x_2^{\max}} \frac{dx_2}{z} P_\Theta^{(1)}\left(1 - \frac{x_2}{z}\right) \tilde{\sigma}_0(z - x_2) = \\ &= \int_{\epsilon/z}^{u_0} du P_\Theta^{(1)}(1 - u) [(\tilde{\sigma}_0(z(1 - u)) - \tilde{\sigma}_0(z)) + \tilde{\sigma}_0(z)] \\ &= \sigma_0(z) \cdot \left[\int_0^{u_0} du P_\Theta^{(1)}(1 - u) \left(\frac{\tilde{\sigma}_0(z(1 - u))}{\tilde{\sigma}_0(z)} - 1 \right) \right. \\ & \quad \left. + 2 \ln z - P_\delta^{(1)} - \int_{u_0}^1 du P_\Theta^{(1)}(1 - u) \right], \end{aligned} \quad (4.11)$$

where in the last step we have extended the u -integration of the IR convergent piece to 0 due to the smallness of ϵ , and we have used the property

$$\int_0^1 du P^{(1)}(u) = 0$$

Method	Q_t^2	x_t	y_t	z'_{\min}	$\mathcal{J}(\hat{x}, \hat{y}; z')$
lepton	$z' \hat{Q}^2$	$\frac{\hat{x} \hat{y} z'}{\hat{y} + z' - 1}$	$\frac{\hat{y} + z' - 1}{z'}$	$\frac{1 - \hat{y}}{1 - \hat{x} \hat{y}}$	$\frac{\hat{y}}{\hat{y} + z' - 1}$
JB	$\frac{1 - \hat{y}_{\text{JB}}}{1 - \hat{y}_{\text{JB}}/z'} \hat{Q}_{\text{JB}}^2$	$\frac{1 - \hat{y}_{\text{JB}}}{1 - \hat{y}_{\text{JB}}/z'} \hat{x}_{\text{JB}}$	$\frac{\hat{y}_{\text{JB}}}{z'}$	$\frac{\hat{y}_{\text{JB}}}{1 - \hat{x}_{\text{JB}}(1 - \hat{y}_{\text{JB}})}$	$\frac{1 - \hat{y}_{\text{JB}}}{z' - \hat{y}_{\text{JB}}}$
Σ	\hat{Q}_{Σ}^2	$\frac{\hat{x}_{\Sigma}}{z'}$	\hat{y}_{Σ}	\hat{x}_{Σ}	$\frac{1}{z'}$

Table 4.1: Scaling properties of the kinematic variables under initial state radiation for different experimental methods of their determination.

in the simplification of the IR divergent piece.

Adding up the contributions (4.5), (4.6), and (4.8), we see that the dependence on the auxiliary parameter ϵ cancels, as it should.

4.1.3 The radiatively corrected cross section

We are now able to write down the result for the leading logarithmic radiative corrections. The correction δ_{RC} is defined via:

$$\frac{d^3\sigma_{\text{RC}}}{d\hat{x} d\hat{y} dz} = \frac{d^3\sigma_{\text{lo}}}{d\hat{x} d\hat{y} dz} \cdot (1 + \delta_{\text{RC}}(\hat{x}, \hat{y}, z)) . \quad (4.12)$$

Since we restricted ourselves to the leading logarithms, we must retain in the correction factor $(1 + \delta_{\text{RC}})$ only the logarithmic terms L_0, L_1 from (4.5), (4.6), and (4.8). We thus obtain:¹

$$\begin{aligned} \delta_{\text{RC}} &= \frac{\alpha L_0}{4\pi} \frac{1 - z}{1 + z^2} P_{\Theta}^{(2)}(z) \\ &+ \frac{\alpha L_1}{2\pi} \left[\int_0^{u_0} du P_{\Theta}^{(1)}(1 - u) \left(\frac{\tilde{\sigma}_0(z(1 - u))}{\tilde{\sigma}_0(z)} - 1 \right) \right. \\ &\left. - \int_{u_0}^1 du P^{(1)}(1 - u) \right] . \end{aligned} \quad (4.13)$$

Remember that the contribution from the undetected hard photon depends on the choice of kinematic variables and on the upper limit u_0 .

¹In contrast to [30] we do not count here the contribution from vacuum polarization as part of the radiative corrections, as it is contained in the leading order tagged photon cross section $d^3\sigma_{\text{lo}}/d\hat{x} d\hat{y} dz$.

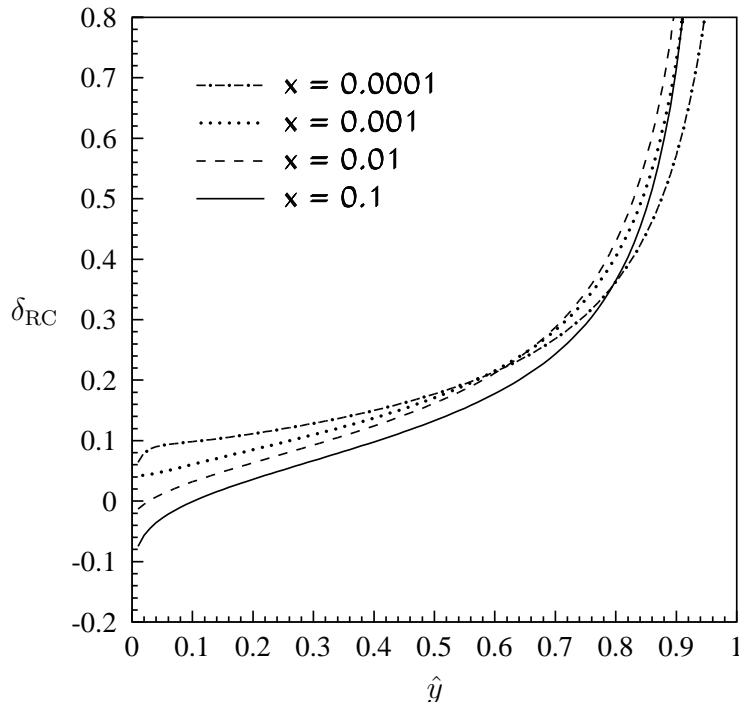


Figure 4.1: The leading logarithmic radiative corrections to the tagged photon cross section for $E_\gamma = 10$ GeV. Lepton method.

4.1.4 Numerical results

To give an impression of the significance of the radiative corrections at leading logarithmic accuracy as given by eq. (4.13), we shall present some typical numerical results. The relations between the measured and the true kinematic variables in (4.9) for some reconstruction methods are given in table 4.1; they agree with those for the calculation of the leading logarithms from initial state radiation to non-radiative DIS (see e.g., [81, 75]). The variable z' corresponds to $1 - u$ in (4.13), so that $u_0 = 1 - z'_{\min}$.

We use the same set of HERA parameters as in section 3.3, eq. (3.84), the ALLM97 parameterization and a fixed ratio $R = F_L/F_T = 0.3$, unless stated otherwise. As a representative intermediate value for the tagged energy we take $E_\gamma = 10$ GeV. No cut will be applied to the energy of the second (“lost”) photon.

Figure 4.1 shows the radiative correction δ_{RC} (4.13) for the reconstruction of the kinematic variables using the electron method. In the region of very small \hat{y}_l , the radiative corrections may become strongly negative. The contributions from virtual and soft photon corrections dominate, because the

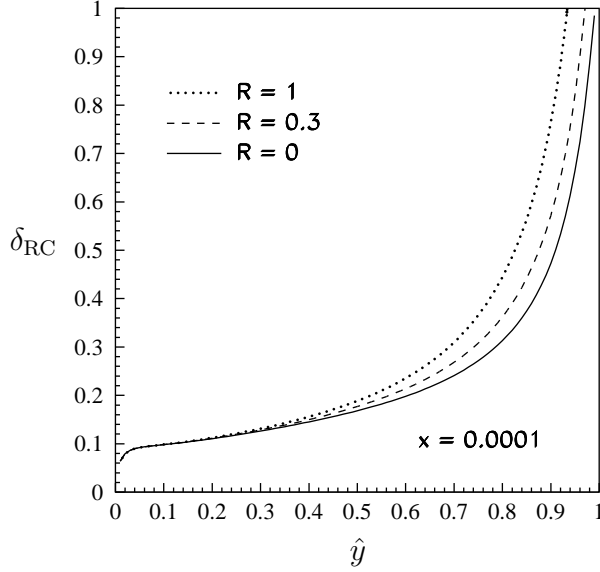


Figure 4.2: R -dependence of the leading logarithmic radiative corrections to the tagged photon cross section for $E_\gamma = 10$ GeV. Lepton method.

kinematic limit on the energy of the undetected photon tends to zero as

$$u_0 = 1 - z'_{\min} = \frac{\hat{y}_l(1 - \hat{x}_l)}{1 - \hat{x}_l\hat{y}_l} . \quad (4.14)$$

For $\hat{y}_l \rightarrow 1$, the phase space for photon emission increases, and we find the typical strong rise of the corrections, which is due to the large shift between the “true” and the measured the kinematic variables under hard photon radiation as discussed in section 3.2.3, and due to the steep dependence of the lowest order neutral current cross section for small \hat{y} , resp. \hat{Q}^2 .

The radiative corrections for the electron method exhibit a very strong dependence on the ratio $R = F_L/F_T$, see fig. 4.2. Again, this effect is largest for large \hat{y} . Increasing R increases the correction, mainly because it reduces the hard cross section σ_0 for $\hat{y} \rightarrow 1$, while hard collinear radiation probes $x_t > \hat{x}$, $y_t < \hat{y}$. This strong dependence of the radiative corrections on a quantity (here: R) poorly known in other regions of phase space is a nice example of the kinematic effects we discussed in section 3.2.3.

Figure 4.3a shows the leading logarithmic radiative corrections for the Jacquet-Blondel method, again for a tagged photon energy of 10 GeV. In this case the corrections are negative for $\hat{y} \rightarrow 1$, because in this limit the phase space for the undetected photon tends to zero,

$$u_0 = 1 - z'_{\min} = \frac{(1 - \hat{x}_{\text{JB}})(1 - \hat{y}_{\text{JB}})}{1 - \hat{x}_{\text{JB}}(1 - \hat{y}_{\text{JB}})} , \quad (4.15)$$

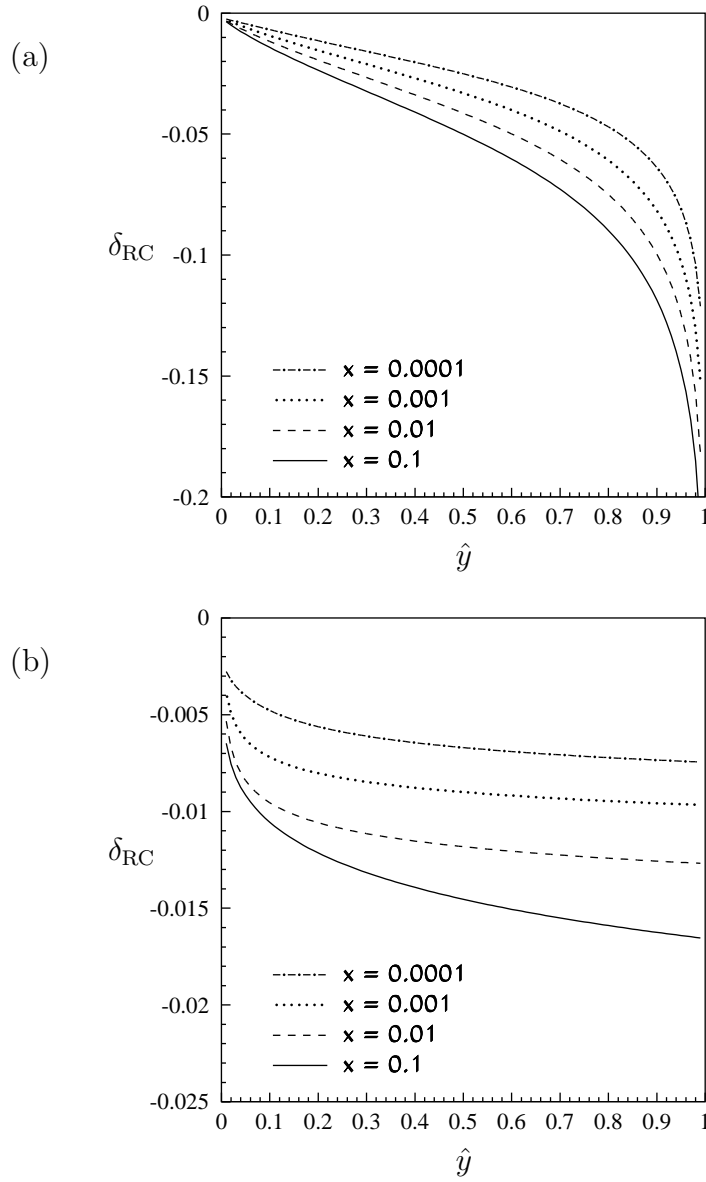


Figure 4.3: Leading logarithmic radiative corrections to the tagged photon cross section for $E_\gamma = 10$ GeV: (a) Jacquet-Blondel method, (b) Σ method.

whereas for small \hat{y}_{JB} the corrections remain moderate. Since the Jacquet-Blondel variables correspond to a “more inclusive” measurement than the leptonic variables, the corrections due to radiation of an additional photon are generally smaller.

Finally, figure 4.3b displays the corresponding results for the Σ method. Here the corrections are surprisingly small. This apparent suppression is easily traced back to the weak dependence on initial state radiation of the reconstruction of the kinematic variables using the Σ method, see table 4.1. At the same time the R -dependence is negligible [33].

4.2 Complete leptonic corrections

As explained in the previous chapter, the subset of leptonic QED corrections to deep inelastic scattering is gauge invariant. Assuming one-photon exchange it also factorizes, thus allowing a discussion isolated from the hadronic part. In the present section, we shall therefore consider the complete set of QED corrections to the Compton subprocess

$$e(p_1) + \gamma^*(-q) \rightarrow e(p_2) + \gamma(k) , \quad (4.16)$$

with the emission angle of the photon being integrated over the PD, while taking into account the corrections from virtual and real QED corrections. While performing this integration, we require that the remaining part of the amplitude of the full process, $\mathcal{M}(\gamma^* + p \rightarrow X)$, depends only weakly on the transverse recoil momentum of the forward photon. This implies the condition $p_1 \cdot k \ll p_1 \cdot p_2$, i.e., $\vartheta_0 \ll \theta$.

The presentation below follows the outline given in [34], but provides more details.

4.2.1 Compton tensor

We start our calculation with the Compton tensor $K_{\mu\nu}$ as defined in (3.7). For the discussion of the radiative corrections to this tensor we write its decomposition up to and including 1-loop contributions as follows [84]:

$$\begin{aligned} K_{\mu\nu}^{1\text{-loop}} &= \frac{1}{2} (P_{\mu\nu} + P_{\nu\mu}^*) , \\ P_{\mu\nu} &= \tilde{g}_{\mu\nu} \left(B_g + \frac{\alpha}{2\pi} T_g \right) + \sum_{i,j=1,2} \tilde{p}_{i\mu} \tilde{p}_{j\nu} \left(B_{ij} + \frac{\alpha}{2\pi} T_{ij} \right) , \\ \tilde{g}_{\mu\nu} &= g_{\mu\nu} - \frac{q_\mu q_\nu}{q^2} , \quad \tilde{p}_{i\mu} = p_{i\mu} - q_\mu \frac{p_i \cdot q}{q^2} , \quad i = 1, 2 . \end{aligned} \quad (4.17)$$

The expressions for the quantities B_{ij} corresponding to the Born approximation are given in (3.12). The general results for the one-loop QED contributions T_g , T_{ij} in the high energy limit can be found in [84]; they are lengthy and will not be reproduced here.

The next step will be the integration over the solid angle of the photon that is tagged in the forward detector. Since we are interested in the region of almost collinear emission, $k \simeq (1-z)p_1$, we neglect the transverse momentum of the emitted photon in the tensor decomposition (4.17), as it is of order $\mathcal{O}(E_e \vartheta_0)$, and use momentum conservation to set $\tilde{p}_2 = z\tilde{p}_1$. To the same accuracy, the kinematic variables of the Compton subprocess are related to those of the radiative DIS process via:

$$\hat{u} = -\frac{\hat{Q}^2}{z}, \quad q^2 = (p_1 - k - p_2)^2 \simeq -\hat{Q}^2, \quad \hat{s} \simeq \frac{1-z}{z} \hat{Q}^2.$$

4.2.2 Virtual and soft corrections

The virtual corrections to the Compton tensor are furthermore conveniently decomposed into a piece containing the universal infrared singular contributions, which are proportional to the Born contributions, and an infrared finite remainder:

$$T_g = \rho B_g + T'_g, \quad T_{ij} = \rho B_{ij} + T'_{ij}, \quad i, j = 1, 2. \quad (4.18)$$

The precise form of the infrared singular expression ρ depends on the regularization procedure. The calculation of the one-loop contributions in [84] uses a fictitious photon mass λ in the calculation of the virtual corrections and obtains:

$$\rho = 4(L_Q - 1) \ln \frac{\lambda}{m} - L_Q^2 + 3L_Q + 3 \ln z + \frac{\pi^2}{3} - \frac{9}{2}, \quad (4.19)$$

with

$$L_Q = \ln \frac{-\hat{u}}{m^2} = \ln \frac{Q^2}{m^2}. \quad (4.20)$$

The integration of the Compton tensor over the solid angle of the collinear photon is described in some detail in appendix A.1. We quote here only the final result:

$$\begin{aligned} \frac{E_e^2}{\pi} \int d\Omega_k K_{\mu\nu}^{1\text{-loop}} &= (-Q_l^2 \tilde{g}_{\mu\nu} + 4z \tilde{p}_{1\mu} \tilde{p}_{1\nu}) \times \\ &\quad \frac{1}{1-z} \left[\left(1 + \frac{\alpha}{2\pi} \rho \right) P(z, L_0) - \frac{\alpha}{2\pi} T \right] + \mathcal{O}(\vartheta_0^2, \zeta_0^{-1}), \end{aligned} \quad (4.21)$$

where

$$\begin{aligned}
T &= (A \ln z + B)P(z, L_0) + CL_0 + D, \\
A &= 2L_Q - L_0 - 2 \ln(1 - z), \\
B &= \ln^2 z - 2 \text{Li}_2(1 - z) - \frac{1}{2}, \\
C &= -\frac{2z}{1 - z} \ln z - z, \\
D &= -\frac{1 - 6z + 4z^2}{1 - z} (\text{Li}_2(1 - z) + \ln z \ln(1 - z)) \\
&\quad - 2z \ln^2(1 - z) + \frac{8z}{1 - z} \ln z - \frac{4\pi^2}{3} z + 1.
\end{aligned} \tag{4.22}$$

Here

$$\text{Li}_2(x) = - \int_0^x \frac{dy}{y} \ln(1 - y) \tag{4.23}$$

is the Spence function or dilogarithm [110]. The single and double logarithmic terms in L_0 and L_Q of expression (4.22) agree with [32].

The dependence of the virtual corrections on the unphysical parameter λ is canceled by the contribution from emission of an additional soft photon, calculated using the same regularization method. Since soft photon emission factorizes, its contribution is proportional to the Born piece $B_{\mu\nu}$ and can be combined with the ρ -piece of the virtual corrections. Requiring that the energy fraction of the second (soft) photon in units of the energy of the incoming electron does not exceed ϵ , with $\epsilon \ll 1$, and adding the contribution from soft photon emission to the virtual correction then amounts to the replacement of the quantity ρ in (4.21) by $\tilde{\rho}$, see [84]:

$$\tilde{\rho} = 2(L_Q - 1) \ln \frac{\epsilon^2}{Y} + 3L_Q + 3 \ln z - \ln^2 Y - \frac{\pi^2}{3} - \frac{9}{2} + 2 \text{Li}_2 \left(\frac{1 + c}{2} \right), \tag{4.24}$$

with

$$Y = \frac{E'_e}{E_e} \quad \text{and} \quad c \equiv \cos \theta = \cos \angle(\vec{p}, \vec{p}') \tag{4.25}$$

being the relative energy of the scattered electron and the cosine of the scattering angle in the lab system, respectively.

4.2.3 Double hard bremsstrahlung: ISR

Kinematics of the double Compton process

The other contributions to the radiative corrections involve the emission of two hard photons. This part is quite elaborate, as we need to keep the elec-

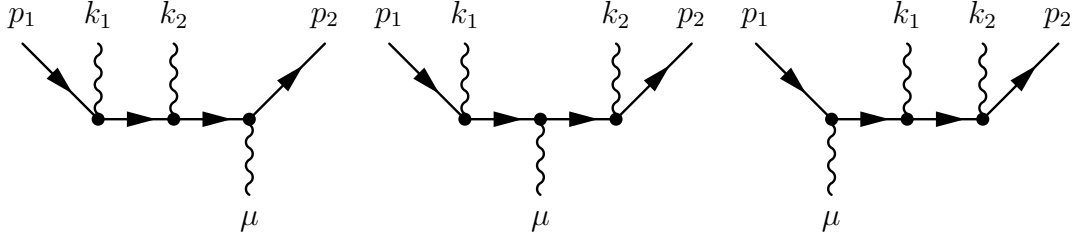


Figure 4.4: Three of the six Feynman diagrams contributing to the double Compton process (4.26). The remaining three diagrams are obtained by exchanging $k_1 \leftrightarrow k_2$.

tron mass different from zero even at high energies. Techniques for the efficient calculation of processes with double photon emission have been developed by the CALKUL collaboration (see [111] and references cited therein). It is however not necessary to deal with the full expressions for our purposes, since we are only interested in the hard photon corrections to the tagged photon cross section. We shall therefore consider the double Compton process of fig. 4.4,

$$e(p_1) + \gamma^*(-q) \rightarrow e(p_2) + \gamma(k_1) + \gamma(k_2) . \quad (4.26)$$

with the implicit assumption that one of the final photons is emitted almost collinearly to the incoming electron. Furthermore, we will keep only those terms that contribute to integrated cross sections at high energy, i.e., for $|(p_1 - p_2)^2|, |q^2| \gg m^2$.

For explicit calculations in the HERA frame the following parameterization of the momenta is convenient:

$$\begin{aligned} p_1 &= (E_e; p_e \vec{e}_z) = E_e \cdot (1; \beta_e \vec{e}_z) , \\ p_2 &= (E'_e; p'_e \vec{n}) = E'_e \cdot (1; \beta'_e \vec{n}) , \quad \vec{n} = (\sin \theta, 0, \cos \theta) , \\ k_i &= x_i E_e \cdot (1; \vec{n}_i) , \quad \vec{n}_i = (\sin \vartheta_i \cos \phi_i, \sin \vartheta_i \sin \phi_i, \cos \vartheta_i) , \quad i = 1, 2 . \end{aligned} \quad (4.27)$$

The $x_i \equiv E_{\gamma,i}/E_e$ are the energy fractions of the photons in units of the electron beam energy.

Instead of the polar angles the photons, ϑ_i , we shall make frequent use of the substitution

$$\tau_i = \frac{1 - \cos \vartheta_i}{2} , \quad (0 \leq \tau_i \leq 1) . \quad (4.28)$$

Collinear emission of photon i obviously corresponds to $\tau_i \rightarrow 0$.

For the kinematic invariants of the Compton subprocess we introduce the notation:

$$z_i = 2p_1 \cdot k_i , \quad z'_i = 2p_2 \cdot k_i ,$$

$$\begin{aligned}
\sigma &= 2k_1 \cdot k_2 = (k_1 + k_2)^2 , \\
\Delta &= -[(p_1 - k_1 - k_2)^2 - m^2] = z_1 + z_2 - \sigma , \\
\Delta' &= [(p_2 + k_1 + k_2)^2 - m^2] = z'_1 + z'_2 + \sigma , \\
Q_l^2 &= -(p_1 - p_2)^2 , \\
Q_h^2 &= -q^2 = Q_l^2 + z_1 + z_2 - z'_1 - z'_2 - \sigma .
\end{aligned}$$

In the kinematic region of interest at least one of the invariants $z_{1,2}$ will be small, i.e., $\mathcal{O}(m^2)$:

$$\begin{aligned}
z_i &= 2p \cdot k_i = 2x_i E_e^2 (1 - \beta_e \cos \vartheta_i) \\
&= 2x_i E_e^2 (1 - \beta_e + 2\beta_e \tau_i) \simeq x_i (m^2 + 4E_e^2 \tau_i) .
\end{aligned} \tag{4.29}$$

In the last line we neglected terms of relative order $\mathcal{O}(m^2/E_e^2)$. Note that also the invariant Δ may become small in the double collinear region, as

$$\begin{aligned}
\sigma &= 2k_1 \cdot k_2 = 2x_1 x_2 E_e^2 (1 - \vec{n}_1 \cdot \vec{n}_2) \\
&= 2x_1 x_2 E_e^2 [1 - \cos \vartheta_1 \cos \vartheta_2 - \sin \vartheta_1 \sin \vartheta_2 \cos(\phi_1 - \phi_2)] \\
&= 4x_1 x_2 E_e^2 \left[\tau_1 + \tau_2 - 2\tau_1 \tau_2 - 2\sqrt{\tau_1 \tau_2 (1 - \tau_1)(1 - \tau_2)} \cos(\phi_1 - \phi_2) \right] .
\end{aligned} \tag{4.30}$$

The kinematic restriction to at least one almost collinear photon allows certain simplifications of the expressions we encounter. To exploit these systematically we used the symbolic manipulation program **FORM** [112].

Double Compton tensor

For the treatment of two photon emission off unpolarized electrons, we normalize the double Compton tensor analogously to (3.7) as [34]²

$$K_{\mu\nu}^{\gamma\gamma} = \frac{1}{(2e^2)^3} \sum_{\text{spins}} M_\mu^{e\gamma^* \rightarrow e'\gamma\gamma} (M_\nu^{e\gamma^* \rightarrow e'\gamma\gamma})^* , \tag{4.31}$$

where now $M_\mu^{e\gamma^* \rightarrow e'\gamma\gamma}$ is the matrix element of the double Compton process (4.26), with the index μ describing the polarization of the virtual photon.

Double collinear emission

When both photons are emitted almost collinearly to the incoming electron, it is convenient to express the photon four-momenta occurring in the numerator of the expression for the double Compton tensor schematically as:

$$k_i = x_i p_1 + k_{i,\perp} . \tag{4.32}$$

²Note that the normalization chosen here differs from [34] by a factor of 1/4 in order to conveniently absorb factors of 4 in other places below.

The components of the transverse parts $k_{i,\perp}$ are typically of the order $\mathcal{O}(m)$ and limited to be smaller than $x_i E_e \vartheta_0$; they can be safely neglected. Similar simplifications can be applied for z'_i , Δ' and Q_h^2 . We will therefore set:

$$\begin{aligned} z'_i &\simeq 2x_i p_1 \cdot p_2 \simeq x_i Q_l^2, \\ \Delta' &\simeq (x_1 + x_2) Q_l^2, \\ Q_h^2 &\simeq (1 - x_1 - x_2) Q_l^2, \\ \tilde{k}_i &\simeq x_i \tilde{p}_1, \end{aligned} \tag{4.33}$$

and by momentum conservation:

$$\tilde{p}_2 \simeq \tilde{p}_1 - \tilde{k}_1 - \tilde{k}_2 = (1 - x_1 - x_2) \tilde{p}_1.$$

The expression for the double Compton tensor simplifies tremendously when we note that in the double collinear region:

$$\frac{z_i}{Q_l^2}, \frac{\Delta}{Q_l^2} \lesssim \mathcal{O}(\vartheta_0^2).$$

Introducing the abbreviations

$$r_1 = 1 - x_1, \quad r_2 = 1 - x_2, \quad z = 1 - x_1 - x_2, \tag{4.34}$$

the double Compton tensor takes a rather compact form:

$$\begin{aligned} K_{\mu\nu}^{2\text{-coll}} &= \left[-\tilde{g}_{\mu\nu} Q_l^2 + 4z (\tilde{p}_{1\mu} \tilde{p}_{1\nu}) \right] \\ &\times \left[\frac{1+z^2}{x_1 x_2} \frac{1}{z_1 z_2} - \frac{z}{\Delta^2} \left(\frac{z_1}{z_2} + \frac{z_2}{z_1} \right) + \frac{1}{x_1 x_2} \left(\frac{r_1^3 + z r_2}{z_1 \Delta} + \frac{r_2^3 + z r_1}{z_2 \Delta} \right) \right. \\ &\quad - 2 \frac{m^2}{\Delta} \left(\frac{r_1^2 + z^2}{x_2 z_1^2} + \frac{r_2^2 + z^2}{x_1 z_2^2} + \frac{(1-z)(r_1 r_2 + z)}{x_1 x_2 z_1 z_2} \right) \\ &\quad \left. - 4z \frac{m^2}{\Delta^2} \left(\frac{1}{z_1} + \frac{1}{z_2} \right) + 4z \frac{m^4}{\Delta^2} \left(\frac{1}{z_1} + \frac{1}{z_2} \right)^2 \right]. \end{aligned} \tag{4.35}$$

This expression is consistent with [108], where leading and next-to-leading logarithms were calculated.

The integration over the photon phase space

We assume that the photon detector measures only the sum of the energies even if the two photons hit in different positions. Taking into account the symmetry factor $1/2!$ for the emitted photons, we need to calculate:

$$\frac{e^4}{4} \cdot \frac{1}{2!} \int_{\text{PD}} \widetilde{\text{d}k_1} \widetilde{\text{d}k_2} \Theta(x_1 - \epsilon) \Theta(x_2 - \epsilon) \delta(x_1 + x_2 - (1 - z)) K_{\mu\nu}^{2\text{-coll}}. \tag{4.36}$$

The infrared cutoff ϵ is necessary to regularize the singularity when either photon becomes soft.

For a general shape of the PD the integrations in (4.36) can only be performed numerically. To proceed analytically we require, in addition to $\vartheta_0 \ll 1$, azimuthal symmetry of the PD. The result obtained then also serves as a useful cross check of a numerical implementation. The integrations over the photons in (4.36) are therefore understood as

$$\int_{\text{PD}} \widetilde{\text{d}k_i} = \frac{1}{(4\pi)^2} \int x_i \text{d}x_i \frac{E_e^2}{\pi} \int \text{d}\Omega_i \Theta(\vartheta_0 - \vartheta_i) , \quad (4.37)$$

with no restriction on the azimuthal integration.

Under these conditions the integrals over the solid angles of the photons can be performed completely. A list of the relevant integrals is given in appendix A.2, along with a description of their calculation.

The remaining integration over the relative photon energies however is very tedious. Nevertheless, one can decompose the result of (4.36) in the following form:

$$\left[-\tilde{g}_{\mu\nu} Q_l^2 + 4z (\tilde{p}_{1\mu} \tilde{p}_{1\nu}) \right] \times \frac{\alpha^2}{8\pi^2} \left[P_{\log}^{(2)}(z) + P_{\text{nonlog}}^{(2),\text{IR-div.}}(z) + P_{\text{nonlog}}^{(2),\text{IR-fin.}}(z) \right] . \quad (4.38)$$

The previously known leading terms containing double and single logarithms L_0 are contained in $P_{\log}^{(2)}(z)$:

$$\begin{aligned} P_{\log}^{(2)}(z) &= \left[-4 \frac{1+z^2}{1-z} \ln \frac{\epsilon}{1-z} + (1+z) \ln z - 2(1-z) \right] L_0^2 \\ &+ \left[6(1-z) + \frac{3+z^2}{1-z} \ln^2 z + 4 \frac{(1+z)^2}{1-z} \ln \frac{\epsilon}{1-z} \right] L_0 \\ &= \left[P_{\Theta}^{(2)}(z) + 2 \frac{1+z^2}{1-z} \left(\ln z - \frac{3}{2} - 2 \ln \epsilon \right) \right] L_0^2 \\ &+ \left[6(1-z) + \frac{3+z^2}{1-z} \ln^2 z + 4 \frac{(1+z)^2}{1-z} \ln \frac{\epsilon}{1-z} \right] L_0 , \end{aligned} \quad (4.39)$$

with the second-order leading-log radiator

$$P_{\Theta}^{(2)}(z) = 2 \left[\frac{1+z^2}{1-z} \left(2 \ln(1-z) - \ln z + \frac{3}{2} \right) + \frac{1}{2} (1+z) \ln z - 1 + z \right] .$$

The nonleading terms are split into an infrared divergent piece that depends on $\ln \epsilon$,

$$P_{\text{nonlog}}^{\text{IR-div.}}(z) = \frac{8z}{1-z} \ln \frac{\epsilon}{1-z} , \quad (4.40)$$

and an infrared finite piece $P_{\text{nonlog}}^{(2),\text{IR-fn.}}(z)$. An outline of the calculation and more information on the last piece are given in appendix A.2.

Inspecting (4.39), (4.40) we find that the terms depending on the soft-photon cutoff parameter ϵ in (4.38) do factor nicely, as expected from the usual soft-photon factorization:

$$\left[-\tilde{g}_{\mu\nu} Q_l^2 + 4z (\tilde{p}_{1\mu} \tilde{p}_{1\nu}) \right] \times \left(\frac{\alpha}{2\pi} \right)^2 P(z, L_0) \cdot 2(L_0 - 1) \ln \frac{1}{\epsilon} . \quad (4.41)$$

4.2.4 Final state collinear radiation

Consider now the kinematic region where one photon is emitted almost collinearly to the incoming electron and the other one close to the outgoing electron. We suppose that the angle between the scattered electron and the second photon is smaller than some angular separation parameter ϑ'_0 , i.e.,

$$\angle(\vec{k}_2, \vec{p}') \leq \vartheta'_0 , \quad \text{with} \quad \vartheta'_0 \ll \theta . \quad (4.42)$$

Without loss of generality we therefore set:

$$k_1 = x_1 p_1 + k_{1,\perp} , \quad k_2 = \frac{\xi}{1-\xi} p_2 + k_{2,\perp} , \quad (4.43)$$

where we again assume that the indicated transverse parts of the photon momenta are small, being typically of the order $\mathcal{O}(m)$, c.f. the discussion of (4.32). These simplifications lead to:

$$\begin{aligned} z'_1 &\simeq x_1 Q_l^2 , & z_2 &\simeq \frac{\xi}{1-\xi} Q_l^2 , \\ \Delta &\simeq (1-x_1) \frac{\xi}{1-\xi} Q_l^2 , \\ \Delta' &\simeq \frac{x_1}{1-\xi} Q_l^2 , \\ Q_h^2 &\simeq \frac{1-x_1}{1-\xi} Q_l^2 \\ \tilde{k}_1 &\simeq x_1 \tilde{p}_1 , & \tilde{k}_2 &\simeq \frac{\xi}{1-\xi} \tilde{p}_2 , \end{aligned} \quad (4.44)$$

and by momentum conservation:

$$\tilde{p}_2 + \tilde{k}_2 = \tilde{p}_1 - \tilde{k}_1 \quad \Rightarrow \quad \tilde{p}_2 \simeq (1-x_1)(1-\xi) \tilde{p}_1 .$$

Furthermore:

$$\frac{z_1}{Q_l^2} \lesssim \mathcal{O}(\vartheta_0^2) , \quad \frac{z'_2}{Q_l^2} \lesssim \mathcal{O}(\vartheta_0'^2) ,$$

and the double Compton tensor considerably simplifies to

$$\begin{aligned}
K_{\mu\nu}^{2\gamma,\text{FSR}} &\simeq \left[-\tilde{g}_{\mu\nu} \frac{Q_l^2}{1-\xi} + 4(1-x_1) \cdot (\tilde{p}_{1\mu} \tilde{p}_{1\nu}) \right] \\
&\times \left[\frac{1+(1-x_1)^2}{x_1} \frac{1}{z_1} - 2(1-x_1) \frac{m^2}{z_1^2} \right] \\
&\times \left[\frac{1+(1-\xi)^2}{\xi} \frac{1}{z_2'} - 2 \frac{m^2}{z_2'^2} \right], \tag{4.45}
\end{aligned}$$

exhibiting a complete factorization of collinear initial and final state radiation, respectively. For the application to the tagged photon process, we have to identify $x_1 = 1 - z$ in the above expressions.

The integration over the photon phase space

Integrating the expression (4.45) for the double Compton tensor over the solid angle of photon 1 at fixed energy we obtain:

$$\begin{aligned}
\frac{E_e^2}{\pi} \int_{\text{PD}} d\Omega_1 K_{\mu\nu}^{2\gamma,\text{FSR}} &= \left[-\tilde{g}_{\mu\nu} \frac{Q_l^2}{1-\xi} + 4(1-x_1) \cdot (\tilde{p}_{1\mu} \tilde{p}_{1\nu}) \right] \times \\
&\frac{1}{x_1} P(1-x_1, L_0) \times \\
&\left[\frac{1+(1-\xi)^2}{\xi} \frac{1}{z_2'} - 2 \frac{m^2}{z_2'^2} \right]. \tag{4.46}
\end{aligned}$$

The corresponding integration over the final state photon depends on the details of the experimental situation, i.e., whether the detector is able to resolve a photon collinear to the electron, or whether it just measures the sum of their energies. We denominated these cases in the discussion in section 3.2.2 as *exclusive* and *calorimetric* measurement, respectively.

Let us consider first the exclusive case, when only p_2 of the scattered electron is measured but the momentum k_2 of the almost collinear photon is missed. The phase space for the second photon can be rewritten as:

$$\int \widetilde{dk}_2 = \frac{1}{(4\pi)^2} \frac{E_e'^2}{\pi} \int \frac{\xi d\xi}{(1-\xi)^3} \int_{\vartheta_2' \leq \vartheta_0'} d\Omega_2', \tag{4.47}$$

with E_e' being the measured energy of the scattered electron and the polar angle ϑ_2' of the photon being measured with respect to the scattered electron.

Performing the integration over the solid angle leads to:

$$\begin{aligned} & \int \widetilde{dk}_2 \left[\frac{1 + (1 - \xi)^2}{\xi} \frac{1}{z'_2} - 2 \frac{m^2}{z'^2_2} \right] \\ &= \frac{1}{(4\pi)^2} \int \frac{d\xi}{(1 - \xi)^2} \left[\frac{1 + (1 - \xi)^2}{\xi} (L' - 1) + \xi \right] , \end{aligned} \quad (4.48)$$

with

$$L' = \ln \frac{E_e^2 \vartheta_0'^2}{m^2} + 2 \ln Y , \quad Y = \frac{E'_e}{E_e} . \quad (4.49)$$

The lower limit of the ξ integration in (4.48) is given by

$$\xi_{\min} = \frac{\epsilon}{Y} , \quad (4.50)$$

while the upper limit depends on details of the full process and on the kinematic reconstruction method. It needs to be discussed in the concrete application.

In the calorimetric case we assume that only the four-momentum of a cluster (or electromagnetic jet) can be measured when condition (4.42) is met:

$$p'_{\text{cal}} \equiv p'_{\text{cluster}} = p_2 + k_2 . \quad (4.51)$$

Expressing the occurrences of p_2 in the numerator of (4.46) in terms of p'_{cal} , the tensor structure in the first line becomes independent of ξ ,

$$[-\tilde{g}_{\mu\nu} (Q_l^2)_{\text{cal}} + 4(1 - x_1) \cdot (\tilde{p}_{1\mu} \tilde{p}_{1\nu})] , \quad (4.52)$$

because the calorimetrically measured invariant momentum transfer is:

$$(Q_l^2)_{\text{cal}} = -(p_1 - p'_{\text{cal}})^2 = \frac{Q_l^2}{1 - \xi} \simeq \frac{Q_h^2}{1 - x_1} . \quad (4.53)$$

In the definition of measured cross sections only p'_{cal} can be used. We therefore replace the phase space of the outgoing electron by the cluster using the substitution:

$$\int \widetilde{dp}_2 \int \widetilde{dk}_2 \quad \rightarrow \quad \int \widetilde{dp}'_{\text{cal}} \int \widetilde{dk}_2 (1 - \xi)^2 . \quad (4.54)$$

Combining the Jacobian $(1 - \xi)^2$ with the integration over the solid angle of the photon yields:

$$\begin{aligned} & \int \widetilde{dk}_2 (1 - \xi)^2 \left[\frac{1 + (1 - \xi)^2}{\xi} \frac{1}{z'_2} - 2 \frac{m^2}{z'^2_2} \right] \\ &= \frac{1}{(4\pi)^2} \int d\xi \left[\frac{1 + (1 - \xi)^2}{\xi} (L'' - 1) + \xi \right] , \end{aligned} \quad (4.55)$$

with

$$L'' = \ln \frac{E_e^2 \vartheta_0'^2}{m^2} + 2 \ln Y + 2 \ln \frac{E_e'}{E_{\text{cluster}}'} = L' + 2 \ln(1 - \xi) , \quad (4.56)$$

since in the inclusive case the ratio Y is given by:

$$Y = \frac{E_{\text{cluster}}'}{E_e} . \quad (4.57)$$

Inserting the limits for the ξ -integration which are now independent of the full process,

$$\frac{\epsilon}{Y} \leq \xi \leq 1 , \quad (4.58)$$

and evaluating the r.h.s. of (4.55) we finally obtain:

$$\frac{1}{(4\pi)^2} \left[\left(2 \ln \frac{Y}{\epsilon} - \frac{3}{2} \right) (L' - 1) + 3 - \frac{2\pi^2}{3} \right] . \quad (4.59)$$

4.2.5 Semi-collinear emission

The final situation covers the configuration where one photon is emitted almost collinearly to the incoming electron, while the other photon is emitted at a large angle with respect to both the incoming and outgoing electron directions, i.e., for $\vartheta_2 > \vartheta_0$ and $\vartheta_2' > \vartheta_0'$. We denote this kinematic domain as the semi-collinear one.

To be consistent with the above treatment of the double collinear emission, we need to perform the solid angle integration over the collinear photon and drop all contributions of the order $\mathcal{O}(\vartheta_0)$ and $\mathcal{O}(\zeta_0^{-1})$. In doing so, a subtlety arises from the propagator denominators $\Delta = z_1 + z_2 - \sigma$. For strongly ordered angles $\vartheta_1 \ll \vartheta_2$, corresponding to $z_1 \ll z_2$, one may approximate:

$$k_1 \simeq x_1 p_1 , \quad \Delta \simeq (1 - x_1) z_2 + \mathcal{O}(z_1) \quad (\text{for } \vartheta_1 \ll \vartheta_2) . \quad (4.60)$$

This leads to a factorized expression not only for the differential cross section, but also after integration over the collinear photon, as long as $\vartheta_2 \gg \vartheta_0$. However, for $\vartheta_1 \approx \vartheta_2$, which can happen if photon 2 is emitted close to the forward cone that is specified by the solid angle of the PD, approximation (4.60) no longer works well. One obtains contributions from further terms of an expansion around the limit $\vartheta_1 \rightarrow 0$, which lead to a more complicated, steeper ϑ_2 -dependence that spoils the factorization. Fortunately, these terms fall off rapidly and essentially contribute only in the small region $\vartheta_0 \lesssim \vartheta_2 < \text{few} \cdot \vartheta_0$. Since these extra-terms are important only for this particular kinematic configuration of almost double collinear emission we shall

denote them the *quasi-collinear contribution*. The details of this calculation are given in appendix B.

Assuming that photons in this narrow region outside the PD will not be measured, we explicitly integrate these additional terms over the photon solid angle and split their contribution schematically as follows:

$$\begin{aligned}
& \frac{E_e^4}{\pi^2} \int_{\vartheta_1 < \vartheta_0} d\Omega_1 \int_{\vartheta_2 > \vartheta_0} d\Omega_2 K_{\mu\nu}^{\text{semi-coll}} \\
& \simeq \frac{E_e^2}{\pi} \int_{\vartheta_2 > \vartheta_0} d\Omega_2 \left\{ \left[-\tilde{g}^{\mu\nu} \frac{(r_1(Q_l^2 + z_2))^2 + (r_1 Q_l^2 - z_2')^2}{r_1 z_2 z_2'} \right. \right. \\
& \quad \left. \left. + 4r_1^2 \tilde{p}_1^\mu \tilde{p}_1^\nu \frac{Q_h^2}{r_1 z_2 z_2'} + 4\tilde{p}_2^\mu \tilde{p}_2^\nu \frac{Q_h^2}{r_1 z_2 z_2'} \right] \cdot \frac{1}{x_1 r_1} P(r_1, L_0) \right\} \\
& + \left[-\tilde{g}_{\mu\nu} Q_l^2 + 4(r_1 - x_2) (\tilde{p}_{1\mu} \tilde{p}_{1\nu}) \right] \cdot \frac{1}{x_1 x_2} H(x_1, x_2) , \tag{4.61}
\end{aligned}$$

with $r_1 = 1 - x_1$. The expression for the function $H(x_1, x_2)$, which collects the non-factorizing, quasi-collinear terms, is given in appendix B, eq. (B.25). It is infrared-finite, ϑ_0 -independent for small ϑ_0 , and does not contain any logarithm of a large scale.

The integrand in the first part on the r.h.s. of (4.61) can be rewritten as

$$\left\{ \dots \right\} \simeq \frac{1}{x_1} P(r_1, L_0) \cdot \frac{1}{r_1} K_{\mu\nu}^{\text{Born}}(r_1 p_1, p_2, k_2) , \tag{4.62}$$

where for the sake of consistency one should drop terms of order m^2 on the r.h.s. in the expression for the lowest order Compton tensor (3.7).

Since in our decomposition of phase space only photon 1 reaches the PD, we have to identify r_1 by z and x_1 by $1 - z$ in the above expressions. However, we still need to integrate over the phase space of the other photon that is emitted at large angles. This calculation depends on the complete scattering process and in general requires a numerical integration.

4.3 Corrections to radiative DIS

Let us turn to the description of the radiative deep inelastic scattering process with photon tagging,

$$e(p) + p(P) \rightarrow e(p') + X(P_X) + \gamma(k_1) \quad (+ \gamma(k_2)) ,$$

including the complete leptonic QED radiative corrections calculated above. It is straightforward to contract the expressions for the radiatively corrected

Compton tensor with the hadron tensor (2.19). We assume here the kinematic reconstruction by measurement of the scattered lepton and later outline the changes for other methods.

Applying the results from the previous section, we find for the contribution from virtual and soft corrections to the cross section:

$$\frac{1}{\hat{y}} \frac{d^3\sigma_{V+S}}{d\hat{x} d\hat{y} dz} = \frac{\alpha^2}{4\pi^2} [P(z, L_0)\tilde{\rho} - T] \tilde{\Sigma}(\hat{x}, \hat{y}, \hat{Q}^2), \quad (4.63)$$

where $\tilde{\rho}$ is taken from (4.24) with

$$\begin{aligned} Y &\equiv \frac{E'_e}{E_e} = z(1 - \hat{y}) + \hat{x}\hat{y} \frac{E_p}{E_e}, \\ c &\equiv \cos\theta = \frac{z(1 - \hat{y})E_e - \hat{x}\hat{y}E_p}{z(1 - \hat{y})E_e + \hat{x}\hat{y}E_p}. \end{aligned} \quad (4.64)$$

In the calculation of the contributions from the emission of two hard photons, we decompose the phase space into three regions discussed in the previous section (see also [32]): (i) both hard photons hit the forward photon detector, i.e., both are emitted within a narrow cone around the electron beam ($\vartheta_{1,2} \leq \vartheta_0$, $\vartheta_0 \ll 1$); (ii) one photon is tagged in the PD, while the other is collinear to the outgoing electron ($\vartheta'_2 \equiv \angle(\vec{k}_2, \vec{p}') \leq \vartheta'_0$); and finally (iii) the second photon is emitted at large angles (i.e., outside the defined narrow cones) with respect to both incoming and outgoing electron momenta. For the sake of simplicity, we assume that $m/E_e \ll \vartheta'_0 \ll \theta$.

The contribution from the kinematic region (i), with both hard photons being tagged in the PD, but only the sum of their energies measured, reads:

$$\frac{1}{\hat{y}} \frac{d^3\sigma_{(i)}^{\gamma\gamma}}{d\hat{x} d\hat{y} dz} = \frac{\alpha^2}{8\pi^2} \left[P_{\log}^{(2)} + P_{\text{nonlog}}^{(2),\text{IR-div.}} + P_{\text{nonlog}}^{(2),\text{IR-fin.}} \right] \tilde{\Sigma}, \quad (4.65)$$

see eq. (4.38).

In region (ii) we need to distinguish between the cases of whether the outgoing electron in the presence of a collinear photon can be measured separately (exclusively), or whether its energy and momentum are detected together with the electron (inclusively), as this affects the reconstructed kinematic variables.

For the exclusive event selection, when only the scattered electron is detected, we obtain from (4.46) and (4.48):

$$\frac{1}{\hat{y}} \frac{d^3\sigma_{(ii),\text{excl}}^{\gamma\gamma}}{d\hat{x} d\hat{y} dz} = \frac{\alpha^2}{4\pi^2} P(z, L_0) \int_{\xi_{\min}}^{\xi_{\max}} \frac{d\xi}{(1 - \xi)^2} \left[\frac{1 + (1 - \xi)^2}{\xi} (L' - 1) + \xi \right] \tilde{\Sigma}_f, \quad (4.66)$$

where

$$\begin{aligned}
\tilde{\Sigma}_f &= \tilde{\Sigma}(x_f, y_f, Q_f^2), \quad L' = \ln \frac{E_e^2 \vartheta_0'^2}{m^2} + 2 \ln Y, \\
x_f &= \frac{\hat{x}\hat{y}}{\hat{y} - \xi}, \quad y_f = 1 - \frac{1 - \hat{y}}{1 - \xi}, \quad Q_f^2 = \frac{\hat{Q}^2}{1 - \xi}, \\
\xi_{\min} &= \frac{\epsilon}{Y}, \quad \xi_{\max} = \frac{(1 - \hat{x})\hat{y} - (\bar{M}^2 - M^2)/(zS)}{1 - (\bar{M}^2 - M^2)/(zS)} \simeq (1 - \hat{x})\hat{y}.
\end{aligned} \tag{4.67}$$

In the case of a calorimetric event selection, where only the sum of the energies of the outgoing electron and collinear photon is measured and taken into account in the determination of the kinematic variables, the corresponding contribution from (4.46) and (4.59) is proportional to the lowest order contribution and reads

$$\begin{aligned}
\frac{1}{\hat{y}} \frac{d^3 \sigma_{(ii), \text{cal}}^{\gamma\gamma}}{d\hat{x} d\hat{y} dz} &= \frac{\alpha^2}{4\pi^2} P(z, L_0) \int_{\xi_{\min}}^1 d\xi \left[\frac{1 + (1 - \xi)^2}{\xi} (L' - 1 + 2 \ln(1 - \xi)) + \xi \right] \tilde{\Sigma} \\
&= \frac{\alpha^2}{4\pi^2} P(z, L_0) \left[\left(2 \ln \frac{Y}{\epsilon} - \frac{3}{2} \right) (L' - 1) + 3 - \frac{2\pi^2}{3} \right] \tilde{\Sigma}, \tag{4.68}
\end{aligned}$$

see also [31, 32, 33].

For the calculation of the contribution from the semi-collinear region (iii) we apply the decomposition (4.61). Due to the factorization property (4.62) of the leading term, it is useful to introduce the “radiation kernel” [32]:

$$\begin{aligned}
I^\gamma(zp, p', k_2) &\equiv \frac{1}{8\pi} K_{\rho\sigma}(zp, p', k_2) H^{\rho\sigma}(P, zp - p' - k_2) \\
&= \frac{1}{zz_2 z_2'} \left[G \cdot F_1(x_h, Q_h^2) + \left(x_h(zS)^2 [1 + (1 - \hat{y})^2] - \frac{x_h M^2}{Q_h^2} G \right. \right. \\
&\quad \left. \left. + (zS)[(1 - \hat{y})(\hat{Q}_l^2 - z_2') - (\hat{Q}_l^2 + zz_2)] \right) F_2(x_h, Q_h^2) \right], \tag{4.69}
\end{aligned}$$

which can be obtained from eqs. (3.19), (3.20). Here:

$$\begin{aligned}
Q_h^2 &= \hat{Q}_l^2 + zz_2 - z_2', \quad z_2 = 2p \cdot k_2, \quad z_2' = 2p' \cdot k_2, \\
x_h &= \frac{Q_h^2}{2P \cdot (zp - p' - k_2)} = \frac{Q_h^2}{\hat{y}zS - 2P \cdot k_2}, \\
G &= \left(\hat{Q}_l^2 + zz_2 \right)^2 + \left(\hat{Q}_l^2 - z_2' \right)^2. \tag{4.70}
\end{aligned}$$

The semi-collinear contribution then reads:

$$\begin{aligned} \frac{1}{\hat{y}} \frac{d^3 \sigma_{(iii)}^{\gamma\gamma}}{d\hat{x} d\hat{y} dz} &= \frac{\alpha^2}{\pi^2} P(z, L_0) \int \frac{d^3 k_2}{|\vec{k}_2|} \frac{\alpha^2(Q_h^2)}{Q_h^4} I^\gamma(zp, p', k_2) \\ &+ \frac{\alpha^2}{4\pi^2} \int_{\epsilon}^{x_2^t} dx_2 \frac{z}{z - x_2} H(1 - z, x_2) \tilde{\Sigma}(x_t, y_t, Q_t^2) . \end{aligned} \quad (4.71)$$

In the integration over the solid angle the cones corresponding to double collinear ISR (region (i), half opening angle ϑ_0) and FSR (region (ii), half opening angle ϑ'_0) have to be excepted. The upper limit on the photon energy is obtained from (3.36) by substituting $E_e \rightarrow zE_e$, $S \rightarrow zS$, $Y \rightarrow Y/z$:

$$E_2^{\max} = \frac{S[z - Y(1 - \tau)] - 4E_e^2 z Y \tau - (\bar{M}^2 - M^2)}{4[E_p(1 - \tau_1) + zE_e \tau_1 - Y E_e \tau_2]} . \quad (4.72)$$

For the second, quasi-collinear part, we have used the abbreviations

$$x_t = \frac{(z - x_2)\hat{x}\hat{y}}{z\hat{y} - x_2} , \quad y_t = \frac{z\hat{y} - x_2}{z - x_2} , \quad Q_t^2 = \hat{Q}^2 \frac{z - x_2}{z} , \quad (4.73)$$

and under HERA conditions and for small \hat{x} the upper integration limit simplifies to

$$x_2^t = z \frac{(1 - \hat{x})\hat{y} - (\bar{M}^2 - M^2)/(zS)}{1 - \hat{x}\hat{y}} \simeq z\hat{y} . \quad (4.74)$$

The total contribution from QED radiative corrections is finally obtained by adding up (4.63), (4.65), (4.71), and, depending on the chosen event selection, (4.66) or (4.68). As has been demonstrated explicitly in [32] the unphysical IR regularization parameter ϵ cancels in the sum.

In the case of a bare electron measurement, the angle ϑ'_0 plays the rôle of an (unphysical) regularization parameter that serves to define the phase space region of collinear final state radiation. It can be shown to cancel between the contributions from regions (ii) and (iii) and to drop out of the final result if chosen small enough, see [32].

For a calorimetric measurement of the scattered electron, ϑ'_0 corresponds to a resolution of the detector and is actually physical. Therefore the cross section will depend on it. However, in this case the mass singularity that is connected with final state collinear emission cancels in the sum of the contributions from virtual and soft corrections and from regions (ii) and (iii), in accordance with the Kinoshita-Lee-Nauenberg theorem [86]. For sufficiently small ϑ'_0 the resulting cross section depends logarithmically on

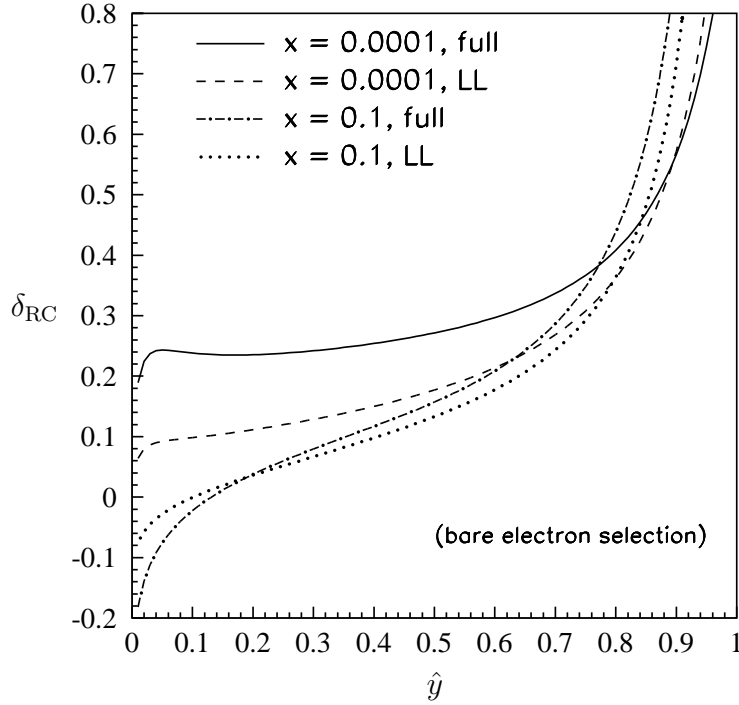


Figure 4.5: Radiative corrections to the tagged photon cross section with leading logarithmic and with full leptonic accuracy for the bare electron selection and for $E_\gamma = 10$ GeV.

ϑ'_0 , while for a coarse detector, i.e., for $\vartheta'_0 \sim \mathcal{O}(1)$, the result agrees at the leading logarithmic level with the correction obtained in section 4.1.

Let us now compare the radiative corrections calculated with full leptonic accuracy to those obtained by considering only the leading logarithms. For the same set of parameters as in section 4.1, figure 4.5 displays the radiative correction

$$\delta_{\text{RC}} = \frac{d^3\sigma}{d^3\sigma_{\text{Born}}} - 1 \quad (4.75)$$

at leading logarithmic and with full leptonic accuracy for the bare electron measurement for $\hat{x} = 0.1$ and $\hat{x} = 10^{-4}$ and for a tagged energy $E_\gamma = 10$ GeV. We find a large difference of the order of 5 to 10 percent between both calculations, especially in the region of small \hat{x} and for large \hat{y} .

In the case of the HERA main detectors, the measurement of the energy of the scattered electron in the electromagnetic calorimeter is performed with a typical separation from an almost collinear photon of the order of (several cm)/(1 meter) $\sim \mathcal{O}(50 \text{ mrad})$. Figure 4.6 displays the corresponding com-

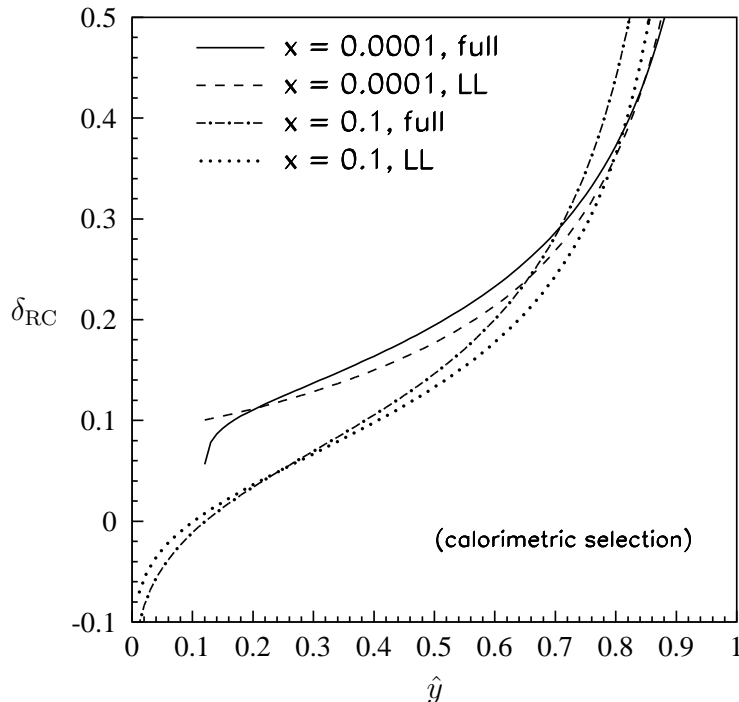


Figure 4.6: Radiative corrections to the tagged photon cross section with leading logarithmic and with full leptonic accuracy for calorimetric event selection with $\vartheta'_0 = 50$ mrad and for $E_\gamma = 10$ GeV.

parison of the radiative corrections for the calorimetric selection, assuming

$$\vartheta'_0 = 50 \text{ mrad} . \quad (4.76)$$

Apparently the difference between the leading logarithmic and the full leptonic result becomes significantly smaller, especially at smaller \hat{x} and for small \hat{y} , reaching a level of the order of 5 percent. This suggests that the leading logarithmic approximation gives a reasonable estimate for the radiative corrections for a sufficiently inclusive measurement, at least for the reconstruction of the kinematic variables using the lepton method.

In the references [31, 32, 33] a calculation of the radiative corrections was performed that takes into account the leading and next-to-leading logarithms of the full corrections. We can now compare this approximation with the full result. It turns out that it is rather close to the full calculation [34], and that the non-logarithmic terms, typically contributing at the per mille level, are potentially significant only at small \hat{x} and for a large tagged photon energy. To demonstrate this we compare in figure 4.7 the corrections in the calorimetric case taking into account the next-to-leading logarithms vs. the

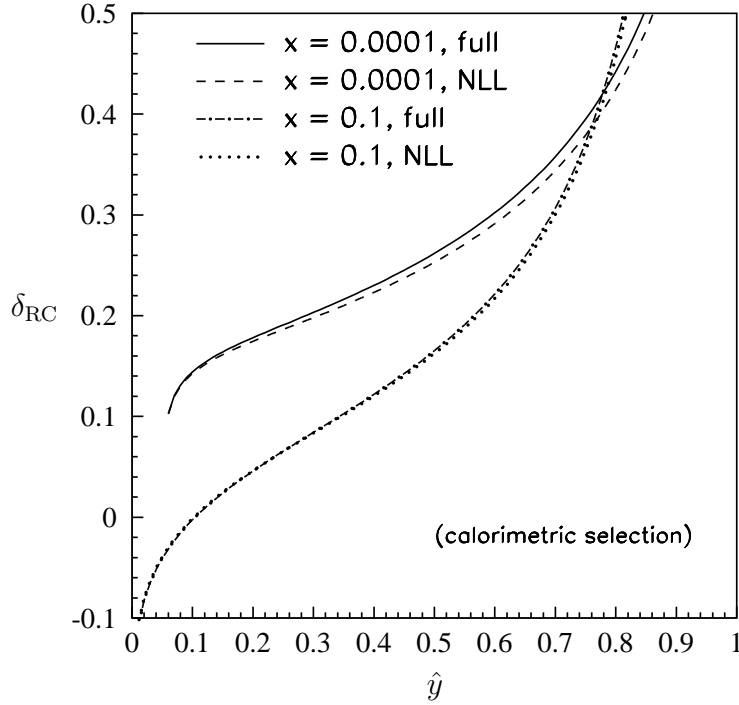


Figure 4.7: Comparison of the radiative corrections with next-to-leading logarithmic and with full leptonic accuracy for a calorimetric event selection with $\vartheta'_0 = 50$ mrad and for $E_\gamma = 20$ GeV.

full leptonic corrections for a higher tagged energy of $E_\gamma = 20$ GeV. Similar results are obtained for the bare electron measurement as the non-logarithmic terms do not change the contribution from region (ii) and the large-angle part of region (iii).

The size of the contribution from hard photon emission to the radiative corrections can be reduced if one applies experimental cuts. As an example which is applicable at HERA we define a “missing longitudinal energy” using longitudinal momentum conservation:

$$E_{\text{miss}} := E_e - E_{\text{PD}} - \frac{\Sigma_h + E'_e(1 + \cos \theta)}{2} = \frac{P \cdot k_2}{2E_p} = \frac{1}{2} (E_\gamma^{(2)} + p_{\gamma,z}^{(2)}) , \quad (4.77)$$

where E_{PD} represents the actually measured energy in the photon detector. Assuming 100% efficiency of the PD and the second photon being lost in the forward beam pipe outside the PD, the quantity E_{miss} is roughly equal to the energy of this lost photon. We then apply the following cut:

$$\Delta_{\text{miss}} := \frac{E_{\text{miss}}}{E_{\text{PD}}} < 0.5 , \quad (4.78)$$

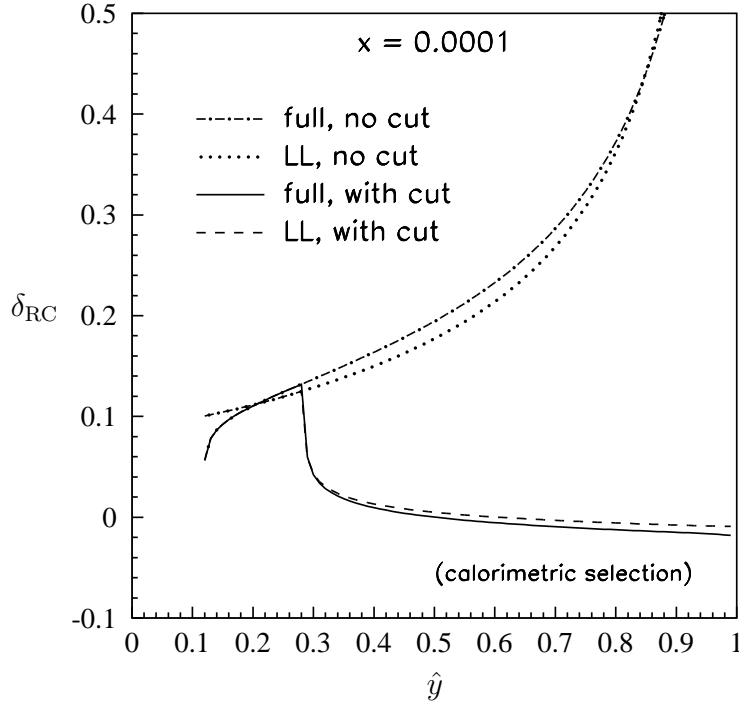


Figure 4.8: Comparison of the radiative corrections with leading logarithmic and with full leptonic accuracy for a calorimetric event selection without cuts and with cut (4.78) for $E_\gamma = 10$ GeV.

and compare the radiative corrections with and without this cut for the calorimetric selection. For the same set of parameters and for $\hat{x} = 10^{-4}$ and $E_\gamma = 10$ GeV the result is displayed in figure 4.8.

We observe that the size of the corrections is much reduced, and that the difference between the leading logarithmic and the full result is also lessened slightly. A main reason is that this cut is mostly efficient for the contribution from very hard lost photons which would lead to the largest shifts between reconstructed and “true” kinematic variables. Therefore this cut is effective only for sufficiently large \hat{y} , see also (4.14). It also affects the QED Compton contribution which plays a rôle only at large \hat{y} .

For other reconstructions of the kinematic variables the above formulae have to be adapted in the contributions from final state radiation (ii) and for the semi-collinear contribution (iii). Ref. [33] discusses the modification of the calculation of the next-to-leading logarithms for the Σ method. The derivation of the boundaries of the photon phase space is more elaborate than for the electron method, so that we will not treat it here and only quote the results.

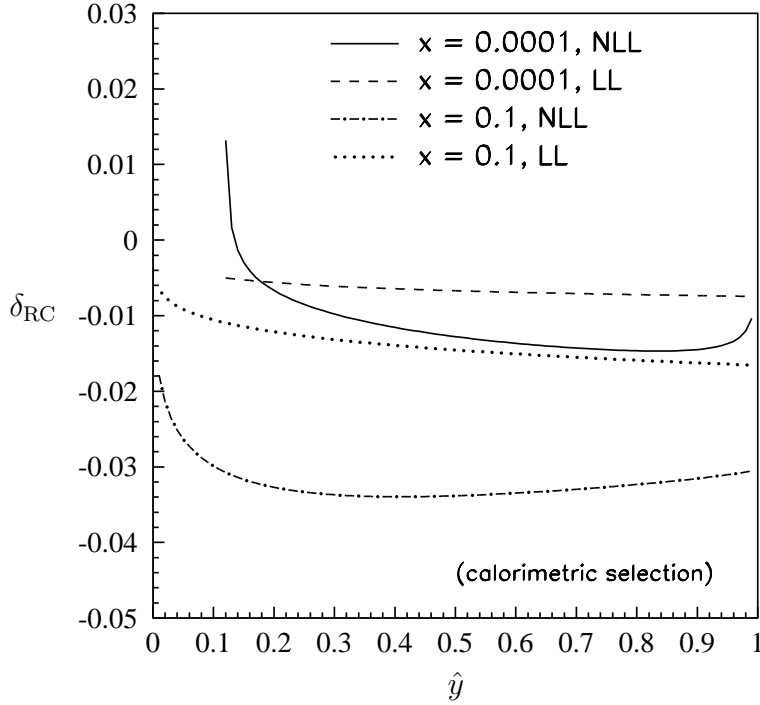


Figure 4.9: Radiative corrections with leading and with next-to-leading logarithmic accuracy for the Σ method for a calorimetric event selection with $\vartheta'_0 = 50$ mrad and for $E_\gamma = 10$ GeV.

We found in section 4.1 that the leading logarithmic corrections for the Σ method were quite small, see fig. 4.3b. The reason for this behavior can be attributed to the scaling properties of the kinematic variables under collinear photon emission, see table 4.1. However, as can be seen from fig. 4.9 the more accurate next-to-leading logarithmic calculation adds terms that are the order of a few percent and thus of similar size as the leading logarithmic estimate, even for the calorimetric selection. As can be expected the corrections become significantly larger for a bare electron measurement but still stay well below those for the kinematic reconstruction using the lepton method. Furthermore, the R dependence of the corrections remains small even after taking into account the next-to-leading logarithmic terms. For more details we refer the reader to [33].

Chapter 5

Estimates of Higher Order QED Corrections

In this chapter we shall attempt to obtain an all orders estimate of the leading logarithmic contributions to the radiative corrections to the deep inelastic scattering process with tagged initial state radiation. To this end, we will first rederive the final result of section 4.1 in a simpler framework. We then generalize the arguments to all orders to find a closed expression after resummation.

Our starting point will be the factorization theorem for the QED radiatively corrected, photon inclusive cross section for high energy scattering processes,

$$\sigma_{\text{RC}}(s) = \int_0^1 dz \, D(z, \mu_F^2) \sigma_h(zs; \mu_F^2) . \quad (5.1)$$

Here s stands for a typical large scale of the process. All large logarithms in the small electron mass m are contained in the radiator function $D(z, \mu_F^2)$, while the “hard cross section” σ_h is finite for $m \rightarrow 0$. Also, the cancellation of infrared singularities from QED virtual corrections and from soft photon emission takes place within this radiator function at all orders. The factorization theorem (5.1) is a corollary of the corresponding theorems for the factorization of infrared and mass singularities in QCD [101], but has also been proven explicitly for QED in [107]. Note that we have suppressed in (5.1) the dependence of the hard cross section on the renormalization scale μ_R^2 , which is formally unrelated to μ_F^2 . The purpose of factorization in QCD in the above example is to extract all soft (long distance) contributions into the distribution D , so that the hard process receives only perturbatively calculable short distance corrections.

Eq. (5.1) introduces on the r.h.s. an arbitrary unphysical scale, μ_F^2 . Physical results, and thus the l.h.s. should in principle be independent of the choice of this so-called factorization scale. This formal independence can be used to derive renormalization group type equations. In practical applications, however, things are more complicated. Calculating the radiator function using a partial resummation of large terms at all orders in the coupling constant while treating the hard part at fixed order in perturbation theory leads to an unavoidable residual dependence of the r.h.s. on μ_F^2 in higher orders that are not completely calculated. On the other hand, one can show that the leading dependence of the uncalculated corrections to σ_h is logarithmic in μ_F^2 . If all small scales can be extracted into the radiator function D , one may hope that the missing logarithmic terms in σ_h will be small if this factorization scale is chosen close to a typical large scale.

In the simplest case, the leading logarithmic approximation, the hard cross section is approximated by the so-called “improved Born cross section” for the hard scattering process by replacing coupling constants by the running couplings taken at the scale μ_F^2 . For the photon inclusive cross section with no explicit registration of the radiated photons there essentially is a single large scale, e.g., the total energy s or a momentum transfer Q^2 . The ambiguity in selecting one of these scales reflects the uncertainty of this approximation; it can only be resolved by a calculation with higher (next-to-leading) accuracy, i.e., taking into account terms beyond the Born cross section. Nevertheless, the leading logarithmic result often gives a reasonable estimate. The structure function method in the form as applied in section 4.1 corresponds to this simple approximation.

5.1 Exclusive photons in the leading logarithmic approximation

The radiator function $D(z, \mu^2)$ appearing in (5.1) satisfies an Altarelli-Parisi type evolution equation. As we shall be interested in the leading logarithmic contribution only, we restrict ourselves to the electron non-singlet structure function $D^{\text{NS}}(z, \mu^2)$, which is the solution of the integro-differential equation,¹

$$\mu^2 \frac{d}{d\mu^2} D^{\text{NS}}(z, \mu^2) = \frac{\alpha}{2\pi} \int_z^1 \frac{dy}{y} P_{ee}(y) D^{\text{NS}}\left(\frac{z}{y}, \mu^2\right), \quad (5.2)$$

¹For the sake of simplicity we shall ignore the running of the QED coupling.

with the electron splitting function

$$P_{ee}(x) = \lim_{\epsilon \rightarrow 0} \left(\Theta(1 - \epsilon - x) \frac{1 + x^2}{1 - x} - \delta(1 - x) \int_0^{1-\epsilon-x} \frac{1 + y^2}{1 - y} dy \right) \quad (5.3)$$

and with initial condition

$$D^{\text{NS}}(z, m^2) = \delta(1 - z) . \quad (5.4)$$

The normalization of the non-singlet structure function,

$$\int_0^1 dz D^{\text{NS}}(z, \mu^2) = 1 , \quad (5.5)$$

valid for any μ^2 , is a consequence of

$$\int_0^1 dx P_{ee}(x) = 0 , \quad (5.6)$$

which expresses the order-by-order cancellation of the infrared singularities between virtual corrections ($x = 1$) and soft photon emission ($x \rightarrow 1$).

The formal solution of the integro-differential equation (5.2) with initial condition (5.4) reads:

$$D^{\text{NS}}(z, \mu^2) = \delta(1 - z) + \frac{\alpha}{2\pi} \int_{m^2}^{\mu^2} \frac{dQ^2}{Q^2} \int_z^1 \frac{dy}{y} P_{ee}(y) D^{\text{NS}}\left(\frac{z}{y}, Q^2\right) . \quad (5.7)$$

A perturbative solution is obtained from (5.7) by iteration. It may be written in different equivalent forms, e.g.,

$$D^{\text{NS}}(z, \mu^2) = \delta(1 - z) + \frac{\alpha}{2\pi} \int_{m^2}^{\mu^2} \frac{dQ_1^2}{Q_1^2} P_{ee}(z) \quad (5.8)$$

$$+ \left(\frac{\alpha}{2\pi}\right)^2 \int_{m^2}^{\mu^2} \frac{dQ_1^2}{Q_1^2} \int_{Q_1^2}^{\mu^2} \frac{dQ_2^2}{Q_2^2} \int_z^1 \frac{dy}{y} P_{ee}(y) P_{ee}\left(\frac{z}{y}\right) + \dots$$

$$= \delta(1 - z) + \frac{\alpha}{2\pi} \int_{m^2}^{\mu^2} \frac{dQ_1^2}{Q_1^2} P_{ee}(z) \quad (5.9)$$

$$+ \frac{1}{2!} \left(\frac{\alpha}{2\pi} \int_{m^2}^{\mu^2} \frac{dQ^2}{Q^2} \right)^2 \int_z^1 \frac{dy}{y} P_{ee}(y) P_{ee}\left(\frac{z}{y}\right) + \dots$$

As long as we are interested in photon inclusive radiative corrections only, both forms (5.8) and (5.9) are equally useful. However, the first variant (5.8) turns out to be powerful for the treatment of exclusive photon emission in QED. This can be seen as follows.

For QED radiative corrections, the origin of the leading large logarithms, $L \equiv \ln(\mu^2/m^2)$, is identified by analyzing the peaking behavior of the squared matrix elements for photon radiation in the region of phase space where the photons are widely separated in polar angle (measured w.r.t. the radiating fermion).

Let us start by considering a typical expression corresponding to single photon emission. In that case, the large logarithm results from the integration over the photon polar angle, which is of the type $(\tau \equiv (1 - \cos \vartheta)/2)$:²

$$\int \frac{d(p \cdot k)}{p \cdot k} \simeq \int \frac{d(\cos \vartheta)}{1 - \beta \cos \vartheta} \simeq \int \frac{d\tau}{\tau + (1 - \beta)/2} \simeq \int \frac{d\tau}{\tau + m^2/(4E_e^2)} . \quad (5.10)$$

In the high-energy limit, one may drop the term $m^2/(4E_e^2)$ in the denominator if one cuts off the τ -integration at

$$\tau^{\min} = \frac{m^2}{4E_e^2} , \quad (5.11)$$

corresponding to a fictitious minimum angle $\vartheta_{\min} \simeq m/E_e$. The large logarithm L of the non-singlet structure function D^{NS} is then mimicked by assuming a fictitious maximum³

$$\tau^{\max} = \frac{\mu^2}{4E_e^2} . \quad (5.12)$$

It must be emphasized that this clearly is an effective but *not* a physical cutoff. First, at large angles the approximations leading to (5.10) will no longer be valid. Second, τ^{\max} in (5.12) obviously is not restricted to be smaller than unity for arbitrary μ^2 .

The n photon contributions ($n \geq 2$) in eq. (5.8) can be interpreted analogously. However, we need to take into account the fact that the leading contributions are obtained from the integration over configurations in phase

²In the approximation of small angles, one may equally well work with the photon rapidity $y = \frac{1}{2} \ln[(1 + \cos \vartheta)/(1 - \cos \vartheta)] \simeq -\frac{1}{2} \ln \tau$.

³For a general discussion of inclusive radiative corrections, the choice of τ^{\min} and τ^{\max} is completely arbitrary, as long as $\tau^{\max}/\tau^{\min} = \mu^2/m^2$. We do know, however, the full $\mathcal{O}(\alpha)$ result, and can match the leading logarithmic result at this order to the full answer, confirming the above choice for τ^{\min} .

space where the photon polar angles are strongly ordered,

$$\vartheta_1 \ll \vartheta_2 \ll \cdots \ll \vartheta_n , \quad (5.13)$$

which is equivalent to saying that the (negative) virtualities of the electron after radiation, roughly given by $2p \cdot k_i$, are strongly ordered for comparable photon energies. This suggests to replace in (5.8) the nested integrations

$$\int_{m^2}^{\mu^2} \frac{dQ_1^2}{Q_1^2} \int_{Q_1^2}^{\mu^2} \frac{dQ_2^2}{Q_2^2} \cdots \int_{Q_{n-1}^2}^{\mu^2} \frac{dQ_n^2}{Q_n^2} \quad (5.14)$$

by

$$\int_{\tau_1^{\max}}^{\tau_1^{\max}} \frac{d\tau_1}{\tau_1} \int_{\tau_1}^{\tau_1^{\max}} \frac{d\tau_2}{\tau_2} \cdots \int_{\tau_{n-1}}^{\tau_{n-1}^{\max}} \frac{d\tau_n}{\tau_n} . \quad (5.15)$$

The method described above corresponds to the introduction of “unintegrated splitting functions” for the generation of exclusive photons from QED photon showers in Monte Carlo event generators like KRONOS [89], which are chosen in such a way that they reproduce the angular distribution for single photon emission in the region of small angles as given by the peaking behavior of the electron propagator,⁴

$$e^2 \int \widetilde{dk}_i \frac{1}{p^{(i)} \cdot k_i} \frac{1 + (1 - x_i)^2}{x_i} = \frac{\alpha}{2\pi} \int_{\tau_i^{\min}}^{\tau_i^{\max}} \frac{d\tau_i}{\tau_i} \int dx_i P_{e\gamma}(x_i) , \quad (5.16)$$

with

$$P_{e\gamma}(x) = \frac{1 + (1 - x)^2}{x} \Theta(x - \epsilon) + \left(2 \ln \epsilon + \frac{3}{2} \right) \delta(x) , \quad (5.17)$$

and the small parameter ϵ serving as infrared-regulator.

In the following we shall assume the photon angle distributions (5.15) for an estimate of the radiative corrections to the tagged photon process.

Although the rewriting of the scale-ordered integrations (5.14) in the perturbative expansion (5.8) by the angular-ordered integrations (5.15) looks very suggestive, a remark on the proper cancellation of infrared singularities is in order.

⁴Although the Monte Carlo event generator KRONOS generates the proper large inclusive logarithms, the actual implementation of the minimum and maximum values for the polar angles generally leads to emission of exclusive photons at too large polar angles.

In fixed order perturbation theory, the Bloch-Nordsieck theorem guarantees that the emission of soft photons is a Poisson process. The probability for emitting n photons in the energy interval $\omega \in [\omega_{\min}, \omega_{\max}]$ is proportional to

$$\frac{1}{n!} \left[\frac{\alpha}{\pi} \ln \left(\frac{\mu^2}{m^2} \right) \ln \left(\frac{\omega_{\max}}{\omega_{\min}} \right) \right]^n . \quad (5.18)$$

The obvious divergence for $\omega_{\min} \rightarrow 0$ is known to be canceled by taking into account all appropriate virtual corrections at the same order of perturbation theory.

From the reasoning further above, we know that in the regime of hard photon radiation the emission of photons is ordered in virtualities resp. angles. Applying this ordering condition to the phase space of the photon leads to a cancellation of the combinatorial factor $1/n!$; the same will happen in eq. (5.18) with the combination $1/n! \cdot \ln^n(\mu^2/m^2)$.

We shall interpret this outcome in the following way: emission of a single (hard) photon results in an off-shell electron. The finite virtuality effectively restricts the phase space accessible to further photon emissions to the range of larger angles. At the same time, the virtual corrections to the amplitude after the i -th photon emission are regularized or “cut off” by the virtuality of the electron, Q_i^2 , instead of m^2 . The ordered perturbative expansion (5.8) then expresses this order-by-order cancellation due to the normalization property (5.6) of the electron splitting function even for our interpretation of ordered photon emission.

5.2 Leading radiative corrections to DIS with tagged ISR

Let us now turn to an alternative derivation of the leading radiative corrections to DIS with tagged initial state radiation using the above reasoning. We shall find that not only can the result of section 4.1 be reproduced with little effort but also generalized.

As a start, the lowest order cross section for the tagged photon process (3.83) follows from the first term of the expansion of the electron non-singlet structure function. Integrating over the solid angle of the forward photon detector, $\vartheta \leq \vartheta_0$, we obtain:

$$\frac{d^3\sigma^{(1)}}{dx dy dz} = \frac{\alpha}{2\pi} \int_{\tau^{\min}}^{\tau_0} \frac{d\tau}{\tau} P_{ee}(z) \frac{d^2\sigma_{\text{Born}}(x, y; z)}{dx dy} = \frac{\alpha L_0}{2\pi} P^{(1)}(z) \sigma_0(x, y; z) , \quad (5.19)$$

with $\tau_0 = (1 - \cos \vartheta_0)/2$, $L_0 = \ln(\tau_0/\tau^{\min})$, and the abbreviation (c.f. section 4.1):

$$\sigma_0(x, y; z) = \frac{d^2 \sigma_{\text{Born}}(x, y; z)}{dx dy} . \quad (5.20)$$

At order $\mathcal{O}(\alpha^2)$, corresponding to double photon emission, we decompose the contributions into two cases. Case (a) corresponds to both photons hitting the photon detector. Assuming that only the sum of their energies is measured, we find:

$$\begin{aligned} \frac{d^3 \sigma^{(2,a)}}{dx dy dz} &= \left(\frac{\alpha}{2\pi}\right)^2 \int_{\tau^{\min}}^{\tau_0} \frac{d\tau_1}{\tau_1} \int_{\tau_1}^{\tau_0} \frac{d\tau_2}{\tau_2} \int_z^1 \frac{d\xi}{\xi} P_{ee}(\xi) P_{ee}\left(\frac{z}{\xi}\right) \sigma_0(x, y; z) \\ &= \frac{1}{2!} \left(\frac{\alpha L_0}{2\pi}\right)^2 P^{(2)}(z) \sigma_0(x, y; z) . \end{aligned} \quad (5.21)$$

In case (b), one photon enters the photon detector, while the other is emitted at a larger angle. Again, to logarithmic accuracy we may neglect the transverse momentum of both photons, as we did in section 4.1. Taking the angle ordering into account yields:

$$\begin{aligned} \frac{d^3 \sigma^{(2,b)}}{dx dy dz} &= \left(\frac{\alpha}{2\pi}\right)^2 \int_{\tau^{\min}}^{\tau_0} \frac{d\tau_1}{\tau_1} P_{ee}(z) \int_{\tau_0}^{\tau^{\max}} \frac{d\tau_2}{\tau_2} \int dz' P_{ee}(z') \tilde{\sigma}_0(z, y; z, z') \\ &= \left(\frac{\alpha}{2\pi}\right)^2 L_0 L_1 P^{(1)}(z) \int_{z'_{\min}}^1 dz' P_{ee}(z') \tilde{\sigma}_0(x, y; z, z') , \end{aligned} \quad (5.22)$$

with $L_1 = \ln(\tau^{\max}/\tau_0) = \ln(Q^2/m^2) - L_0$. Remember that the semi-collinear contribution does depend on the method of reconstruction of the kinematic variables. Therefore, $\tilde{\sigma}_0$ in the above expression is understood to be expressed in terms of the “true” kinematic variables of the hard subprocess,

$$\tilde{\sigma}_0(x, y; z, z') \equiv \sigma_0(x_{\text{true}}, y_{\text{true}}; z z') \cdot \mathcal{J}(x, y; x_{\text{true}}, y_{\text{true}}; z') , \quad (5.23)$$

with the Jacobian \mathcal{J} depending on the chosen set of kinematic variables, see table 4.1. The integration limit z'_{\min} also depends on kinematic cuts.

Inserting the regularized form of the electron splitting function (5.3) in the last line of (5.22) leads to:

$$\frac{d^3 \sigma^{(2,b)}}{dx dy dz} = \left(\frac{\alpha}{2\pi}\right)^2 L_0 L_1 P^{(1)}(z)$$

$$\times \left[\int_{z'_{\min}}^1 dz' P^{(1)}(z') (\tilde{\sigma}_0(x, y; z, z') - \tilde{\sigma}_0(x, y; z, z' = 1)) - \tilde{\sigma}_0(x, y; z, z' = 1) \int_0^{z'_{\min}} dz' P^{(1)}(z') \right] . \quad (5.24)$$

Adding contributions (5.21) and (5.24), identifying $z' = 1 - u$, and noting that

$$\tilde{\sigma}_0(x, y; z, z' = 1) = \sigma_0(x, y; z) ,$$

we recover result (4.13).

The above procedure may be generalized to higher orders in α ; we only need to pay attention to the angle ordering to find the proper combinatorial factors. As a further explicit example we sketch the application at order α^3 .

The contribution from three forward (collinear) photons reads:

$$\frac{1}{3!} \left(\frac{\alpha L_0}{2\pi} \right)^3 P_{\Theta}^{(3)}(z) \int dz' \delta(1 - z') \tilde{\sigma}_0(x, y; z, z') . \quad (5.25)$$

The semi-collinear part receives contributions from two collinear and one large-angle photon,

$$\frac{1}{2!} \left(\frac{\alpha L_0}{2\pi} \right)^2 P_{\Theta}^{(2)}(z) \int dz' \left(\frac{\alpha L_1}{2\pi} \right) P^{(1)}(z') \tilde{\sigma}_0(x, y; z, z') , \quad (5.26)$$

and from one collinear and two large-angle photons:

$$\left(\frac{\alpha L_0}{2\pi} \right) P_{\Theta}^{(1)}(z) \int dz' \frac{1}{2!} \left(\frac{\alpha L_1}{2\pi} \right)^2 P^{(2)}(z') \tilde{\sigma}_0(x, y; z, z') . \quad (5.27)$$

It is now straightforward to perform a summation of the leading contributions to all orders. Those parts corresponding to collinear emission with no photon at large angles obviously add up to

$$D^{\text{NS}}(z; L_0) \cdot \int dz' \delta(1 - z') \tilde{\sigma}_0(x, y; z, z') , \quad (5.28)$$

with the suggestive notation $D^{\text{NS}}(z; L_0)$ indicating that it coincides with the inclusive non-singlet structure function,

$$D^{\text{NS}}(z; L) = \sum_{n=0}^{\infty} \frac{1}{n!} \left(\frac{\alpha L}{2\pi} \right)^n P^{(n)}(z) , \quad (5.29)$$

and thus satisfies an evolution equation,

$$\frac{\partial}{\partial L} D^{\text{NS}}(z; L) = \frac{\alpha}{2\pi} \int_z^1 \frac{dy}{y} P_{ee}(y) D^{\text{NS}}\left(\frac{z}{y}; L\right) , \quad D^{\text{NS}}(z; 0) = \delta(1 - z) . \quad (5.30)$$

The slight change in notation here is intended in order to emphasize that the present version of D^{NS} has no exclusive meaning in the sense of the discussion in the previous subsection; it just represents the formal sum on the r.h.s. of (5.29). Furthermore, and even more importantly, while $D^{\text{NS}}(z; L)$ appears to be well defined, the partial cross section (5.28) with only forward photons is by itself *not* a meaningful, physical expression, as it lacks contributions from large angle photons. This is tacitly expressed by the δ -function in the variable z' that is related to the energy loss outside the solid angle covered by the forward photon detector, indicating that it is a virtual correction part. Strictly speaking, (5.29) has to be multiplied by the probability for *no emission at large angles*.

The full result for the cross section is therefore obtained by summing the contributions from *any* number of collinear and *any* number of large-angle photon emissions while taking into account the angle ordering. It is easily seen that this procedure finally leads to the following expression for the all-order leading logarithmic result:

$$\begin{aligned} \frac{d^3 \sigma_{\text{RC}}^{\text{LL}(\infty)}}{dx dy dz} &= D^{\text{NS}}(z; L_0) \cdot \int_{z'_{\min}}^1 dz' D^{\text{NS}}(z'; L_1) \tilde{\sigma}_0(x, y; z, z') \\ &= D^{\text{NS}}(z; L_0) \cdot \left[\sigma_0(x, y; z) \cdot \left(1 - \int_0^{z'_{\min}} D^{\text{NS}}(z'; L_1) dz' \right) \right. \\ &\quad \left. + \int_{z'_{\min}}^1 D^{\text{NS}}(z'; L_1) (\tilde{\sigma}_0(x, y; z, z') - \tilde{\sigma}_0(x, y; z, 1)) dz' \right] . \end{aligned} \quad (5.31)$$

In the last step we have used the normalization (5.5) of the non-singlet structure function and exhibited the cancellation of the singular behavior for $z' \rightarrow 1$.

Expanding the all-order result (5.31) in powers of α confirms that the terms up to order $\mathcal{O}(\alpha^2)$ terms agree with the result of section 4.1.

5.3 The non-singlet structure function

In the previous section we found a very compact expression for the tagged photon cross section including the leading QED radiative corrections resummed to all orders. It involves the electron non-singlet structure function $D^{\text{NS}}(z; L)$, where L stands for any of the large logarithms $L_0 = \ln(E_e^2 \vartheta_0^2/m^2)$, $L_1 = \ln(Q^2/m^2) - L_0$. During the calculation of the one-loop radiative corrections to this process in chapter 4, we already encountered the first two orders of a perturbative expansion in α of D^{NS} . We shall now sketch methods aimed at practical determinations of this function for numerical applications, mostly following Jeřábek [113], Przybycień [114], and references quoted in these papers.

Introducing the parameter⁵

$$\beta = \frac{2\alpha}{\pi} L , \quad (5.32)$$

the Gribov-Lipatov evolution equation for the electron non-singlet structure function reads:

$$\frac{\partial D^{\text{NS}}(z, \beta)}{\partial \beta} = \frac{1}{4} \int_z^1 \frac{dy}{y} P_{ee}(y) D^{\text{NS}}\left(\frac{z}{y}, \beta\right) , \quad (5.33)$$

with boundary condition

$$D^{\text{NS}}(z, 0) = \delta(1 - z) . \quad (5.34)$$

The integro-differential equation (5.33) can be solved in various ways.

A perturbative solution is obtained by a power series ansatz,

$$D^{\text{NS}}(z, \beta) = \sum_{n=0}^N \frac{1}{n!} \left(\frac{\beta}{4}\right)^n P^{(n)}(z) + \mathcal{O}(\beta^{N+1}) , \quad (5.35)$$

⁵In the usual treatment of the Gribov-Lipatov equation, the running of the QED coupling α is incorporated by replacing β by

$$\beta(\mu^2) = \frac{2}{\pi} \int_{m^2}^{\mu^2} \frac{\alpha(Q^2) dQ^2}{Q^2} .$$

This modification serves to take into account the additional corrections from pair radiation. However, the forward taggers at HERA clearly detect only real (on-shell) photons. We shall therefore disregard these contributions at least for the tagged collinear initial state radiation and work with constant α .

yielding

$$P^{(0)}(z) = \delta(1 - z) , \quad (5.36)$$

and the recurrence relation

$$P^{(n)}(z) = \int_z^1 \frac{dy}{y} P_{ee}(y) P^{(n-1)}\left(\frac{z}{y}\right) , \quad n \geq 1 . \quad (5.37)$$

From (5.6) we find:

$$\int_0^1 dz P^{(n)}(z) = 0 , \quad n \geq 1 . \quad (5.38)$$

The coefficient functions $P^{(n)}$ are clearly divergent for $z \rightarrow 1$ and need regularization. Using a small auxiliary parameter $\epsilon \rightarrow 0$ as in (5.3), the first few terms obtained from recurrence relation (5.37) read (see also [115, 114, 116] and references):

$$P^{(i)}(z) = \lim_{\epsilon \rightarrow 0} \left[P_\delta^{(i)} \delta(1 - z) + P_\Theta^{(i)}(z) \Theta(1 - z - \epsilon) \right] , \quad (5.39)$$

$$P_\Theta^{(1)}(z) = \frac{1 + z^2}{1 - z} , \quad P_\delta^{(1)} = 2 \ln \epsilon + \frac{3}{2} ,$$

$$P_\Theta^{(2)}(z) = 2 \left[\frac{1 + z^2}{1 - z} \left(2 \ln(1 - z) - \ln z + \frac{3}{2} \right) + \frac{1}{2} (1 + z) \ln z - 1 + z \right] ,$$

$$P_\delta^{(2)} = \left(2 \ln \epsilon + \frac{3}{2} \right)^2 - \frac{2\pi^2}{3} ,$$

$$P_\Theta^{(3)}(z) = 24 \frac{1 + z^2}{1 - z} \left(\frac{1}{2} \ln^2(1 - z) + \frac{3}{4} \ln(1 - z) - \frac{1}{2} \ln z \ln(1 - z) \right. \\ \left. + \frac{1}{12} \ln^2 z - \frac{3}{8} \ln z + \frac{9}{32} - \frac{\pi^2}{12} \right) \quad (5.40)$$

$$+ 6(1 + z) \ln z \ln(1 - z) - 12(1 - z) \ln(1 - z) + \frac{3}{2} (5 - 3z) \ln z$$

$$- 3(1 - z) - \frac{3}{2} (1 + z) \ln^2 z + 6(1 + z) \text{Li}_2(1 - z) ,$$

$$P_\delta^{(3)} = \left(2 \ln \epsilon + \frac{3}{2} \right)^3 - 2\pi^2 \left(2 \ln \epsilon + \frac{3}{2} \right) + 16\zeta(3) .$$

As can already be seen from these expressions, the power series expansion (5.35) does not converge uniformly. As $z \rightarrow 1$, the coefficients behave as

$$P_\Theta^{(n)}(z) \sim n \cdot 2^n \cdot \frac{\ln^{n-1}(1 - z)}{1 - z} . \quad (5.41)$$

This is an obvious hint towards a closed form of the solution to the evolution equation in the limit $z \rightarrow 1$ which was found by Gribov:

$$D_G(z, \beta) = \frac{\exp[\beta/2 \cdot (3/4 - \gamma)]}{\Gamma(1 + \beta/2)} \frac{\beta}{2} (1 - z)^{\beta/2 - 1} . \quad (5.42)$$

Here $\gamma = 0.57721 \dots$ is Euler's constant. The softening of the perturbative behavior of the non-integrable singularity, $(1 - z)^{-1}$, to an integrable one is a consequence of the resummation of multiple soft photon emission to all orders ("exponentiation").

The knowledge of the solution (5.42) has lead to several proposals to improve the accuracy of finite order perturbative approximations to D^{NS} . This was pioneered by Kuraev and Fadin [105] who suggested the prescription

$$D^{\text{NS}}(z, \beta) = D_G(z, \beta) + \sum_{n=1}^N \beta^n \xi_n(z) + \mathcal{O}(\beta^{N+1}) , \quad (5.43)$$

where the functions $\xi_n(z)$ are derived from the requirement that (5.35) and (5.43) are identical up to order β^N .

An alternative prescription was formulated by Jadach and Ward [117]. They suggested a factorized ansatz,

$$\begin{aligned} D^{\text{NS}}(z, \beta) &= D_G(z, \beta) \Phi(z, \beta) \\ &= D_G(z, \beta) \sum_{n=0}^{N-1} \left(\frac{\beta}{2}\right)^n \phi_n(z) + \mathcal{O}(\beta^{N+1}) . \end{aligned} \quad (5.44)$$

Again, the coefficient functions $\phi_n(z)$ can in principle be determined by comparing the expansions (5.35) and (5.44). It is however advantageous to first derive an evolution equation for the function $\Phi(z, \beta)$, which can in turn be used to obtain a recurrence formula for the $\phi_n(z)$ [113]. The first three coefficients read:

$$\begin{aligned} \phi_0(z) &= \frac{1 + z^2}{2} , \\ \phi_1(z) &= -\frac{1}{8} [2(1 - z)^2 + (1 + 3z^3) \ln z] , \\ \phi_2(z) &= \frac{1}{8} \left[(1 - z)^2 + \frac{1 - 4z + 3z^2}{2} \ln z + \frac{1 + 7z^2}{12} \ln^2 z \right. \\ &\quad \left. + (1 - z^2) \text{Li}_2(1 - z) \right] . \end{aligned} \quad (5.45)$$

Further coefficients of the Jadach-Ward series were calculated analytically and numerically by Przybycień [114], where it was also found that the higher

order terms approach a very regular pattern. It is worthwhile to mention that the known coefficients of this series are much more compact than those of the perturbative series (5.39).

Numerical studies of the solutions to the Gribov-Lipatov equation obtained by Monte Carlo calculation and by inverse Mellin transforms show that, if truncated at the same order, the Jadach-Ward series converges significantly better than the Kuraev-Fadin series and provides a particularly good approximation to the full result already with the first three terms for typical LEP and HERA energies [118, 119, 115] except for very small z . However, even this can be remedied. Inspecting the coefficient functions (5.45) for $z \rightarrow 0$ it is evident that the poor convergence in this limit is due to $\phi_n(z) \sim \ln^n z$. Studying the $z \rightarrow 0$ behavior of the Gribov-Lipatov equation, this has lead Jeřabek to suggest a further improvement of the Jadach-Ward series that we will not pursue here. For details we refer the reader to [113].

5.4 Numerical results for higher order corrections

In order to assess the importance of the higher order QED corrections to the tagged photon process, we have calculated the radiative correction factor

$$\delta_{\text{h.o.}} = \left(\frac{d^3\sigma_{\text{h.o.}}}{dx dy dz} \bigg/ \frac{d^3\sigma_{\text{l.o.}}}{dx dy dz} \right) - 1, \quad (5.46)$$

with $\sigma_{\text{l.o.}}$ being the purely leading order, logarithmic part of the lowest order radiative cross section (5.19), and $\sigma_{\text{h.o.}}$ being the radiatively corrected cross section taking into account corrections at the level of leading logarithms as discussed above.

We have used the same sets of parameters as in the previous cases and the ALLM97 parameterization of the structure function of the proton, with fixed $R = 0.3$. As an example, we have performed the numerical calculation for the electron method. Tables 5.1 and 5.2 compare the numerical results for the radiative correction factor $\delta_{\text{h.o.}}$ for the leading logarithmic correction as obtained in section 4.1 with the all-order resummed result (5.31), evaluated using the Jadach-Ward approximation (5.44) of the electron non-singlet structure function, taking into account the first three coefficients (5.45) of the expansion.

As can be seen from these tables, the difference between the first-order corrections and the all-order resummed result is typically at the level of a few per mille. The difference slightly increases for small x and $y \rightarrow 0$, where

$\delta_{\text{h.o.}}$	$x = 10^{-4}$		$x = 10^{-1}$	
	$\mathcal{O}(\alpha)$ LL	all-order LL	$\mathcal{O}(\alpha)$ LL	all-order LL
$y = 0.05$	0.074	0.068	-0.040	-0.043
$y = 0.2$	0.093	0.089	0.024	0.019
$y = 0.5$	0.159	0.156	0.120	0.116
$y = 0.8$	0.344	0.344	0.351	0.350
$y = 0.95$	0.842	0.849	1.412	1.438

Table 5.1: Comparison of higher order leading logarithmic radiative corrections at $\mathcal{O}(\alpha)$ versus the all-order LL resummed calculation for the electron method for a tagged energy of 5 GeV

$\delta_{\text{h.o.}}$	$x = 10^{-4}$		$x = 10^{-1}$	
	$\mathcal{O}(\alpha)$ LL	all-order LL	$\mathcal{O}(\alpha)$ LL	all-order LL
$y = 0.05$	0.118	0.113	-0.016	-0.019
$y = 0.2$	0.148	0.146	0.049	0.045
$y = 0.5$	0.212	0.213	0.147	0.145
$y = 0.8$	0.385	0.393	0.379	0.387
$y = 0.95$	0.681	0.702	1.428	1.486

Table 5.2: Comparison of higher order leading logarithmic radiative corrections at $\mathcal{O}(\alpha)$ versus the all-order LL resummed calculation for the electron method for a tagged energy of 20 GeV

the phase space for photon emission is strongly constrained and effects of multiple soft photon emission become important.

For $y \rightarrow 1$, there is also a significant difference between the $\mathcal{O}(\alpha)$ and the all-order corrections. To understand and to check this finding, we have also calculated the $\mathcal{O}(\alpha^2)$ leading logarithmic corrections using eqs. (5.25ff). It turns out that the difference between the $\mathcal{O}(\alpha^2)$ and the all-order result is at the level of only a few $\times 10^{-4}$ for $0.01 < y < 0.99$, establishing that the differences in these tables also for large y are truly an indication of the size of higher order corrections beyond the first order, being essentially saturated by the contributions at $\mathcal{O}(\alpha^2)$. Note, however, that the effects from higher-order corrections are small compared to the uncertainties of the radiative corrections due the present errors in the ratio R even for rather small values of y .

Finally, there is still the question of the appropriate scale to be used in the leading logarithmic approximation. For the lowest order contribution to the radiative cross section, we can determine the “optimal” scale by “matching” the cross section (5.19) to the cross section obtained by a fixed order calculation, by comparing

$$\frac{1+z^2}{1-z} L_0^{\text{LLA}} \quad \text{vs.} \quad \frac{1+z^2}{1-z} L_0 - \frac{2z}{1-z} \equiv \frac{1+z^2}{1-z} (L_0 - 1) + 1 - z. \quad (5.47)$$

Obviously, the complete lowest order cross section is better approximated by $L_0^{\text{LLA}} \simeq L_0$ for $z \rightarrow 0$, corresponding to emission of a very hard collinear photon, while it appears more reasonable to set $L_0^{\text{LLA}} \simeq L_0 - 1$ for $z \rightarrow 1$. Taking this variation as an indication of the intrinsic uncertainty of the leading logarithmic approximation, we have checked the contributions from higher order corrections by varying the collinear logarithm from L_0 to $L_0 - 1$. We found a change in the contributions from higher order corrections being typically of the order of a few $\times 10^{-4}$ except in the region of large x and $y \rightarrow 1$, where it can reach the per mille level. However, this remaining scale ambiguity, which is resolvable by a calculation of the next-to-leading logarithmic contributions at order $\mathcal{O}(\alpha^2)$, appears to be well below the anticipated statistical accuracy of the corresponding experiments even after the upgrade of the HERA collider.

Chapter 6

Concluding Remarks and Outlook

In this report we have considered QED radiative processes at HERA, focusing on deep inelastic scattering with an exclusive photon being tagged in a forward photon detector. These processes can be used to extend the effective kinematic range for structure function measurements accessible with the HERA experiments down to lower values of the invariant momentum transfer Q^2 . The information obtained this way is important for accurate calculations of the radiative corrections to non-radiative deep inelastic scattering. The extended range allows testing the domain of applicability of perturbative QCD, as well as studying the transition into the non-perturbative regime which is described by phenomenological models. Furthermore, a measurement of the triple differential cross section $d^3\sigma/d\hat{x}d\hat{y}dz$, eq. (3.83), enables the separation of the structure functions of the proton $F_2(x, Q^2)$ and $F_L(x, Q^2)$ and thus a direct measurement of the longitudinal structure function without the need to run the HERA collider at different c.m.s. energies.

The understanding and control of the radiative corrections is crucial for precise theoretical predictions of cross sections. We discussed the calculation of the most important QED corrections to the tagged photon cross section in various approximations. The leading logarithmic approximation provides a rough estimate of the radiative corrections. It is quite useful for inclusive measurements, when final state radiation off the electron is unimportant (“calorimetric selection”), and describes the full leptonic corrections with an accuracy of several percent. Its compact expressions make it suitable for a qualitative understanding of the leading contributions to the corrections for different kinematic reconstruction methods.

The most important result presented in this work is the calculation of the full gauge-invariant set of leptonic QED corrections. We find that the differ-

ence between the full corrections and the leading logarithmic approximation is very significant. Depending on the reconstruction method and whether the measurement is calorimetric or exclusive, this difference can easily reach 5 or even 10 percent. Nevertheless, an approximation that keeps only the leading and next-to-leading logarithms appears to work well within an accuracy of typically a few per mille.

Finally, we estimated the size of the QED corrections at higher orders. Motivating an exclusive interpretation of the Gribov-Lipatov equation similar to QED photon shower algorithms in some Monte Carlo event generators, we obtained a compact, closed expression for the all-order leading logarithmic contributions to the tagged photon cross section. For this particular process, these higher order corrections turn out to be less important than the full corrections at relative order $\mathcal{O}(\alpha)$. Furthermore, they are typically smaller than those induced by the present uncertainty in the longitudinal structure function, F_L , at low Q^2 .

The apparently large dependence of the radiative corrections on F_L for the lepton method is not a real problem. Provided sufficient data is available, it can be solved similar to the case of non-radiative DIS by iteration, where the result of the analysis is fed back into the calculation of the radiative corrections. We thus conclude that the QED radiative corrections to the tagged photon process at HERA are well under control with the calculations described in this report. What remains to be done is an implementation of the QED corrections in a Monte Carlo event generator that is able to perform the calculations also for less symmetric and more complicated setups than assumed here.

For an overview of the experimental situation, figure 6.1 displays the kinematic coverage of the (x, Q^2) plane as presented at the ICHEP98 conference in Vancouver [120]. The contributions from HERA to the determination of the structure function F_2 essentially lie to the left of and above the dashed line that roughly describes the acceptance limit of the HERA experiments, while those from the fixed-target experiments are to the right and below this line. The HERA experiments cover a wide range in $y = Q^2/(xS)$ at sufficiently large x and Q^2 by combining several measurements, but in the interesting region of low x and for $Q^2 \lesssim 1 \text{ GeV}^2$ the kinematically domain accessible to non-radiative DIS becomes very narrow. The large, dark blue area in that region, indicated “H1 96 ISR prel.” corresponds to the kinematic domain that was added by analyzing events with tagged initial state radiation [23]; it overlaps with other measurements only at the left and upper boundaries. The analyzed radiative events obviously populate only the region of rather low Q^2 , justifying a posteriori our calculation that took into account only photon exchange and neglected contributions from the Z boson.

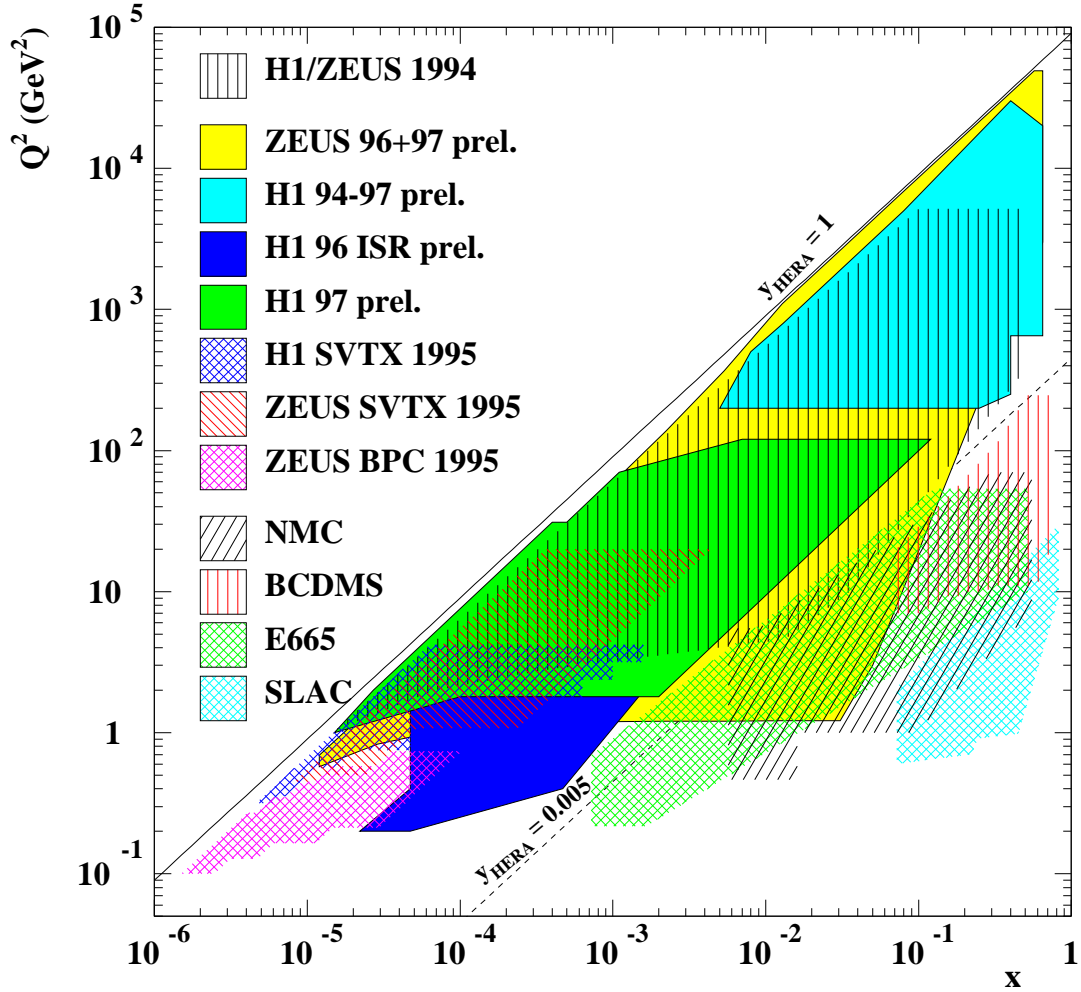


Figure 6.1: Measured regions of F_2 in the (x, Q^2) kinematic plane, as shown at the ICHEP98 conference. The nominal acceptance region of the HERA measurements corresponds to $y_{\text{HERA}} > 0.005$. The fixed-target experimental data occupy the region of high x at low Q^2 . (Taken from [120]).

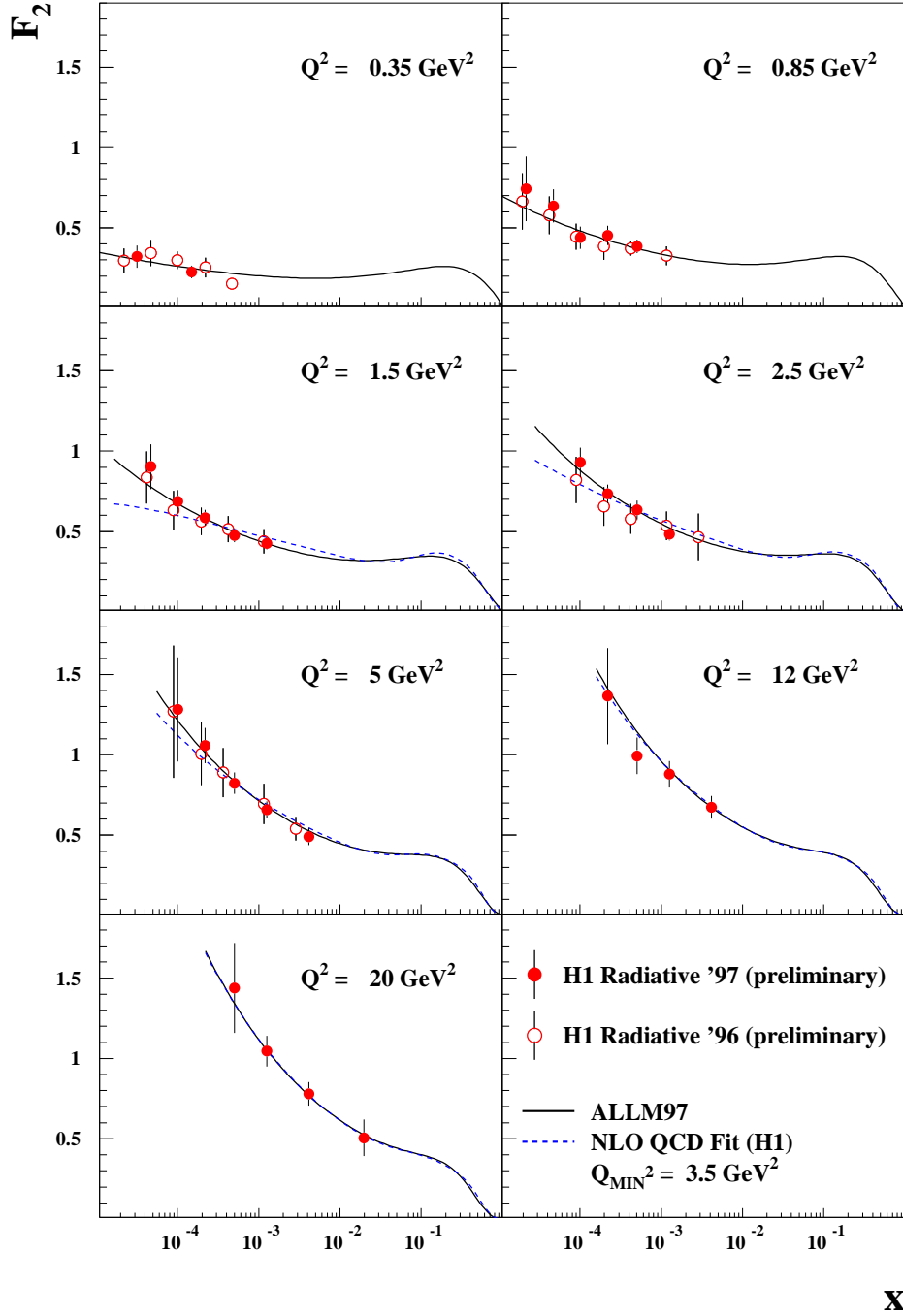


Figure 6.2: The structure function F_2 as determined from tagged ISR events as a function of x for fixed values of Q^2 . The data are compared to the ALLM97 parameterization (solid curve) and a NLO QCD fit to non-radiative F_2 data for $Q^2 \geq 3.5 \text{ GeV}^2$ (dashed curve). (Taken from [25]).

An improved determination of the structure function F_2 from tagged ISR events including the H1 97 ISR data has been presented at the DIS01 conference by the H1 collaboration [25] and is shown in fig. 6.2. The results of this analysis look very promising. There is good agreement with results on F_2 from non-radiative events in the kinematic regions where both methods overlap. Furthermore, it should be emphasized that the ISR data on F_2 describe the important domain where the transition from perturbative QCD ($Q^2 \gg 1 \text{ GeV}^2$) to photoproduction ($Q^2 \approx 0 \text{ GeV}^2$) occurs, within a single, coherent data set. This eliminates systematic errors stemming from uncertainties in the normalization when combining different data sets.

In principle it should be possible to simultaneously obtain the ratio $R = F_L/F_T$ during this analysis from the \hat{y} -dependence of the tagged photon cross section (3.83) at fixed \hat{x} and \hat{Q}^2 . The extraction method described in [28] has been applied to the H1 1996-97 data set [24], resulting so far only in upper limits on F_L and R which are not yet competitive with more model dependent indirect determinations. Improvements in the detectors and more data may change the situation.

In the present paper we have concentrated on DIS with unpolarized beams. For polarized protons there are additional spin-dependent structure functions g_1, g_2 . These are being measured at the HERMES experiment at HERA and at low Q^2 , using the polarization of the lepton beam and a polarized fixed target.

At the upgraded HERA machine, large longitudinal polarization of the lepton beams can also be expected for the H1 and ZEUS experiments. A primary motivation for lepton polarization is the spin dependence of weak interactions which can be exploited in searches for physics beyond the Standard Model, e.g., extensions to the electroweak sector with heavy vector bosons which couple to right-handed currents, or supersymmetry.

If acceleration of polarized protons were possible in the HERA ring, the kinematic domain accessible to spin-dependent lepton-proton scattering could be dramatically extended. Gakh et al. [121] have considered DIS with tagged photons for polarized beams and performed calculations for the corresponding leptonic QED radiative corrections with logarithmic accuracy. The leading logarithmic corrections coincide with those discussed in this work, but the next-to-leading logarithms are spin-dependent. The model-dependent lepton-quark interference terms which contribute to asymmetries such as spin-dependence have not yet been calculated. However, the initial plans for proton polarization in the HERA ring were set back with the recent HERA upgrade.

In the description of radiative processes in this report we have neglected the contributions which are due to emission off the hadron side; we argued

that they are not relevant for the determination of the lepton production structure functions. On the other hand, the case of radiative (quasi-)elastic scattering,

$$e + p \rightarrow e + \gamma + p ,$$

with the photon being well separated from the incident and scattered lepton, has recently received much attention. This process receives contributions from bremsstrahlung off from the lepton (Bethe-Heitler process, BH) as discussed in this report, but also from Deeply Virtual Compton Scattering (DVCS) on the proton,

$$\gamma^* + p \rightarrow \gamma + p ,$$

which gives access to the new class of so-called *generalized* or *non-forward* or *skewed* parton distributions (GPDs) [122]. Briefly put, GPDs are probability amplitudes to knock out a parton from a hadron and to put it back with a different longitudinal momentum. DVCS has a reliable theoretical basis within perturbative QCD. Its measurement provides a further opportunity to gain more insight into nucleon properties such as spin content [123]. The extraction of DVCS from the HERA data also requires to properly take into account the irreducible background from the BH process including the QED radiative corrections.

Radiative processes also play an important rôle at e^+e^- colliders. Most prominent are the “radiative return events” at LEP when running at energies far beyond the Z resonance: an incoming electron or positron may lose just as much energy as needed so that the effective collision energy matches the Z mass. Similar radiative return processes are also visible at other colliders, e.g., B and ϕ factories, and can be used to measure hadron production cross sections and resonances below the nominal machine c.m.s. energy [124]. The high luminosity of these factories can easily compensate the large suppression of the radiative process by a factor α/π despite the absence of a dedicated photon detector at small angles.

Another important application of radiative return events is the improvement of measurements of the ratio

$$R_{\text{had}}(s) \equiv \frac{\sigma(e^+e^- \rightarrow \text{hadrons})}{\sigma(e^+e^- \rightarrow \mu^+\mu^-)} ,$$

which is needed as input in the determination of the hadronic contribution to the running QED coupling $\alpha(Q^2)$. Measurements performed at the DAΦNE collider have provided encouraging results [125] and have also been used in the determination of the hadronic contributions to the muon $g - 2$ [126].

Acknowledgments

I would like to take this opportunity to thank Andrej B. Arbuzov and Eduard A. Kuraev for a fruitful collaboration on the subject. Edward E. Boos, Hans D. Dahmen, Panagiotis Manakos and Thorsten Ohl deserve special thanks for providing continuous support and helping in various ways to “keep me going”. I enjoyed discussions with colleagues, especially the organizers of the HERA 1998 Monte Carlo workshop [127] and in particular the convenors of the working group WG70 on QED radiative effects. Furthermore, I thank Manfred Fleischer for drawing my attention to this interesting subject, and finally Çiğdem İşsever for actually using some of the results presented here in the difficult radiative F_2 analysis.

Financial support from the Bundesministerium für Bildung und Forschung (BMBF), Germany, is gratefully acknowledged.

Appendix A

Auxiliary Calculations

In this appendix we present some details on how to efficiently perform the integration over the solid angle of the radiated photons in the forward region for the virtual corrections and the double collinear contributions.

Denoting the energy fraction of the i -th photon in units of the incident electron energy, $x_i = E_{\gamma,i}/E_e$, we write:

$$\int \widetilde{dk}_i = \frac{1}{(4\pi)^2} \int x_i dx_i \frac{E_e^2}{\pi} \int d\Omega_i . \quad (\text{A.1})$$

When a photon is almost collinear to a fermion it is convenient to rewrite the scalar product between the fermion and photon momenta as follows:

$$\begin{aligned} z_i &= 2p \cdot k_i = 2E_e E_{\gamma,i} (1 - \beta_e \cos \vartheta_i) = 2E_e E_{\gamma,i} (1 - \beta_e + \beta_e \tau_i) \\ &= \frac{2}{1 + \beta_e} x_i \left(m^2 + \frac{2\beta_e(1 + \beta_e)}{4} 4E_e^2 \tau_i \right) \\ &\simeq x_i (m^2 + 4E_e^2 \tau_i) =: x_i m^2 (1 + \zeta_i) . \end{aligned} \quad (\text{A.2})$$

In the last line we neglected terms of order $\mathcal{O}(m^2/E_e^2)$, and we introduced the variable

$$\zeta_i = \frac{4E_e^2}{m^2} \tau_i , \quad (\text{A.3})$$

which varies between 0 and $4E_e^2/m^2$.

Inserting this relation between in the expression for the photon phase space we obtain the parameterization:

$$\int \widetilde{dk}_i = \frac{1}{(4\pi)^2} \int x_i dx_i m^2 \int \frac{d\phi_i}{2\pi} d\zeta_i . \quad (\text{A.4})$$

A.1 Integrals for virtual corrections

For the calculation of the virtual corrections to the tagged photon process we need to integrate the virtually corrected Compton tensor (4.17) over the phase space of the (single) radiated photon, which is the solid angle of the photon detector PD:

$$\int_{\text{PD}} d\Omega_\gamma K_{\mu\nu} . \quad (\text{A.5})$$

We shall assume throughout that the photon detector be azimuthally symmetric with respect to the direction of the incoming electron direction and covering the range of polar angles $0 \leq \vartheta_\gamma \leq \vartheta_0$, with $\vartheta_0 \ll \theta$, where $\theta \sim \mathcal{O}(1)$ represents the scattering angle of the outgoing electron.

Introducing

$$\zeta_0 := \frac{E_e^2 \vartheta_0^2}{m^2} \gg 1 , \quad L_0 := \ln \zeta_0 \gg 1 , \quad (\text{A.6})$$

we can treat L_0 as a *large logarithm* for the conditions of the HERA photon detectors. It is large in the same sense as $L_Q = \ln(Q_l^2/m^2) \gg 1$. We therefore denote as large logarithmic terms those ones that contain at least one factor of L_0 or L_Q .

Consistently neglecting of terms of order $\mathcal{O}(\vartheta_0^2)$, we may drop terms proportional to the transverse momentum of the radiated photon with respect to the incoming lepton. Therefore we take $k \simeq (1-z)p_1$ and set

$$\tilde{p}_2 \simeq z\tilde{p}_1 \quad (\text{A.7})$$

in the integrand. Among the kinematic invariants of the Compton subprocess, \hat{s} , \hat{t} , \hat{u} and q^2 , only \hat{t} is small and may become of order m^2 . We parameterize it as

$$\hat{t} \equiv -2p_1 \cdot k = -m^2(1-z)(1+\zeta) , \quad 0 \leq \zeta \leq \zeta_0 . \quad (\text{A.8})$$

Furthermore, we set

$$\hat{s} = q^2 - \hat{t} - \hat{u} , \quad \hat{u} = -Q_l^2 , \quad q^2 = -(1-z)Q_l^2 . \quad (\text{A.9})$$

Inserting the decomposition (4.18) into (4.17), we obtain:

$$\begin{aligned} \frac{E_e^2}{\pi} \int_{\text{PD}} d\Omega_\gamma K_{\mu\nu} &= \frac{1}{1-z} (-Q_l^2 \tilde{g}_{\mu\nu} + 4z\tilde{p}_{1\mu}\tilde{p}_{1\nu}) \left(1 + \frac{\alpha}{2\pi}\rho\right) P(z, L_0) \\ &+ \frac{E_e^2}{\pi} \int_{\text{PD}} d\Omega_\gamma \frac{\alpha}{2\pi} \left[\tilde{g}_{\mu\nu} T'_g \right. \\ &\quad \left. + \tilde{p}_{1\mu}\tilde{p}_{1\nu} (T'_{11} + z^2 T'_{22} + z(T'_{12} + T'_{21})) \right] . \end{aligned} \quad (\text{A.10})$$

The straightforward integration of T'_g is essentially elementary and leads to transcendent functions including logarithms and dilogarithms. In the convention of Lewin [110], the dilogarithm (Spence function) reads:

$$\text{Li}_2(x) = - \int_0^x \frac{dy}{y} \ln(1-y) . \quad (\text{A.11})$$

Neglecting terms of $\mathcal{O}(\zeta_0^{-1})$ we find:

$$\begin{aligned} \frac{E_e^2}{\pi} \int d\Omega_\gamma T'_g &= \frac{Q_l^2}{1-z} [(A \ln z + B)P(z, L_0) + CL_0 + D] =: \frac{Q_l^2}{1-z} T , \\ A &= 2L_Q - L_0 - 2 \ln(1-z) , \\ B &= \ln^2 z - 2 \text{Li}_2(1-z) - \frac{1}{2} , \\ C &= -\frac{2z}{1-z} \ln z - z , \\ D &= -\frac{1-6z+4z^2}{1-z} (\text{Li}_2(1-z) + \ln z \ln(1-z)) \\ &\quad - 2z \left(\ln^2(1-z) + \frac{2\pi^2}{3} \right) + \frac{8z}{1-z} \ln z + 1 . \end{aligned} \quad (\text{A.12})$$

The integration over solid angle for the other coefficients of the tensor decomposition, T'_{ij} , $i, j = 1, 2$, is more involved. In that case the evaluation of the non-logarithmic terms (in the sense of being free of L_Q and L_0 in the final result) unavoidably leads to trilogarithms, defined as (see [110]):

$$\text{Li}_3(t) = \int_0^t \frac{dt'}{t'} \text{Li}_2(t') . \quad (\text{A.13})$$

The trilogarithms originate from a common integral that can be expressed in the following way:

$$\begin{aligned} \int_{t_0+\delta}^{\infty} dt \left(\frac{1}{t} - \frac{1}{t-t_0} \right) \text{Li}_2(1-t) &= \ln(\delta) \text{Li}_2(1-t_0) + \text{Li}_3(t_0) - \text{Li}_3(1-t_0) \\ &\quad + \text{Li}_3(1) - \frac{\pi^2}{6} \ln t_0 + \frac{1}{2} \ln^2 t_0 \ln(1-t_0) \\ &\quad + \mathcal{O}(\delta) . \end{aligned} \quad (\text{A.14})$$

This expression, regularized by a small parameter, $\delta \ll 1$, is valid for $0 < t_0 < 1$. As the integral converges at the upper limit, we have extended the

upper limit to infinity. We shall not reproduce here the somewhat lengthy calculation which can be done with the help of [110] and only requires some care in finding the proper analytic continuations of intermediate expressions.

The results for the integrations over the photon solid angle read:

$$\begin{aligned}
\frac{E_e^2}{\pi} \int d\Omega_\gamma T'_{11} &= \frac{z}{(1-z)^3} \left[-2(A \ln z + B) \frac{1+(1-z)^2}{1-z} L_0 - (3-z)AL_0 \right. \\
&\quad - \frac{4z(2-z)}{1-z} E + \left(\frac{3-8z}{z} C + \frac{5-11z+5z^2}{1-z} \right) L_0 + 2C \\
&\quad + 2z - 4 - \frac{2(1-4z+z^2)}{1-z} (\text{Li}_2(1-z) + \ln z \ln(1-z)) \\
&\quad \left. + (3-z) \left(\ln^2(1-z) + \frac{2\pi^2}{3} \right) - \frac{2(1-z)}{z} \ln(1-z) \right], \\
\frac{E_e^2}{\pi} \int d\Omega_\gamma T'_{22} &= \frac{1}{z(1-z)^3} \left[-2z^2 (A \ln z + B) \frac{1+2(1-z)^2}{1-z} L_0 \right. \\
&\quad + (1-3z)AL_0 + 8z(1-z)(A \ln z + B) - 4(1-z)^2 D \\
&\quad - \left(\frac{1-4z^2+8z^3}{z} C + \frac{(1-2z)(3-2z)(1-z-z^2)}{1-z} \right) L_0 \\
&\quad - \frac{2(1+4z-15z^2+8z^3)}{1-z} (\text{Li}_2(1-z) + \ln z \ln(1-z)) \\
&\quad - (1-11z+8z^2) \left(\ln^2(1-z) + \frac{2\pi^2}{3} \right) - \frac{4z(4-3z)}{1-z} E \\
&\quad \left. - \frac{2(1-z)(1+2z)}{z} \ln(1-z) + 2C + 4 - 6z \right], \quad (\text{A.15}) \\
\frac{E_e^2}{\pi} \int d\Omega_\gamma T'_{12} &= \frac{1}{(1-z)^3} \left[\frac{2z(2-z)}{1-z} [(A \ln z + B) L_0 + 2E] \right. \\
&\quad + (3-z)AL_0 - \left(\frac{3-8z}{z} C + \frac{5-11z+5z^2}{1-z} \right) L_0 - 2C \\
&\quad + 2z + \frac{2(3-6z+z^2)}{1-z} (\text{Li}_2(1-z) + \ln z \ln(1-z)) \\
&\quad \left. - (3-z) \left(\ln^2(1-z) + \frac{2\pi^2}{3} \right) + \frac{2(1-z)}{z} \ln(1-z) \right], \\
\frac{E_e^2}{\pi} \int d\Omega_\gamma T'_{21} &= \frac{1}{(1-z)^3} \left[(A \ln z + B) \frac{2z^2}{1-z} L_0 - (1-3z)AL_0 - 2C + 2z \right. \\
&\quad + \left(\frac{1-4z^2+8z^3}{z} C + \frac{(1-2z)(3-2z)(1-z-z^2)}{1-z} \right) L_0 \\
&\quad \left. + \frac{2(1-6z+15z^2-8z^3)}{1-z} (\text{Li}_2(1-z) + \ln z \ln(1-z)) \right]
\end{aligned}$$

$$\begin{aligned}
& + (1 - 11z + 8z^2) \left(\ln^2(1 - z) + \frac{2\pi^2}{3} \right) + \frac{4z(4 - 3z)}{1 - z} E \\
& + \frac{2(1 - z)(1 + 2z)}{z} \ln(1 - z) - 4(1 - z)^2 C L_0 \Big] ,
\end{aligned}$$

with the abbreviations A , B , C and D as given above and

$$\begin{aligned}
E &= \text{Li}_3(1 - z) - \text{Li}_3(z) + \text{Li}_3(1) - \frac{\pi^2}{6} \ln(z) \\
&- \left(\text{Li}_2(1 - z) + \frac{1}{2} \ln z \ln(1 - z) \right) \ln(1 - z) . \quad (\text{A.16})
\end{aligned}$$

The single and double logarithmic terms in L_0 and L_Q of the above expressions (A.12) and (A.15) agree with ref. [32].

It is easy to verify that the above integrals satisfy the relation

$$\int_{\text{PD}} d\Omega_\gamma \left\{ 4zT'_g + Q_l^2 [T'_{11} + z^2 T'_{22} + z(T'_{12} + T'_{21})] \right\} = 0 , \quad (\text{A.17})$$

which, after insertion into (A.10), leads to the factorization of the virtual corrections as in eq. (4.22).

As a further check we test the proper behavior in the soft photon limit, i.e., for $z \rightarrow 1$. The coefficients A , B , C and D are at most logarithmically divergent, and we find up to terms of order $\mathcal{O}((1 - z)^0)$:

$$\begin{aligned}
\left. \frac{E_e^2}{\pi} \int_{\text{PD}} d\Omega_\gamma K_{\mu\nu} \right|_{z \rightarrow 1} &\simeq (-Q_l^2 \tilde{g}_{\mu\nu} + 4\tilde{p}_{1\mu} \tilde{p}_{1\nu}) \frac{L_0 - 1}{1 - z} \left[1 + \frac{\alpha}{2\pi} \left(\rho + \frac{1}{2} \right) \right] \\
&= (-Q_l^2 \tilde{g}_{\mu\nu} + 4\tilde{p}_{1\mu} \tilde{p}_{1\nu}) \frac{L_0 - 1}{1 - z} \left(F_1^{(e)}(-Q_l^2) \right)^2 . \quad (\text{A.18})
\end{aligned}$$

Here $F_1^{(e)}(-Q_l^2)$ is the Dirac form factor of the electron in the one-loop approximation. The result (4.22) thus fulfills soft photon factorization as required, see also [84], eq. (36).

A.2 Integrals for double collinear emission

The calculation of the contribution from double collinear emission in section 4.2.3 assumes that only the sum of the photon energies, $(1 - z)E_e$, will be measured in the forward photon detector.

With the help of (A.1) we split the integration of expression (4.38) over the restricted two-photon phase space in the following way:

$$\begin{aligned} & \int \widetilde{dk}_1 \widetilde{dk}_2 \Theta(\vartheta_0 - \vartheta_1) \Theta(\vartheta_0 - \vartheta_2) \delta((1-z) - (x_1 + x_2)) \left[\dots \right] \\ &= \frac{1}{(4\pi)^4} \int x_1 dx_1 \int x_2 dx_2 \delta((1-z) - (x_1 + x_2)) \overline{\left[\dots \right]} . \end{aligned} \quad (\text{A.19})$$

In the last line we adopted the notation of Arbuzov et al. [128],

$$\overline{\left[\dots \right]} := \frac{E_e^4}{\pi^2} \int d\Omega_1 d\Omega_2 \Theta(\vartheta_0 - \vartheta_1) \Theta(\vartheta_0 - \vartheta_2) \left[\dots \right] , \quad (\text{A.20})$$

for the angular part of the integrals.

Equation (A.2) shows that in the collinear region the z_i are typically of the order of or larger than m^2 , even in the limit of high energies. This knowledge allows us to perform the proper counting of powers in selecting those terms in the differential cross section for single and double photon emission that contribute in the collinear region. For example,

$$\begin{aligned} \sigma &= 2k_1 \cdot k_2 = 2E_e^2 x_1 x_2 (1 - \vec{n}_1 \cdot \vec{n}_2) \\ &= 2x_1 x_2 E_e^2 [1 - \cos \vartheta_1 \cos \vartheta_2 - \sin \vartheta_1 \sin \vartheta_2 \cos(\phi_1 - \phi_2)] \\ &= 4x_1 x_2 E_e^2 \left[\tau_1 + \tau_2 - 2\tau_1 \tau_2 - 2\sqrt{\tau_1 \tau_2 (1 - \tau_1)(1 - \tau_2)} \cos(\phi_1 - \phi_2) \right] \\ &= x_1 x_2 m^2 \left[\zeta_1 (1 - \tau_2) + \zeta_2 (1 - \tau_1) \right. \\ &\quad \left. - 2\sqrt{\zeta_1 \zeta_2} \sqrt{(1 - \tau_1)(1 - \tau_2)} \cos(\phi_1 - \phi_2) \right] \\ &\simeq x_1 x_2 m^2 \left[\zeta_1 + \zeta_2 - 2\sqrt{\zeta_1 \zeta_2} \cos(\phi_1 - \phi_2) \right] . \end{aligned} \quad (\text{A.21})$$

In the last line it is assumed that both angles $\tau_{1,2} \ll 1$ in the collinear region. We then find:

$$\begin{aligned} \Delta &= z_1 + z_2 - \sigma \\ &\simeq m^2 \left[x_1 + x_2 + x_1 \zeta_1 r_2 + x_2 \zeta_2 r_1 + 2x_1 x_2 \sqrt{\zeta_1 \zeta_2} \cos(\delta\phi) \right] , \end{aligned} \quad (\text{A.22})$$

with $r_{1,2} = 1 - x_{1,2}$ and $\delta\phi \equiv \phi_2 - \phi_1$.

In the double collinear limit, the only non-trivial dependence on the azimuthal angles of the photons appears in the expression Δ . Performing the integration over the relative azimuthal angles of the two photons yields:

$$\int_{-\pi}^{\pi} \frac{d(\delta\phi)}{2\pi} \frac{1}{\Delta} \simeq \frac{1}{m^2} \left[(x_1 \zeta_1 r_2 + x_2 \zeta_2 r_1 + x_1 + x_2)^2 - 4x_1^2 x_2^2 \zeta_1 \zeta_2 \right]^{-1/2}$$

$$\begin{aligned}
& =: \frac{1}{m^2} D^{-1/2} , \\
\int_{-\pi}^{\pi} \frac{d(\delta\phi)}{2\pi} \frac{1}{\Delta^2} & \simeq \frac{1}{m^4} \cdot \frac{x_1 \zeta_1 r_2 + x_2 \zeta_2 r_1 + x_1 + x_2}{D^{3/2}} .
\end{aligned} \tag{A.23}$$

At this point it turns out to be useful to introduce yet another substitution for the polar angle variables of the photons:

$$\eta_1 = x_1 r_2 (1 + \zeta_1) , \quad \eta_2 = x_2 r_1 (1 + \zeta_2) . \tag{A.24}$$

Inserting these definitions into the above expression for D , we obtain:

$$\begin{aligned}
D(\eta_1, \eta_2) & = \eta_1^2 + \eta_2^2 + 2\eta_1 \eta_2 \frac{1 - x_1 - x_2 - x_1 x_2}{r_1 r_2} + \frac{4x_1 x_2}{r_1 r_2} (r_1 \eta_1 + r_2 \eta_2) \\
& = \eta_1^2 + \eta_2^2 + 2\eta_1 \eta_2 \cos \psi + 2(r_1 \eta_1 + r_2 \eta_2)(1 - \cos \psi) ,
\end{aligned} \tag{A.25}$$

where

$$\cos \psi := \frac{1 - x_1 - x_2 - x_1 x_2}{r_1 r_2} = 1 - \frac{2x_1 x_2}{r_1 r_2} . \tag{A.26}$$

Obviously, $-1 < \cos \psi \leq 1$ in the physically allowed range $0 \leq x_i < 1$, $0 \leq x_1 + x_2 < 1$. Therefore we find:

$$\begin{aligned}
\int_{-\pi}^{\pi} \frac{d(\delta\phi)}{2\pi} \frac{1}{\Delta} & \simeq \frac{1}{m^2} \cdot \frac{1}{\sqrt{D(\eta_1, \eta_2)}} , \\
\int_{-\pi}^{\pi} \frac{d(\delta\phi)}{2\pi} \frac{1}{\Delta^2} & \simeq \frac{1}{m^4} \cdot \frac{\eta_1 + \eta_2 + 2x_1 x_2}{[D(\eta_1, \eta_2)]^{3/2}} .
\end{aligned}$$

A.2.1 Integrals over photon angles

We shall now provide the relevant angular integrals needed for the contribution of two photons emitted almost collinearly to the incoming electron. With the replacement (A.24) definition (A.20) reads:

$$\begin{aligned}
\overline{[\dots]} & = m^4 \int_0^{\zeta_0} d\zeta_1 d\zeta_2 \int_{-\pi}^{\pi} \frac{d\phi_1}{2\pi} \frac{d\phi_2}{2\pi} [\dots] \\
& = \frac{m^4}{x_1 x_2 r_1 r_2} \int_{x_1 r_2}^{x_1 r_2 (1 + \zeta_0)} d\eta_1 \int_{x_2 r_1}^{x_2 r_1 (1 + \zeta_0)} d\eta_2 \int_{-\pi}^{\pi} \frac{d\phi_1}{2\pi} \frac{d\phi_2}{2\pi} [\dots] ,
\end{aligned} \tag{A.27}$$

and we have:

$$z_1 = \frac{m^2 \eta_1}{r_2} , \quad z_2 = \frac{m^2 \eta_2}{r_1} . \quad (\text{A.28})$$

The calculation is performed under the assumption that $\zeta_0 \gg 1$ and $\vartheta_0^2 \ll 1$.

We begin with the integrals that give rise to double and single large logarithms L_0 .

1/($\mathbf{z}_1 \mathbf{z}_2$):

This one is really trivial:

$$\overline{\left[\frac{1}{z_1 z_2} \right]} = \frac{1}{x_1 x_2} L_0^2 . \quad (\text{A.29})$$

1/($\mathbf{z}_1 \Delta$):

We start with the integration over azimuthal angles:

$$m^4 \int d\zeta_1 d\zeta_2 \int_{-\pi}^{\pi} \frac{d\phi_1}{2\pi} \frac{d\phi_2}{2\pi} \frac{1}{z_1 \Delta} = \frac{1}{x_1 x_2 r_1} \int \frac{d\eta_1}{\eta_1} \int \frac{d\eta_2}{\sqrt{D(\eta_1, \eta_2)}} . \quad (\text{A.30})$$

Next, the integral over η_2 is easily evaluated:

$$\int \frac{d\zeta_2}{\sqrt{D(\eta_1, \eta_2)}} = \ln E(\eta_1, \eta_2) , \quad (\text{A.31})$$

with

$$E(\eta_1, \eta_2) = \sqrt{D} + \frac{1}{2} \frac{\partial D}{\partial \eta_2} = \eta_1 \cos \psi + \eta_2 + r_2(1 - \cos \psi) + \sqrt{D} . \quad (\text{A.32})$$

Let us also define

$$\begin{aligned} \tilde{D}(\eta_1, \eta_2) &:= \eta_1^2 + \eta_2^2 + 2\eta_1 \eta_2 \cos \psi , \\ \tilde{E}(\eta_1, \eta_2) &:= \sqrt{\tilde{D}} + \frac{1}{2} \frac{\partial \tilde{D}}{\partial \eta_2} = \eta_1 \cos \psi + \eta_2 + \sqrt{\tilde{D}} , \end{aligned} \quad (\text{A.33})$$

which reproduce the leading asymptotic behavior of D and E for $\eta_{1,2} \gg 1$. Some special values that will be needed below are:

$$\begin{aligned} \sqrt{D(\eta_1, \eta_2 = x_2 r_1)} &= \eta_1 + x_2(1 + x_1) , \\ E(\eta_1, \eta_2 = x_2 r_1) &= \frac{2}{r_1 r_2} (\chi \eta_1 + x_2 r_2) , \end{aligned} \quad (\text{A.34})$$

$$\begin{aligned}
\sqrt{\tilde{D}(\eta_1, \eta_2 = 0)} &= \eta_1 , \\
\tilde{E}(\eta_1, \eta_2 = 0) &= (1 + \cos \psi) \eta_1 = \frac{2\chi}{r_1 r_2} \eta_1 , \\
\sqrt{\tilde{D}(\eta_1 = 0, \eta_2)} &= \eta_2 , \\
\tilde{E}(\eta_1 = 0, \eta_2) &= 2\eta_2 ,
\end{aligned}$$

where

$$\chi = 1 - x_1 - x_2 . \quad (\text{A.35})$$

Before proceeding with the η_1 integration, let us note that we are finally interested in definite integrals over η_2 , with lower limit $\eta_2^{\min} = x_2 r_1$. Choosing the integration constant in (A.31) appropriately so that the antiderivative vanishes if η_2 is taken at the lower limit, we can decompose the logarithm in the integrand in the following way:

$$\ln \frac{E(\eta_1, \eta_2)}{E(\eta_1, x_2 r_1)} = \ln \frac{\tilde{E}(0, \eta_2)}{\tilde{E}(\eta_1, 0)} - \ln \frac{E(\eta_1, x_2 r_1)}{\tilde{E}(\eta_1, 0)} + \ln \frac{\tilde{E}(\eta_1, \eta_2)}{\tilde{E}(0, \eta_2)} + \ln \frac{E(\eta_1, \eta_2)}{\tilde{E}(\eta_1, \eta_2)} . \quad (\text{A.36})$$

Since we shall be interested in the case $\eta_2^{\max} \gg 1$, there will be certain simplifications possible when considering the integral over η_1 .

The first integral is readily evaluated,

$$\begin{aligned}
\int \frac{d\eta_1}{\eta_1} \ln \frac{\tilde{E}(0, \eta_2)}{\tilde{E}(\eta_1, 0)} &= \int \frac{d\eta_1}{\eta_1} \ln \frac{2\eta_2}{(1 + \cos \psi) \eta_1} \\
&= \ln \eta_1 \ln \frac{2\eta_2}{1 + \cos \psi} - \frac{1}{2} \ln^2 \eta_1 . \quad (\text{A.37})
\end{aligned}$$

We shall later see that this term contributes to the leading double logarithms.

The second term in the decomposition (A.36) gives:

$$\begin{aligned}
\int \frac{d\eta_1}{\eta_1} \ln \frac{E(\eta_1, x_2 r_1)}{\tilde{E}(\eta_1, 0)} &= \int \frac{d\eta_1}{\eta_1} \ln \frac{\chi \eta_1 + x_2 r_2}{\chi \eta_1} = \int \frac{d\eta_1}{\eta_1} \ln \left(1 + \frac{x_2 r_2}{\chi \eta_1} \right) \\
&= \text{Li}_2 \left(-\frac{x_2 r_2}{\chi \eta_1} \right) . \quad (\text{A.38})
\end{aligned}$$

The third piece gives:

$$\begin{aligned}
\int \frac{d\eta_1}{\eta_1} \ln \frac{\tilde{E}(\eta_1, \eta_2)}{\tilde{E}(0, \eta_2)} &= \int \frac{d\eta_1}{\eta_1} \ln \frac{\eta_1 \cos \psi + \eta_2 + \sqrt{\tilde{D}}}{(1 + \cos \psi) \eta_1} \\
&= \Xi \left(\cos \psi, \frac{\eta_1}{\eta_2} \right) , \quad (\text{A.39})
\end{aligned}$$

where we introduced the auxiliary function

$$\Xi(t; x) := \int_0^x \frac{d\xi}{\xi} \ln \frac{\sqrt{1 + 2t\xi + \xi^2} + t\xi + 1}{2} . \quad (\text{A.40})$$

Evaluating the integral for $-1 < t \leq 1$ and using various identities for dilogarithms (see e.g., [110]) yields:

$$\begin{aligned} \Xi(t; x) &= \frac{1}{2} \ln^2 \left(\frac{\sqrt{1 + 2tx + x^2} + tx + 1}{2} \right) \\ &+ \text{Li}_2 \left(\frac{(1+t)x}{\sqrt{1 + 2tx + x^2} + tx + 1} \right) \\ &+ \text{Li}_2 \left(-\frac{(1-t)x}{\sqrt{1 + 2tx + x^2} + tx + 1} \right) . \end{aligned} \quad (\text{A.41})$$

The asymptotic behavior of this expression for $x \rightarrow +\infty$ is found to be:

$$\Xi(t; x) = \frac{1}{2} \ln^2 \left(\frac{(1+t)x}{2} \right) + \frac{\pi^2}{6} + \text{Li}_2 \left(-\frac{1-t}{1+t} \right) - \frac{1}{x} + \mathcal{O}(x^{-2}) . \quad (\text{A.42})$$

We are finally left with the fourth contribution,

$$\int \frac{d\eta_1}{\eta_1} \ln \frac{E(\eta_1, \eta_2)}{\tilde{E}(\eta_1, \eta_2)} = \int \frac{d\eta_1}{\eta_1} \ln \frac{\eta_1 \cos \psi + \eta_2 + r_2(1 - \cos \psi) + \sqrt{D}}{\eta_1 \cos \psi + \eta_2 + \sqrt{\tilde{D}}} , \quad (\text{A.43})$$

which appears quite elaborate but can nevertheless be reduced to dilogarithms. Fortunately, this effort is not necessary as we need this expression for large $\eta_2 = x_2 r_1 (1 + \zeta_0) \gg 1$. As a consequence the ratio $\xi = \eta_1 / \eta_2$ does not become very large, since we integrate symmetrically over the polar angles of the photons. Substituting $\eta_1 = \xi \eta_2$ and expanding the integrand for large η_2 , we obtain:

$$\int \frac{d\xi}{\xi} \left[\frac{1}{\eta_2} (r_2(1 - \cos \psi) + \mathcal{O}(\xi)) + \mathcal{O}\left(\frac{1}{\eta_2^2}\right) \right] \sim \frac{1}{\eta_2} \ln \frac{\eta_1}{\eta_2} . \quad (\text{A.44})$$

Therefore, this expression is $\mathcal{O}(1/\eta_2)$ and therefore always negligible for symmetric integration.

Collecting the contributions from the first three terms of the decomposition, inserting the integration limits and keeping only terms that are not suppressed by factors $1/\zeta_0$, we find:

$$\overline{\left[\frac{1}{z_1 \Delta} \right]} = \frac{1}{x_1 x_2 r_1} \left[\frac{1}{2} L_0^2 + L_0 \ln \frac{x_2 r_1^2}{x_1 z} + \text{Li}_2 \left(-\frac{x_2}{x_1 z} \right) + \Xi \left(\cos \psi; \frac{x_1 r_2}{x_2 r_1} \right) \right] . \quad (\text{A.45})$$

$\mathbf{m}^2/(\mathbf{z}_1^2\Delta)$:

With the same steps as in the previous case we first find:

$$\begin{aligned} m^4 \int d\zeta_1 d\zeta_2 \int_{-\pi}^{\pi} \frac{d\phi_1}{2\pi} \frac{d\phi_2}{2\pi} \frac{m^2}{z_1^2\Delta} &= \frac{r_2}{x_1 x_2 r_1} \int \frac{d\eta_1}{\eta_1^2} \int \frac{d\eta_2}{\sqrt{D(\eta_1, \eta_2)}} \\ &= \frac{r_2}{x_1 x_2 r_1} \int \frac{d\eta_1}{\eta_1^2} \ln E(\eta_1, \eta_2) . \end{aligned} \quad (\text{A.46})$$

Again we apply the decomposition (A.36) to the logarithm in the integrand. Integrating the sum of the first and second term, we obtain:

$$\begin{aligned} \int \frac{d\eta_1}{\eta_1^2} \ln \frac{\tilde{E}(0, \eta_2)}{E(\eta_1, x_2 r_1)} &= \int \frac{d\eta_1}{\eta_1^2} \ln \frac{r_1 r_2 \eta_2}{\chi \eta_1 + x_2 r_2} \\ &= \frac{\chi}{x_2 r_2} \ln \left(\frac{\chi \eta_1 + x_2 r_2}{\eta_1} \right) - \frac{1}{\eta_1} \ln \frac{r_1 r_2 \eta_2}{\chi \eta_1 + x_2 r_2} . \end{aligned} \quad (\text{A.47})$$

The third term can be neglected for symmetric integration over the photon polar angles. This can be seen by substituting $\eta_1 = \eta_2/\xi'$, leading to

$$\begin{aligned} \frac{1}{\eta_2} \int d\xi' \ln \frac{\tilde{E}(\eta_2/\xi', \eta_2)}{\tilde{E}(0, \eta_2)} &= \frac{1}{\eta_2} \int d\xi' \ln \frac{\xi' + \cos \psi + \sqrt{1 + 2\xi' \cos \psi + \xi'^2}}{1 + \cos \psi} \\ &= \mathcal{O}\left(\frac{1}{\eta_2}\right) . \end{aligned} \quad (\text{A.48})$$

The contribution from the fourth term of decomposition (A.36) turns out to be negligible for the same reason. We thus obtain:

$$\left[\frac{m^2}{z_1^2\Delta} \right] = \frac{1}{x_1^2 x_2 r_1} \left[L_0 + \ln \frac{x_2 r_1}{1-z} \right] - \frac{z}{x_1 x_2^2 r_1} \ln \frac{r_1(1-z)}{x_1 z} . \quad (\text{A.49})$$

$\mathbf{z}_2/(\mathbf{z}_1\Delta^2)$:

After integration over azimuthal angles we have:

$$m^4 \int d\zeta_1 d\zeta_2 \int_{-\pi}^{\pi} \frac{d\phi_1}{2\pi} \frac{d\phi_2}{2\pi} \frac{z_2}{z_1 \Delta^2} = \frac{1}{x_1 x_2 r_1^2} \int d\eta_1 \int d\eta_2 \frac{\eta_2(\eta_1 + \eta_2 + 2x_1 x_2)}{\eta_1 [D(\eta_1, \eta_2)]^{3/2}} . \quad (\text{A.50})$$

It is interesting to note that the integral over η_2 can be split into one piece that is precisely the same as occurred in the discussion of $1/(z_1\Delta)$, plus

another one which at this stage is free from logarithms and involves only algebraic functions.

$$\begin{aligned}
\int d\eta_2 \frac{\eta_2(\eta_1 + \eta_2 + 2x_1x_2)}{\eta_1 [D(\eta_1, \eta_2)]^{3/2}} &= \frac{1}{\eta_1} \int \frac{d\eta_2}{\sqrt{D(\eta_1, \eta_2)}} \\
&- \frac{1}{1 + \cos \psi} \frac{1}{\sqrt{D(\eta_1, \eta_2)}} \\
&- (2 - r_1) \frac{\eta_2}{\eta_1 \sqrt{D(\eta_1, \eta_2)}} \\
&+ \left(\frac{1}{1 + \cos \psi} - r_1 \right) \frac{\chi \eta_2 + x_2(x_1 - \chi)}{(\chi \eta_1 + x_2 r_2) \sqrt{D(\eta_1, \eta_2)}}.
\end{aligned} \tag{A.51}$$

The integration of the r.h.s. over η_1 now is quite simple. The first term leads to an expression that has been discussed further above. The remaining antiderivatives read:

$$\begin{aligned}
\int \frac{d\eta_1}{\sqrt{D(\eta_1, \eta_2)}} &= \ln F(\eta_1, \eta_2), \\
\int \frac{\eta_2}{\eta_1 \sqrt{D(\eta_1, \eta_2)}} d\eta_1 &= G(\eta_1, \eta_2), \\
\int \frac{\chi \eta_2 + x_2(x_1 - \chi)}{(\chi \eta_1 + x_2 r_2) \sqrt{D(\eta_1, \eta_2)}} d\eta_1 &= \ln K(\eta_1, \eta_2),
\end{aligned} \tag{A.52}$$

with

$$\begin{aligned}
F(\eta_1, \eta_2) &= \sqrt{D} + \frac{1}{2} \frac{\partial D}{\partial \eta_1} = \eta_2 \cos \psi + \eta_1 + r_1(1 - \cos \psi) + \sqrt{D}, \\
G(\eta_1, \eta_2) &= \sqrt{\frac{\eta_2}{\eta_2 + 2r_2(1 - \cos \psi)}} \left\{ \ln \eta_1 \right. \\
&\quad \left. - \ln \left[\sqrt{D} + \frac{\eta_2^2 + \eta_1 \eta_2 \cos \psi + (1 - \cos \psi)(\eta_1 r_1 + 2\eta_2 r_2)}{\sqrt{\eta_2[\eta_2 + 2r_2(1 - \cos \psi)]}} \right] \right\}, \\
K(\eta_1, \eta_2) &= \frac{\sqrt{D} - \eta_1 \cos \psi - \eta_2 - r_2(1 - \cos \psi)}{\chi \eta_1 + x_2 r_2} + \frac{(1 - \chi)(1 - \cos \psi)}{\chi \eta_2 + x_2(x_1 - \chi)}.
\end{aligned} \tag{A.53}$$

Collecting the above expressions and inserting limits, we obtain for the contribution in the doubly collinear region:

$$\overline{\left[\frac{z_2}{z_1 \Delta^2} \right]} = \frac{1}{x_1 x_2 r_1^2} \left\{ \frac{1}{2} L_0^2 + L_0 \left[\ln \frac{x_2 r_1^2}{x_1 \chi} - 1 + \frac{x_1 x_2}{\chi} \right] \right\}$$

$$\begin{aligned}
& + \text{Li}_2 \left(-\frac{x_2}{x_1 \chi} \right) + \Xi \left(\cos \psi; \frac{x_1 r_2}{x_2 r_1} \right) \\
& + \frac{r_1 r_2 - 2\chi}{\chi} \ln(2x_2) + \frac{r_1(r_2 - 2\chi)}{\chi} \ln \frac{x_1}{1 - \chi} \\
& + \frac{r_1(3r_2 - 4\chi)}{2\chi} \ln \chi - \frac{r_1 r_2 + 4x_1 \chi}{2\chi} \ln r_1 - \frac{r_1 r_2}{2\chi} \ln r_2 \\
& + \frac{4\chi - r_1 r_2}{2\chi} \ln (\eta + x_2 r_1 + x_1 r_2 \cos \psi) \\
& - \frac{r_1 r_2}{2\chi} \ln (\eta + x_1 r_2 + x_2 r_1 \cos \psi) \Big\} ,
\end{aligned} \tag{A.54}$$

with the abbreviation

$$\eta = \sqrt{\tilde{D}(x_1 r_2, x_2 r_1)} = \sqrt{(x_1 + x_2)(x_1 + x_2 - 4x_1 x_2)} . \tag{A.55}$$

Comparing so far the above results with [108, 128], we find that we reproduce the double and single logarithms in L_0 . Furthermore, our expressions also contain the ‘finite’ terms for $\zeta_0 \gg 1$.

The double Compton tensor in the double collinear region (4.35) contains also further terms that contribute only non-(logarithmically-)enhanced terms. The corresponding integrals are convergent if we remove the upper limit by taking $\zeta_0 \rightarrow \infty$. Inspecting the expressions for these additional terms reveals that the corresponding integrands contribute only when $\eta_i \lesssim \mathcal{O}(1)$, i.e., the angle of both photons is of the order of $\vartheta_{1,2} \lesssim \mathcal{O}(m/E_e)$. Taking one photon at a large angle immediately leads to a strong suppression. We therefore take the upper limit of both integration variables η_i as infinite.

$\mathbf{m}^2/(\mathbf{z}_1 \mathbf{z}_2 \Delta)$:

$$m^4 \int d\zeta_1 d\zeta_2 \int_{-\pi}^{\pi} \frac{d\phi_1}{2\pi} \frac{d\phi_2}{2\pi} \frac{m^2}{z_1 z_2 \Delta} = \frac{1}{x_1 x_2} \int \frac{d\eta_1 d\eta_2}{\eta_1 \eta_2 \sqrt{D(\eta_1, \eta_2)}} \tag{A.56}$$

One integration, e.g., over η_2 , is elementary:

$$\int \frac{d\eta_2}{\eta_2 \sqrt{D(\eta_1, \eta_2)}} = \frac{\ln \eta_2 - \ln \left[\sqrt{D} + \frac{\eta_1^2 + \eta_1 \eta_2 \cos \psi + (1 - \cos \psi)(2\eta_1 r_1 + \eta_2 r_2)}{\sqrt{\eta_1 [\eta_1 + 2r_1(1 - \cos \psi)]}} \right] + c_1}{\sqrt{\eta_1 [\eta_1 + 2r_1(1 - \cos \psi)]}} . \tag{A.57}$$

The integral is convergent for $\eta_2 \rightarrow \infty$, so we are free to choose the constant c_1 (w.r.t. η_2) in such a way that the r.h.s. of (A.57) vanishes in that limit:

$$c_1 = \ln \left[1 + \frac{\eta_1 \cos \psi + r_2(1 - \cos \psi)}{\sqrt{\eta_1 [\eta_1 + 2r_1(1 - \cos \psi)]}} \right] . \tag{A.58}$$

We therefore obtain for the definite integral:

$$\int_{x_2 r_1}^{\infty} \frac{d\eta_2}{\eta_2 \sqrt{D(\eta_1, \eta_2)}} = \frac{\ln \left[\eta_1 + x_2(1 + x_1) + \frac{\eta_1^2 + r_1 \eta_1 [x_2 \cos \psi + 2(1 - \cos \psi)] + 2x_1 x_2^2}{\sqrt{\eta_1 [\eta_1 + 2r_1(1 - \cos \psi)]}} \right]}{\sqrt{\eta_1 [\eta_1 + 2r_1(1 - \cos \psi)]}} - \frac{\ln(x_2 r_1) + c_1}{\sqrt{\eta_1 [\eta_1 + 2r_1(1 - \cos \psi)]}}. \quad (\text{A.59})$$

The integration over η_1 is attacked with the help of the substitution

$$\eta_1 = \frac{2r_1(1 - \cos \psi)}{\rho_1(\rho_1 + 2)}, \quad \frac{d\eta_1}{\eta_1^{3/2} \sqrt{\eta_1 + 2r_1(1 - \cos \psi)}} = \frac{d\rho_1}{r_1(1 - \cos \psi)}, \quad (\text{A.60})$$

leading to:

$$\int_{x_1 r_2}^{\infty} \frac{d\eta_1}{\eta_1} \int_{x_2 r_1}^{\infty} \frac{d\eta_2}{\eta_2 \sqrt{D(\eta_1, \eta_2)}} = \frac{r_2}{2x_1 x_2} \int_0^{2x_2/r_2} d\rho_1 \ln \frac{(\rho_1 + 1)(\rho_1 + 2x_1/r_2)}{\rho_1(\rho_1 + 2\chi/r_2)}. \quad (\text{A.61})$$

Its evaluation yields:

$$\left[\frac{m^2}{z_1 z_2 \Delta} \right] = \frac{1}{x_1^2 x_2^2} \left[(1 - \chi) \ln(1 - \chi) + \chi \ln \chi - r_1 \ln r_1 - r_2 \ln r_2 - x_1 \ln x_1 - x_2 \ln x_2 \right]. \quad (\text{A.62})$$

$m^2/(z_1 \Delta^2)$:

$$m^4 \int d\zeta_1 d\zeta_2 \int_{-\pi}^{\pi} \frac{d\phi_1}{2\pi} \frac{d\phi_2}{2\pi} \frac{m^2}{z_1 \Delta^2} = \frac{1}{x_1 x_2 r_1} \int d\eta_1 d\eta_2 \frac{\eta_1 + \eta_2 + 2x_1 x_2}{\eta_1 [D(\eta_1, \eta_2)]^{3/2}}. \quad (\text{A.63})$$

Performing the integration over η_2 , one finds for the r.h.s.:

$$\frac{1}{2x_1 x_2^2} \int \frac{d\eta_1}{\sqrt{D(\eta_1, \eta_2)}} \left[\frac{\eta_2 - 2x_2}{\eta_1} - \frac{\chi \eta_2 + x_2(x_1 - \chi)}{\chi \eta_1 + x_2 r_2} \right] \quad (\text{A.64})$$

Obviously, this can be expressed in terms of the already known expressions G and $\ln K$ given in (A.53). However, this is not really necessary, as we only need the definite integral which is absolutely convergent. Evaluating (A.64) in the limits $\eta_2 = x_2 r_1 \dots \infty$, we arrive at a much simpler expression:

$$\frac{1}{x_1 x_2^2} \int d\eta_1 \frac{x_2 r_2}{\eta_1 [\chi \eta_1 + x_2 r_2]}. \quad (\text{A.65})$$

This immediately leads to

$$\overline{\left[\frac{m^2}{z_1 \Delta^2}\right]} = \frac{1}{x_1 x_2^2} \ln \frac{r_1(1-\chi)}{x_1 \chi} . \quad (\text{A.66})$$

$\mathbf{m}^4/(\mathbf{z}_1^2 \Delta^2)$:

This integral can be dealt with in a similar way. Starting from the expression

$$m^4 \int d\zeta_1 d\zeta_2 \int_{-\pi}^{\pi} \frac{d\phi_1}{2\pi} \frac{d\phi_2}{2\pi} \frac{m^4}{z_1^2 \Delta^2} = \frac{r_2}{x_1 x_2 r_1} \int d\eta_1 d\eta_2 \frac{\eta_1 + \eta_2 + 2x_1 x_2}{\eta_1^2 [D(\eta_1, \eta_2)]^{3/2}} , \quad (\text{A.67})$$

and performing the integration over η_2 , we arrive at the following expression for the r.h.s.:

$$\frac{1}{2x_1 x_2^3} \int \frac{d\eta_1}{\eta_1 \sqrt{D(\eta_1, \eta_2)}} \left[\frac{\eta_2 - 2x_2}{\eta_1} - \frac{\chi \eta_2 + x_2(x_1 - \chi)}{\chi \eta_1 + x_2 r_2} \right] . \quad (\text{A.68})$$

Again, we evaluate this in the limits $\eta_2 = x_2 r_1 \dots \infty$, to obtain:

$$\frac{r_2}{x_1 x_2^2} \int d\eta_1 \frac{x_2 r_2}{\eta_1^2 [\chi \eta_1 + x_2 r_2]} . \quad (\text{A.69})$$

The remaining integral is trivial, yielding:

$$\overline{\left[\frac{m^4}{z_1^2 \Delta^2}\right]} = \frac{1}{x_1^2 x_2^2} \left[1 - \frac{x_1 \chi}{x_2} \ln \frac{r_1(1-\chi)}{x_1 \chi} \right] . \quad (\text{A.70})$$

$\mathbf{m}^4/(\mathbf{z}_1 \mathbf{z}_2 \Delta^2)$:

The last and most involved integral among the non-logarithmic ones that is needed for the double collinear region is the following:

$$m^4 \int d\zeta_1 d\zeta_2 \int_{-\pi}^{\pi} \frac{d\phi_1}{2\pi} \frac{d\phi_2}{2\pi} \frac{m^4}{z_1 z_2 \Delta^2} = \frac{1}{x_1 x_2} \int d\eta_1 d\eta_2 \frac{\eta_1 + \eta_2 + 2x_1 x_2}{\eta_1 \eta_2 [D(\eta_1, \eta_2)]^{3/2}} . \quad (\text{A.71})$$

We start with the integration over η_2 to obtain:

$$\begin{aligned} \frac{1}{x_1 x_2} \int \frac{d\eta_1}{\sqrt{D(\eta_1, \eta_2)}} & \left[\frac{r_2(r_1 \eta_2 + 4x_1 x_2)}{4x_1 x_2 \eta_1^2} + \frac{r_1 \chi [\chi \eta_2 + x_2(x_1 - \chi)]}{2x_2^2(x_1 - \chi) [\chi \eta_1 + x_2 r_2]} \right. \\ & \left. + \frac{r_1^2 + x_1^2 - x_2^2}{4x_1 x_2 \eta_1} - \frac{r_1 \eta_2 [\chi^2 + x_1(4\chi - x_1)]}{16x_1^2 x_2^2 \eta_1} \right] \end{aligned} \quad (\text{A.72})$$

$$\begin{aligned}
& -\frac{r_1 r_2^4 \eta_2}{16x_1^2 x_2^2 (x_1 - \chi)[r_2 \eta_1 + 4x_1 x_2]} - \frac{r_2^2(1+x_2)}{4x_1 x_2 [r_2 \eta_1 + 4x_1 x_2]} \Bigg] \\
& + \frac{1}{x_1 x_2} \int d\eta_1 \frac{\eta_1 + r_1 r_2 (1 - \cos \psi)}{\eta_1^{5/2} \sqrt{\eta_1 + 2r_1(1 - \cos \psi)}}^3 \left[\ln \eta_2 \right. \\
& \quad \left. - \ln \left[\sqrt{D(\eta_1, \eta_2)} + \frac{\eta_1^2 + \eta_1 \eta_2 \cos \psi + (1 - \cos \psi)(2\eta_1 r_1 + \eta_2 r_2)}{\sqrt{\eta_1 [\eta_1 + 2r_1(1 - \cos \psi)]}} \right] \right].
\end{aligned}$$

Again, these expressions confirm that the integrals are absolutely convergent. We therefore immediately insert the limits for η_2 . The remaining η_1 integration is straightforward for the first part of (A.72); the second is part is tackled with the help of the substitution (A.60):

$$\begin{aligned}
& \frac{1}{x_1 x_2} \left[-\frac{1}{2x_1 x_2} + \frac{r_1 \chi}{x_2^2 (\chi - x_1)} \ln \frac{r_1 (1 - \chi)}{x_1 \chi} + \frac{r_2^2 (1 + x_2)}{4x_1 x_2^2 (\chi - x_1)} \ln \frac{r_2}{1 + x_2} \right] \\
& + \frac{r_2^2}{x_1^3 x_2^3} \int_0^{2x_2/r_2} d\rho_1 \frac{\rho_1 (2 + \rho_1) [r_2 (\rho_1 + 1)^2 + 2 - r_2]}{16(\rho_1 + 1)^2} \ln \frac{(\rho_1 + 2)(\rho_1 + 2x_1/r_2)}{\rho_1 (\rho_1 + 2\chi/r_2)} \\
& = \frac{1}{6x_1^3 x_2^3} \left[x_1^2 (3 - 2x_1) \ln \frac{(1 - \chi)r_1}{x_1 \chi} + x_2^2 (3 - 2x_2) \ln \frac{(1 - \chi)r_2}{x_2 \chi} \right. \\
& \quad \left. + \ln \frac{\chi}{r_1 r_2} - 2x_1 x_2 \right]. \tag{A.73}
\end{aligned}$$

Fortunately, an intermediate spurious singularity in $(\chi - x_1)$ cancels, and we find:

$$\begin{aligned}
\left[\frac{m^4}{z_1 z_2 \Delta^2} \right] & = \frac{1}{6x_1^3 x_2^3} \left[x_1^2 (3 - 2x_1) \ln \frac{(1 - \chi)r_1}{x_1 \chi} + x_2^2 (3 - 2x_2) \ln \frac{(1 - \chi)r_2}{x_2 \chi} \right. \\
& \quad \left. + \ln \frac{\chi}{r_1 r_2} - 2x_1 x_2 \right]. \tag{A.74}
\end{aligned}$$

The remaining integrals can be obtained from those given above by exchanging the labels 1 and 2, i.e., $x_1 \leftrightarrow x_2$ and $r_1 \leftrightarrow r_2$.

Once again we stress that the coefficients of the double and single logarithmic terms (L_0^2 and L_0) in eqs. (A.29), (A.45), (A.49) and (A.54) agree with refs. [108, 128]. Furthermore we have calculated also the non-logarithmic contributions.

A.2.2 Integrals over relative photon energy

Having performed the angular integration, we still need to integrate over the relative photon energy, see (A.19). As this integral will be infrared-divergent,

we introduce a soft-photon cutoff ϵ on the minimum energy fraction of each photon, which is identical to the one used in the soft-photon contribution. We thus define:

$$\left\langle [\cdots] \right\rangle := \int_{\epsilon}^1 x_1 dx_1 \int_{\epsilon}^1 x_2 dx_2 \delta((1-z) - (x_1 + x_2)) [\cdots] . \quad (\text{A.75})$$

With the substitution $x_1 \rightarrow (1-z) \cdot u$ and the abbreviation $\tilde{\epsilon} = \epsilon/(1-z)$, we have, after elimination of the trivial δ -function:

$$\left\langle [\cdots] \right\rangle = (1-z) \int_{\tilde{\epsilon}}^{1-\tilde{\epsilon}} du \, x_1 x_2 [\cdots]_{x_1=(1-z)u, x_2=(1-z)(1-u), \dots}$$

For the logarithmically (L_0) enhanced leading terms, we find the familiar result (4.39).

The analytic calculation of the remaining, non-enhanced terms is quite tedious, leading to lengthy expressions involving many dilogarithms and trilogarithms (see e.g., [110]). As these terms also contain IR-divergent contributions, we shall pursue here the following approach. We analytically extract those terms in the integrand that either contribute to the infrared-divergence as $\epsilon \rightarrow 0$ or survive in the limit $z \rightarrow 1$, before performing the integral over the remaining expression numerically. Besides, this separation improves the stability of the numerical integration.

For the IR-divergent pieces of the non-enhanced terms we find

$$P_{\text{nonlog}}^{\text{IR-div}} = \left\langle \frac{4z}{(x_1 x_2)^2} \right\rangle = \frac{4z}{1-z} \int_{\tilde{\epsilon}}^{1-\tilde{\epsilon}} du \frac{1}{u(1-u)} \simeq \frac{8z}{1-z} \ln \tilde{\epsilon} . \quad (\text{A.76})$$

We then decompose the infrared-finite pieces as follows:

$$P_{\text{nonlog}}^{(2), \text{IR-fin.}}(z) = P_{\text{nonlog}}^{z \rightarrow 1} + P_{\text{nonlog}}^{\text{rem}}(z) , \quad (\text{A.77})$$

so that $P_{\text{nonlog}}^{\text{rem}}(z=1) = 0$. The first term on the r.h.s., obtained in the limit $z \rightarrow 1$ reads:

$$\begin{aligned} P_{\text{nonlog}}^{z \rightarrow 1} &= \left\langle \frac{8}{3x_1 x_2} \left[\frac{x_1 + 3x_2}{x_2^2} \ln x_1 + \frac{3x_1 + x_2}{x_1^2} \ln x_2 \right. \right. \\ &\quad \left. \left. - \frac{(1-z)^3}{x_1^2 x_2^2} \ln(1-z) + \frac{1-z}{x_1 x_2} \right] \right\rangle \\ &= \int_{\tilde{\epsilon}}^{1-\tilde{\epsilon}} du \frac{8}{3} \left[\frac{1}{u(1-u)} + \frac{3-2u}{(1-u)^2} \ln u + \frac{1+2u}{u^2} \ln(1-u) \right] \\ &= -\frac{16}{9} (3 + \pi^2) , \end{aligned} \quad (\text{A.78})$$

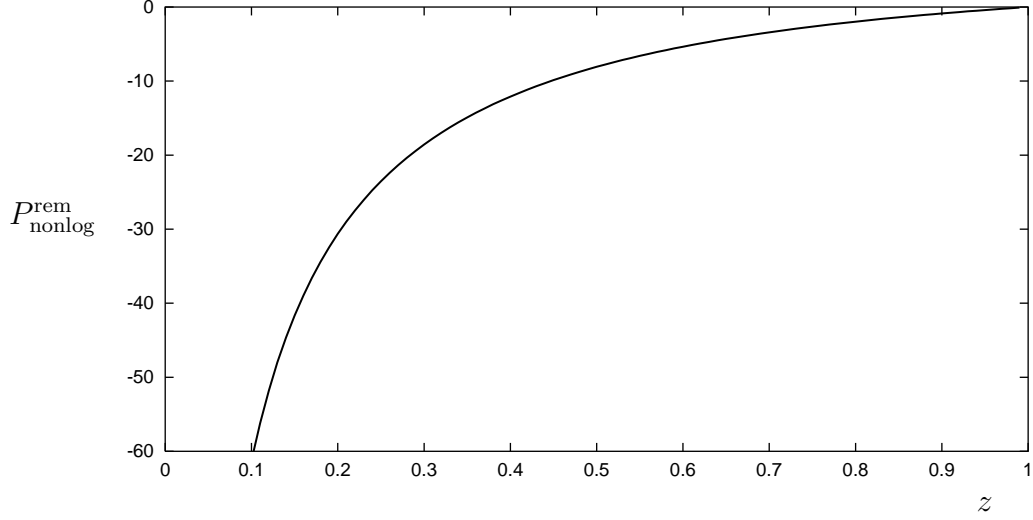


Figure A.1: The infrared-finite, ‘normalized’ part of the double-collinear contribution, $P_{\text{nonlog}}^{\text{rem}}(z)$.

where we neglected terms of order ϵ .

Finally, we plot in figure A.1 the ‘remainder’ $P_{\text{nonlog}}^{\text{rem}}(z)$, which we evaluated numerically.

Appendix B

The Semi-Collinear Contribution

In this appendix we shall describe the steps leading to the almost factorization (4.61) of the contributions from double photon emission in the region of semi-collinear kinematics.

We assume that one photon, say photon 1, is almost collinear to the incident electron and thus detected in the forward PD, i.e., $\vartheta_1 < \vartheta_0$, while the other one, photon 2, is radiated at larger angles, $\vartheta_2 > \vartheta_0$. For the computation of this contribution we formally need to perform the phase space integration for the two photons. The solid angle part of this integral schematically reads:¹

$$\frac{E_e^4}{\pi^2} \int_{\vartheta_1 < \vartheta_0} d\Omega_1 \int_{\vartheta_2 > \vartheta_0} d\Omega_2 K_{\mu\nu}^{\text{semi-coll}}(\vartheta_1, \vartheta_2; \phi_1, \phi_2, \dots) H^{\mu\nu}(\vartheta_1, \vartheta_2; \dots) . \quad (\text{B.1})$$

The hadron tensor $H^{\mu\nu}$ depends on the photon angles only through the transferred momentum $q = p - p' - k_1 - k_2$. It is thus natural to expect that the tensor $H^{\mu\nu}(P, q)$ is a smooth function of the photon angles, as long as the invariant mass of the final hadronic system, $W^2 = (P + q)^2$, stays well above the inelastic threshold of pion production, $W^2 \gg (M + m_\pi)^2$. Within the desired accuracy, which implies dropping terms of $\mathcal{O}(\vartheta_0^2)$, we set ϑ_1 to 0 in the argument of $H^{\mu\nu}$.

In principle, given $K_{\mu\nu}^{\text{semi-coll}}$, this allows us to perform the integrations over ϕ_1 and ϑ_1 immediately. Before doing this, however, we must first determine those terms of the full expression for the double Compton tensor

¹For the discussion below it is useful to temporarily consider the contraction of the Compton tensor with the hadron tensor.

that lead to nonvanishing contributions in the semi-collinear region. Second, we have to find a procedure to systematically expand the result in the limit of large ζ_0 , which means to find the analogue of the logarithmic and non-logarithmic terms in the double collinear region. This last step is actually non-trivial, which will become clear in the discussion below.

Let us first assume that photon 2 is sufficiently hard, $x_2 \sim \mathcal{O}(x_1) \sim \mathcal{O}(1)$, and that it is emitted at a large angle, $\vartheta_2 \gg \vartheta_0$, so that $z_2 \gg z_1$. We find that under these conditions the double Compton tensor simplifies considerably. Approximating $k_1 \simeq x_1 p$, one has $1/\Delta \simeq 1/(r_1 z_2)$, with $r_1 = 1 - x_1$, etc. Terms of order $\mathcal{O}((z_1)^0)$ can be dropped, as they are expected not to contribute when integrated over the solid angle of photon 1. It is now straightforward to verify that the double Compton tensor in this limit factorizes into a collinear radiation factor and the Compton tensor for single photon emission, as in the quasi-real electron approximation [109]:

$$K_{\mu\nu}^{\text{semi-coll}}(p, p', k_1, k_2) \Big|_{z_2 \gg z_1} \simeq \frac{1}{r_1} \left[\frac{1 + (1 - x_1)^2}{x_1} \frac{1}{z_1} - 2(1 - x_1) \frac{m^2}{z_1^2} \right] \times K_{\mu\nu}^{1\gamma}(r_1 p, p', k_2) . \quad (\text{B.2})$$

Strictly speaking, this expression is correct for emission at large angles and for radiation collinear to the final state electron, while one should drop those terms from the Compton tensor in the last line that are of order m^2 and contribute only for small angles, i.e., terms like m^2/z_2^2 .

However, if ϑ_2 is small, eq. (B.2) not only fails to reproduce the indicated terms that we dropped, it completely misses the behavior of the angular distribution of photon 2 in that region. To understand this, let us consider the integral over the azimuthal angle ϕ_1 . Neglecting terms that are always suppressed by a factor m^2/E_e^2 relative to the leading ones, we have:

$$\int_{-\pi}^{\pi} \frac{d\phi_1}{2\pi} \frac{1}{\Delta} \simeq \left[(r_2 z_1)^2 + (r_1 z_2)^2 + 2r_1 r_2 z_1 z_2 \cos \psi + 4x_1 x_2 m^2 (z_1 + z_2) + \frac{(z_1 + z_2) z_1 z_2}{E_e^2} \right]^{-1/2} , \quad (\text{B.3})$$

with $\cos \psi$ defined in (A.26).

Requiring one photon being almost collinear and the other one at a large angle, we see that the terms in the last line of (B.3) can be neglected in comparison to those of the first line. Thus, for the semi-collinear case we obtain:

$$\int_{-\pi}^{\pi} \frac{d\phi_1}{2\pi} \frac{1}{\Delta} \simeq \frac{1}{\sqrt{(r_2 z_1)^2 + (r_1 z_2)^2 + 2r_1 r_2 z_1 z_2 \cos \psi}} . \quad (\text{B.4})$$

Under the same conditions, we find:

$$\int_{-\pi}^{\pi} \frac{d\phi_1}{2\pi} \frac{1}{\Delta^2} \simeq \frac{r_2 z_1 + r_1 z_2}{[(r_2 z_1)^2 + (r_1 z_2)^2 + 2r_1 r_2 z_1 z_2 \cos \psi]^{3/2}}. \quad (\text{B.5})$$

It is easy to see that it is not sufficient to keep just the first terms of the expansions for large z_2 when we are going to smaller angles for photon 2. Consider e.g., the r.h.s. of (B.4):

$$\frac{1}{\sqrt{(r_2 z_1)^2 + (r_1 z_2)^2 + 2r_1 r_2 z_1 z_2 \cos \psi}} = \frac{1}{r_1 z_2} - \frac{r_2 z_1 \cos \psi}{(r_1 z_2)^2} + \mathcal{O}\left(\frac{z_1^2}{z_2^3}\right). \quad (\text{B.6})$$

A similar expansion holds for $1/\Delta^2$. Retaining only the first term of this expansion in the expression for K integrated over ϕ_1 leads to the factorized form (B.2), as discussed above. However, when integrating over the polar angle ϑ_1 , we find that the higher terms in (B.6) lead to expressions of the type:

$$\frac{E_e^2 \vartheta_0^2}{z_2^2}, \quad \frac{(E_e^2 \vartheta_0^2)^2}{z_2^3}, \quad \dots \quad (\text{B.7})$$

Although these expressions appear to be of formal order $\mathcal{O}(\vartheta_0^2)$, they do contribute when integrating over the polar angle of the second photon, ϑ_2 . Since they fall off much faster as a function of ϑ_2 than the leading terms (B.2), their contribution is essentially concentrated in a small region $\vartheta_2 \gtrsim \vartheta_0$. We express this by formally splitting the double Compton tensor as follows:

$$\begin{aligned} K_{\mu\nu}^{\text{semi-coll}} &\rightarrow \frac{1}{r_1} \left[\frac{1 + (1 - x_1)^2}{x_1} \frac{1}{z_1} - 2(1 - x_1) \frac{m^2}{z_1^2} \right] K_{\mu\nu}^{1\gamma}(r_1 p, p', k_2) \\ &+ R_{\mu\nu}(p, p', k_1, k_2), \end{aligned} \quad (\text{B.8})$$

thereby introducing the “remainder” $R_{\mu\nu}$ which falls off rapidly as a function of ϑ_2 .

Inserting (B.8) into (B.1) yields

$$\begin{aligned} &\frac{1}{x_1 r_1} P(r_1, L_0) \cdot \frac{E_e^2}{\pi} \int_{\vartheta_2 > \vartheta_0} d\Omega_2 K_{\mu\nu}^{1\gamma}(r_1 p, p', k_2) H^{\mu\nu}(P, q) \Big|_{q=r_1 p - p' - k_2} \\ &+ H^{\mu\nu}(P, q) \Big|_{q=(r_1 - x_2)p - p'} \cdot \frac{E_e^4}{\pi^2} \int_{\vartheta_1 < \vartheta_0 < \vartheta_2} d\Omega_1 d\Omega_2 R_{\mu\nu}(p, p', k_1, k_2). \end{aligned} \quad (\text{B.9})$$

In the second line we exploited again our assumption that the hadron tensor is a smooth function of its arguments and the above finding that $R_{\mu\nu}$ contributes to the integral only in a narrow region of the ϑ_2 integration.

We have not yet discussed the actual form of $R_{\mu\nu}$. From current conservation and the kinematic restrictions it is obvious that its tensor structure should be as follows:

$$R_{\mu\nu}(p, p', k_1, k_2) \simeq -\tilde{g}_{\mu\nu}R_g + \tilde{p}_\mu\tilde{p}_\nu R_{11} . \quad (\text{B.10})$$

Furthermore, we can actually guess the coefficients R_g and R_{11} without great effort just from the considerations above and from the knowledge of the double Compton tensor in the double collinear region, for the simple reason being that the “problematic” semi-collinear terms must fall off at least like $1/z_2$, as well as contribute in the double collinear case, too. The “remainder” $R_{\mu\nu}$ is thus given by:

$$R_{\mu\nu} \simeq K_{\mu\nu}^{2-\text{coll}} - [K_{\mu\nu}^{2-\text{coll}}]_{\Delta \rightarrow r_1 z_2} . \quad (\text{B.11})$$

Looking at the expression for the Compton tensor in the double collinear region (4.35) and requiring that the resulting contribution not be suppressed by a factor $1/\zeta_0$ after integration over the solid angle of photon 1, we identify the following candidates with a denominator Δ for closer investigation:

$$\frac{1}{z_1\Delta} , \quad \frac{1}{z_2\Delta} , \quad \frac{z_2}{z_1\Delta^2} , \quad \frac{z_1}{z_2\Delta^2} . \quad (\text{B.12})$$

All other terms, e.g., $m^2/(z_1^2\Delta)$, will be suppressed and thus harmless.

Analogous to the double collinear case it is convenient to define the following abbreviation for the semi-collinear situation:

$$\overline{\{\dots\}} := \frac{E_e^4}{\pi^2} \int d\Omega_1 d\Omega_2 \Theta(\vartheta_0 - \vartheta_1) \Theta(\vartheta_2 - \vartheta_0) \{\dots\} . \quad (\text{B.13})$$

We shall also use the substitutions described in appendix A.2 and exploit the fact that all integrals below will be convergent even if the upper limit on the variable ϑ_2 is removed.

By straightforward calculation we obtain:

$$\begin{aligned} \overline{\left\{ \frac{1}{z_1\Delta} - \frac{1}{z_1(r_1 z_2)} \right\}} &\simeq \frac{1}{x_1 x_2 r_1} \int_{x_1 r_2}^{x_1 r_2 \zeta_0} \frac{d\eta_1}{\eta_1} \int_{x_2 r_1 \zeta_0}^{\infty} d\eta_2 \left[\frac{1}{\sqrt{D(\eta_1, \eta_2)}} - \frac{1}{\eta_2} \right] \\ &= \frac{1}{x_1 x_2 r_1} \left[\left[\Xi \left(\cos \psi, \frac{\eta_1}{\eta_2} \right) \right]_{\eta_1=x_1 r_2}^{x_1 r_2 \zeta_0} \right]_{\eta_2=x_2 r_1 \zeta_0}^{\infty} \\ &=: \frac{1}{x_1 x_2 r_1} H_1(x_1, x_2) , \end{aligned} \quad (\text{B.14})$$

with the function Ξ being defined in (A.40), and the abbreviation:

$$H_1(x_1, x_2) = -\Xi\left(\cos\psi, \frac{x_1 r_2}{x_2 r_1}\right). \quad (\text{B.15})$$

The second candidate of (B.12) does not contribute to the naive factorization (B.2) at large angles. Therefore no ‘subtraction’ is necessary, and we have:

$$\begin{aligned} \overline{\left\{\frac{1}{z_2 \Delta}\right\}} &\simeq \frac{1}{x_1 x_2 r_2} \int_{x_2 r_1 \zeta_0}^{\infty} \frac{d\eta_2}{\eta_2} \int_{x_1 r_2}^{x_1 r_2 \zeta_0} \eta_1 \left[\frac{1}{\sqrt{D(\eta_1, \eta_2)}} \right] \\ &= \frac{1}{x_1 x_2 r_2} \left[\left[\ln \eta_1 \ln \eta_2 + \Xi\left(\cos\psi, \frac{\eta_2}{\eta_1}\right) \right]_{\eta_1=x_1 r_2}^{x_1 r_2 \zeta_0} \right]_{\eta_2=x_2 r_1 \zeta_0}^{\infty} \\ &=: \frac{1}{x_1 x_2 r_2} H_2(x_1, x_2), \end{aligned} \quad (\text{B.16})$$

with $(\chi = 1 - x_1 - x_2)$:

$$H_2 = \frac{1}{2} \ln^2 \frac{x_1 r_2^2}{x_2 \chi} + \frac{\pi^2}{6} + \text{Li}_2\left(-\frac{x_1 x_2}{\chi}\right) - \Xi\left(\cos\psi, \frac{x_2 r_1}{x_1 r_2}\right). \quad (\text{B.17})$$

Similarly, the third candidate yields:

$$\begin{aligned} \overline{\left\{\frac{z_2}{z_1 \Delta^2} - \frac{z_2}{z_1 (r_1 z_2)^2}\right\}} &\simeq \frac{1}{x_1 x_2 r_1^2} \int_{x_1 r_2}^{x_1 r_2 \zeta_0} \frac{d\eta_1}{\eta_1} \int_{x_2 r_1 \zeta_0}^{\infty} d\eta_2 \left[\frac{(\eta_1 + \eta_2) \eta_2}{\sqrt{D(\eta_1, \eta_2)}^3} - \frac{1}{\eta_2} \right] \\ &= \frac{1}{x_1 x_2 r_1^2} \left[\Xi\left(\cos\psi, \frac{\eta_1}{\eta_2}\right) + \Psi(\cos\psi; \eta_1, \eta_2) \right]_{\eta_1=x_1 r_2}^{x_1 r_2 \zeta_0} \\ &=: \frac{1}{x_1 x_2 r_1^2} H_3, \end{aligned} \quad (\text{B.18})$$

where

$$\begin{aligned} \Psi(\cos\psi; \eta_1, \eta_2) &= \frac{1 + 2 \cos\psi}{1 + \cos\psi} \ln \frac{\eta_2 + \eta_1 \cos\psi + \sqrt{D(\eta_1, \eta_2)}}{\eta_1} \\ &\quad - \frac{\ln[\eta_1 + \eta_2 \cos\psi + \sqrt{D(\eta_1, \eta_2)}]}{1 + \cos\psi}. \end{aligned} \quad (\text{B.19})$$

One finds:

$$\begin{aligned} H_3 &= H_1 + \frac{2 \cos\psi}{1 + \cos\psi} \ln(2x_2 r_1) - \frac{1}{1 + \cos\psi} \ln \frac{1 + \cos\psi}{2} \\ &\quad - \frac{1 + 2 \cos\psi}{1 + \cos\psi} \ln(\eta + x_2 r_1 + x_1 r_2 \cos\psi) \\ &\quad + \frac{1}{1 + \cos\psi} \ln(\eta + x_1 r_2 + x_2 r_1 \cos\psi). \end{aligned} \quad (\text{B.20})$$

For the last candidate, the same arguments apply as to the second, and we obtain:

$$\begin{aligned}
\overline{\left\{ \frac{z_1}{z_2 \Delta^2} \right\}} &\simeq \frac{1}{x_1 x_2 r_2^2} \int_{x_2 r_1 \zeta_0}^{\infty} \frac{d\eta_2}{\eta_2} \int_{x_1 r_2}^{x_1 r_2 \zeta_0} d\eta_1 \left[\frac{(\eta_1 + \eta_2) \eta_1}{\sqrt{D(\eta_1, \eta_2)}^3} \right] \\
&= \frac{1}{x_1 x_2 r_2^2} \left[\ln \eta_1 \ln \eta_2 + \Xi \left(\cos \psi, \frac{\eta_2}{\eta_1} \right) + \Psi(\cos \psi; \eta_2, \eta_1) \right]_{\eta_1 = x_1 r_2}^{x_1 r_2 \zeta_0} \\
&=: \frac{1}{x_1 x_2 r_2^2} H_4, \tag{B.21}
\end{aligned}$$

with

$$\begin{aligned}
H_4 &= H_2 + \frac{2 \cos \psi}{1 + \cos \psi} \ln[(1 + \cos \psi) x_2 r_1] + \frac{1}{1 + \cos \psi} \ln \frac{1 + \cos \psi}{2} \\
&+ \frac{1}{1 + \cos \psi} \ln(\eta + x_2 r_1 + x_1 r_2 \cos \psi) \\
&- \frac{1 + 2 \cos \psi}{1 + \cos \psi} \ln(\eta + x_1 r_2 + x_2 r_1 \cos \psi). \tag{B.22}
\end{aligned}$$

As a representative of the harmless terms, we shall investigate whether the contribution of $m^2/(z_1^2 \Delta)$ at large angles of the second photon deviates from the naive approximation. We find:

$$\begin{aligned}
\overline{\left\{ \frac{m^2}{z_1^2 \Delta} - \frac{m^2}{z_1^2 (r_1 z_2)} \right\}} &\simeq \frac{r_2}{x_1 x_2 r_1} \int_{x_1 r_2}^{x_1 r_2 \zeta_0} \frac{d\eta_1}{\eta_1^2} \int_{x_2 r_1 \zeta_0}^{\infty} d\eta_2 \left[\frac{1}{\sqrt{D(\eta_1, \eta_2)}} - \frac{1}{\eta_2} \right] \\
&= \frac{r_2}{x_1 x_2 r_1} \int_{x_2 r_1 \zeta_0}^{\infty} \frac{d\eta_2}{\eta_2^2} \left[\frac{\eta_2 - \sqrt{D(\eta_1, \eta_2)}}{\eta_1} \right. \\
&\quad \left. - \cos \psi \ln \frac{\eta_2 + \eta_1 \cos \psi + \sqrt{D(\eta_1, \eta_2)}}{\eta_1} \right]_{\eta_1 = x_1 r_2}^{x_1 r_2 \zeta_0}. \tag{B.23}
\end{aligned}$$

One can see even without explicit evaluation of the last integral that both terms in the integrand actually contribute only at order $\mathcal{O}(1/\zeta_0)$ and are thus negligible. We leave it as an exercise to the reader to verify that the contributions of all other terms beyond the factorization (B.2) in the semi-collinear limit are suppressed by a power of $1/\zeta_0$ for each power of m^2 in the numerator, except to those given in (B.12) which after integration are leading to $H_1 \dots H_4$.

To summarize, the integral over the non-factorizing contribution is found to be:

$$\frac{E_e^4}{\pi^2} \int_{\vartheta_1 < \vartheta_0 < \vartheta_2} d\Omega_1 d\Omega_2 R_{\mu\nu} = [-\tilde{g}_{\mu\nu} Q_l^2 + 4(r_1 - x_2) (\tilde{p}_\mu \tilde{p}_\nu)] \cdot \frac{1}{x_1 x_2} H(x_1, x_2) , \quad (\text{B.24})$$

with $(\chi = 1 - x_1 - x_2)$:

$$H(x_1, x_2) = \frac{r_1^3 + \chi r_2}{x_1 x_2 r_1} H_1 + \frac{r_2^3 + \chi r_1}{x_1 x_2 r_2} H_2 - \chi \left(\frac{H_3}{r_1^2} + \frac{H_4}{r_2^2} \right) . \quad (\text{B.25})$$

This quasi-collinear contribution corresponding to one lost photon, i.e., being emitted outside the PD, is to be treated in collinear kinematics and only depends on the energies of the photons. Obviously, this can only be true as long as the strong hierarchy $m/E_e \ll \vartheta_0 \ll \theta$ exists, so that the indicated approximations remain valid.

As a check on the quasi-collinear contribution, let us finally investigate the leading behavior for $x_2 \rightarrow 0$. We find:

$$\begin{aligned} H_1 &\simeq - \left[\frac{1}{2} \ln^2 \frac{x_1}{x_2 r_1} + \frac{\pi^2}{6} \right] + \mathcal{O}(x_2) , \\ H_2 &\simeq \frac{1}{2} \ln^2 \frac{x_1}{x_2 r_1} + \frac{\pi^2}{6} + \mathcal{O}(x_2) , \end{aligned} \quad (\text{B.26})$$

leading to a cancellation of the apparent $1/x_2$ singularity in $H(x_1, x_2)$ and leaving an expression that is integrable for $x_2 \rightarrow 0$. The entire soft behavior for photon 2 is thus contained in the factorizing piece (B.2).

Bibliography

- [1] E. Rutherford, Phil. Mag. Vol. 21 (1911) 669
- [2] R. Hofstadter and R. W. McAllister, Phys. Rev. **98** (1955) 217.
- [3] M. Breidenbach *et al.*, Phys. Rev. Lett. **23** (1969) 935.
- [4] The LEP Collaborations ALEPH, DELPHI, L3, OPAL, the LEP Electroweak Working Group and the SLD Heavy Flavour and Electroweak Working Group, *A Combination of Preliminary Electroweak Measurements and Constraints on the Standard Model*, [arXiv:hep-ex/0112021].
- [5] C. Grosso-Pilcher [for the CDF and D0 Collaborations], in: Proceedings of 29th International Conference on High-Energy Physics (ICHEP 98), Vancouver, Canada, 23-29 Jul 1998, vol. 2, p. 1355, FERMILAB-CONF-98-306-E.
- [6] C. Adloff *et al.* [H1 Collaboration], Phys. Lett. B **479** (2000) 358 [arXiv:hep-ex/0003002];
J. Breitweg *et al.* [ZEUS Collaboration], Eur. Phys. J. C **14** (2000) 239 [arXiv:hep-ex/9905039].
- [7] E. A. Kuraev, L. N. Lipatov and V. S. Fadin, Sov. Phys. JETP **44** (1976) 443 [Zh. Eksp. Teor. Fiz. **71** (1976) 840];
E. A. Kuraev, L. N. Lipatov and V. S. Fadin, Sov. Phys. JETP **45** (1977) 199 [Zh. Eksp. Teor. Fiz. **72** (1977) 377];
I. I. Balitsky and L. N. Lipatov, Sov. J. Nucl. Phys. **28** (1978) 822 [Yad. Fiz. **28** (1978) 1597].
- [8] For a recent review on BFKL see e.g., C. R. Schmidt, in: Proc. of the 5th International Symposium on Radiative Corrections (RADCOR 2000) ed. Howard E. Haber, arXiv:hep-ph/0106181.
- [9] A. M. Staśto, K. Golec-Biernat and J. Kwieciński, Phys. Rev. Lett. **86** (2001) 596 [arXiv:hep-ph/0007192].

- [10] L. V. Gribov, E. M. Levin and M. G. Ryskin, Phys. Rept. **100** (1983) 1.
- [11] For a recent review see e.g., M. Lublinsky, Eur. Phys. J. C **21** (2001) 513 [arXiv:hep-ph/0106112].
- [12] V. Lemaitre [H1 and ZEUS Collaborations], Nucl. Phys. Proc. Suppl. **64** (1998) 184;
C. Adloff *et al.* [H1 Collaboration], Eur. Phys. J. C **5** (1998) 575 [arXiv:hep-ex/9806009];
J. Olsson [H1 and ZEUS Collaborations], Nucl. Phys. Proc. Suppl. **82** (2000) 432.
- [13] V. Arkadov [H1 Collaboration], Nucl. Phys. Proc. Suppl. **79** (1999) 179.
- [14] C. Adloff *et al.* [H1 Collaboration], Eur. Phys. J. C **21** (2001) 33 [hep-ex/0012053].
- [15] A. Dubak [H1-Collaboration], presentation at the DIS 2001 International Workshop on Deep Inelastic Scattering, Bologna, 27 April - 1 May, 2001, and H1-prelim-01-053.
- [16] ZEUS Collaboration, *The ZEUS NLOQCD fit to determine parton distribution functions and α_s* , contributed paper no. 628 to the EPS 2001 conference (Budapest, Hungary, July 2001).
- [17] T. Gehrmann, Phys. Lett. B **480** (2000) 77 [hep-ph/0003156].
- [18] M. W. Krasny, W. Płaczek and H. Spiesberger, Z. Phys. C **53** (1992) 687.
- [19] T. Ahmed *et al.* [H1 Collaboration], Z. Phys. C **66** (1995) 529.
- [20] J. Andruszkow *et al.* [ZEUS Luminosity Group Collaboration], Acta Phys. Polon. B **32** (2001) 2025.
- [21] H. Bethe and W. Heitler, Proc. Roy. Soc. Lond. A **146** (1934) 83.
- [22] B. Foster, *ZEUS at HERA II*, arXiv:hep-ex/0107066.
- [23] M. Klein [H1 collaboration], talk no. 404 given at the ICHEP98 conference, (Vancouver, Canada, July 1998), and contributed paper no. 535

- [24] Ç. İssever, *Messung der Protonstrukturfunktionen $F_2(x, Q^2)$ und $F_L(x, Q^2)$ bei HERA in radiativer ep Streuung*, Ph.D. thesis, Dortmund, December 2000; DESY-THESIS-2001-032.
- [25] Ç. İssever [H1 collaboration], presentation at the DIS 2001 International Workshop on Deep Inelastic Scattering, Bologna, 27 April - 1 May, 2001, and H1-prelim-01-042.
- [26] H1 Collaboration, *Measurement of the Proton Structure Function using Radiative Events at HERA*, contributed paper to the EPS 2001 (Budapest, Hungary, July 2001) and LP 2001 (Rome, Italy, July 2001) conferences.
- [27] M. Derrick *et al.* [ZEUS Collaboration], Z. Phys. C **69** (1996) 607 [hep-ex/9510009].
- [28] L. Favart, M. Gruwé, P. Marage and Z. Zhang, Z. Phys. C **72** (1996) 425 [hep-ph/9606465].
- [29] D. Y. Bardin, L. Kalinovskaya and T. Riemann, Z. Phys. C **76** (1997) 487 [hep-ph/9612203].
- [30] H. Anlauf, A. B. Arbuzov, E. A. Kuraev and N. P. Merenkov, Phys. Rev. D **59** (1999) 014003 [hep-ph/9711333].
- [31] H. Anlauf, A. B. Arbuzov, E. A. Kuraev, N. P. Merenkov, JETP Lett. **66** (1997) 391 [Erratum-ibid. **67** (1997) 305].
- [32] H. Anlauf, A. B. Arbuzov, E. A. Kuraev and N. P. Merenkov, JHEP **9810** (1998) 013 [hep-ph/9805384].
- [33] H. Anlauf, Eur. Phys. J. C **9** (1999) 69 [hep-ph/9901258].
- [34] H. Anlauf, Eur. Phys. J. C **22** (2002) 627 [hep-ph/0110120].
- [35] S. Bentvelsen, J. Engelen and P. Kooijman, Proceedings of the Workshop on Physics at HERA, vol. 1, W. Buchmüller, G. Ingelman, DESY (1992) 23.
- [36] F. Jacquet and A. Blondel, in *Proceedings of the study of an ep facility for Europe* U. Amaldi (ed.), DESY 79/48 (1979), 391.
- [37] U. Bassler and G. Bernardi, Nucl. Instrum. Meth. A **361** (1995) 197 [arXiv:hep-ex/9412004].

- [38] U. Bassler and G. Bernardi, Nucl. Instrum. Meth. A **426** (1999) 583 [arXiv:hep-ex/9801017].
- [39] L. A. Bauerdick, A. Glazov and M. Klein, *Future measurement of the longitudinal proton structure function at HERA*, arXiv:hep-ex/9609017.
- [40] H. Spiesberger *et al.*, *Radiative corrections at HERA*, CERN-TH-6447-92, in: Workshop on Physics at HERA, Hamburg, Germany, Oct 29-30, 1991, p. 798.
- [41] G. Altarelli, Phys. Rept. **81** (1982) 1.
- [42] A. J. Buras, Rev. Mod. Phys. **52** (1980) 199.
- [43] Y. L. Dokshitzer, D. Diakonov and S. I. Troian, Phys. Rept. **58** (1980) 269.
- [44] E. Reya, Phys. Rept. **69** (1981) 195.
- [45] R. K. Ellis, W. J. Stirling, B. R. Webber, *QCD and Collider Physics*, Cambridge University Press, 1996.
- [46] T. Muta, *Foundations of Quantum Chromodynamics: An Introduction to perturbative methods in gauge theories*, Lectures Notes in Physics, Vol. 57, World Scientific, 1998.
- [47] R. G. Roberts *The Structure of the Proton. Deep Inelastic Scattering*, Cambridge University Press, Cambridge, 1990.
- [48] R. T. Herrod and S. Wada, Phys. Lett. B **96** (1980) 195.
- [49] G. Altarelli, R. K. Ellis and G. Martinelli, Nucl. Phys. B **143** (1978) 521 [Erratum-ibid. B **146** (1978) 544].
- [50] J. Kubar-André and F. E. Paige, Phys. Rev. D **19** (1979) 221.
- [51] G. Altarelli, R. K. Ellis and G. Martinelli, Nucl. Phys. B **157** (1979) 461.
- [52] G. Altarelli and G. Parisi, Nucl. Phys. B **126** (1977) 298.
- [53] Y. L. Dokshitzer, Sov. Phys. JETP **46** (1977) 641 [Zh. Eksp. Teor. Fiz. **73** (1977) 1216].

- [54] V. N. Gribov and L. N. Lipatov, *Yad. Fiz.* **15** (1972) 1218 [*Sov. J. Nucl. Phys.* **15** (1972) 675].
- [55] L. N. Lipatov, *Sov. J. Nucl. Phys.* **20** (1975) 94 [*Yad. Fiz.* **20** (1975) 181].
- [56] H. Plathow-Besch, *Comput. Phys. Commun.* **75** (1993) 396;
PDFLIB version 8.04 (April 2000), CERN program library.
- [57] B. Badelek and J. Kwieciński, *Rev. Mod. Phys.* **68** (1996) 445
[arXiv:hep-ph/9408318].
- [58] B. Badelek, J. Kwieciński and A. Staśto, *Z. Phys. C* **74** (1997) 297
[arXiv:hep-ph/9603230].
- [59] B. Badelek, M. Krawczyk, K. Charchula and J. Kwieciński, *Rev. Mod. Phys.* **64** (1992) 927.
- [60] A. M. Cooper-Sarkar, R. C. Devenish and A. De Roeck, *Int. J. Mod. Phys. A* **13** (1998) 3385 [arXiv:hep-ph/9712301].
- [61] T. H. Bauer, R. D. Spital, D. R. Yennie and F. M. Pipkin, *Rev. Mod. Phys.* **50** (1978) 261 [Erratum-ibid. **51** (1978) 407].
- [62] P.D.B. Collins, *An Introduction to Regge Theory and High Energy Physics*, Cambridge University Press, Cambridge, 1977.
- [63] A. Donnachie and P. V. Landshoff, *Phys. Lett. B* **296** (1992) 227
[arXiv:hep-ph/9209205].
- [64] C. Adloff *et al.* [H1 Collaboration], *Phys. Lett. B* **520** (2001) 183
[arXiv:hep-ex/0108035].
- [65] A. Donnachie and P. V. Landshoff, *Phys. Lett. B* **437** (1998) 408
[arXiv:hep-ph/9806344].
- [66] A. Donnachie and P. V. Landshoff, *Phys. Lett. B* **518** (2001) 63
[arXiv:hep-ph/0105088].
- [67] J. R. Forshaw, D. A. Ross, *Quantum Chromodynamics and the Pomeron*, Cambridge Lecture Notes in Physics, vol. 9, Cambridge University Press, Cambridge, 1997.
- [68] J. R. Forshaw, G. Kerley and G. Shaw, *Phys. Rev. D* **60** (1999) 074012
[arXiv:hep-ph/9903341].

- [69] A. Donnachie and H. G. Dosch, Phys. Rev. D **65** (2002) 014019 [arXiv:hep-ph/0106169].
- [70] H. Abramowicz, E. M. Levin, A. Levy and U. Maor, Phys. Lett. B **269** (1991) 465.
- [71] H. Abramowicz, A. Levy, DESY 97-251, 1997, arXiv:hep-ph/9712415.
- [72] K. Adel, F. Barreiro and F. J. Yndurain, Nucl. Phys. B **495** (1997) 221 [arXiv:hep-ph/9610380].
- [73] A. Capella, A. Kaidalov, C. Merino and J. Tran Thanh Van, Phys. Lett. B **337** (1994) 358 [arXiv:hep-ph/9405338];
A. B. Kaidalov, C. Merino and D. Pertermann, Eur. Phys. J. C **20** (2001) 301 [arXiv:hep-ph/0004237].
- [74] P. Desgrolard, L. Jenkovszky and F. Paccanoni, Eur. Phys. J. C **7** (1999) 263 [arXiv:hep-ph/9803286].
- [75] A. Arbuzov, D. Bardin, J. Blümlein, L. Kalinovskaya and T. Riemann, Comput. Phys. Commun. **94** (1996) 128 [hep-ph/9511434].
- [76] W. L. van Neerven, *Review of higher order QCD corrections to structure functions*, arXiv:hep-ph/9609243.
- [77] R. Beyer, E. Elsen, S. Riess, F. Zetsche and H. Spiesberger, *Electroweak Precision Tests With Deep Inelastic Scattering At HERA*, in: Proceedings of the Workshop on Future Physics at HERA, Hamburg, Germany.
- [78] E. Boos and T. Ohl, Phys. Rev. Lett. **83** (1999) 480 [arXiv:hep-ph/9903357];
E. Boos and T. Ohl, *Forests and groves: Minimal gauge invariant classes of tree diagrams in gauge theories*, arXiv:hep-ph/9909487.
- [79] H. Burkhardt and B. Pietrzyk, Phys. Lett. B **356** (1995) 398;
H. Burkhardt and B. Pietrzyk, Phys. Lett. B **513** (2001) 46.
- [80] L. W. Mo and Y. S. Tsai, Rev. Mod. Phys. **41** (1969) 205.
- [81] A. A. Akhundov, D. Y. Bardin, L. Kalinovskaya and T. Riemann, Fortsch. Phys. **44** (1996) 373 [arXiv:hep-ph/9407266].
- [82] M. Böhm and H. Spiesberger, Nucl. Phys. B **304** (1988) 749.
- [83] D. Y. Bardin, K. C. Burdik, P. K. Khristova and T. Riemann, Z. Phys. C **44** (1989) 149.

- [84] E. A. Kuraev, N. P. Merenkov and V. S. Fadin, *Yad. Fiz.* **45** (1987) 782 [*Sov. J. Nucl. Phys.* **45** (1987) 486].
- [85] E. Byckling, K. Kajantie, *Particle Kinematics* John Wiley & Sons, 1973.
- [86] T. Kinoshita, *J. Math. Phys.* **3** (1962) 650;
T. D. Lee and M. Nauenberg, *Phys. Rev.* **133** (1964) B1549.
- [87] J. Blümlein, G. Levman and H. Spiesberger, *Large Angle Radiative Scattering At HERA*, in: Snowmass 1990, Proceedings, Research directions for the decade, p. 554; *J. Phys. G* **19** (1993) 1695.
- [88] H. Anlauf, H. D. Dahmen, P. Manakos, T. Mannel and T. Ohl, *Z. Phys. C* **52** (1991) 655.
- [89] H. Anlauf, H. D. Dahmen, P. Manakos, T. Mannel and T. Ohl, *Comput. Phys. Commun.* **70** (1992) 97.
- [90] A. Courau and P. Kessler, *Phys. Rev. D* **46** (1992) 117.
- [91] A. De Rújula and W. Vogelsang, *Phys. Lett. B* **451** (1999) 437 [[arXiv:hep-ph/9812231](#)].
- [92] M. W. Krasny, *Proceedings of the Workshop on Physics at HERA*, vol. 2, W. Buchmüller, G. Ingelman, DESY (1992) 850;
M. W. Krasny, *J. Phys. G* **19** (1993) 1479.
- [93] M. Böhm and H. Spiesberger, *Nucl. Phys. B* **294** (1987) 1081.
- [94] M. Klein, *On the Q^2 , x Range at HERA*, in: *Proceedings of the Workshop on Physics at HERA*, vol. 1, W. Buchmüller, G. Ingelman, DESY (1992) 71.
- [95] S. Jadach, W. Płaczek and M. Jeżabek, *Phys. Lett. B* **248** (1990) 417.
- [96] S. Aid *et al.* [H1 Collaboration], *Nucl. Phys. B* **470** (1996) 3 [[arXiv:hep-ex/9603004](#)].
- [97] F. Cornet, R. Graciani and J. I. Illana, [arXiv:hep-ph/9609259](#).
- [98] T. Helbig and H. Spiesberger, *Nucl. Phys. B* **373** (1992) 73.
- [99] A. Heister *et al.* [ALEPH Collaboration], *Eur. Phys. J. C* **21** (2001) 423 [[arXiv:hep-ex/0104034](#)].

- [100] J. Kripfganz and H. Perlt, Z. Phys. C **41** (1988) 319.
- [101] J. C. Collins and G. Sterman, Nucl. Phys. B **185** (1981) 172;
J. C. Collins, D. E. Soper and G. Sterman, Nucl. Phys. B **261** (1985) 104;
G. T. Bodwin, Phys. Rev. D **31** (1985) 2616 [Erratum-ibid. D **34** (1985) 3932].
- [102] H. Spiesberger, Phys. Rev. D **52** (1995) 4936 [hep-ph/9412286].
- [103] N. P. Merenkov, Nucl. Phys. Proc. Suppl. **29A** (1992) 229.
- [104] D. Hoffmann and L. Favart, *Lepton pair Monte Carlo generators for HERA physics*, IIHE-99-01, in: Proceedings of the Workshop on Monte Carlo Generators for HERA Physics, Hamburg, Germany, 27-30 Apr 1998.
- [105] E. A. Kuraev and V. S. Fadin, Sov. J. Nucl. Phys. **41** (1985) 466 [Yad. Fiz. **41** (1985) 733].
- [106] G. Altarelli and G. Martinelli, *In Ellis, J. (Ed.), Peccei, R.d. (Ed.): Physics at LEP, Vol. 1, 47-57*, CERN 86-02, Geneva 1986.
- [107] W. Beenakker, F. A. Berends and W. L. van Neerven, *Applications Of Renormalization Group Methods To Radiative Corrections*, in: Proceedings of the Workshop on Electroweak Radiative Corrections, Ringberg Castle, Germany, Apr 3-7, 1989.
- [108] N. P. Merenkov, Sov. J. Nucl. Phys. **48** (1988) 1073 [Yad. Fiz. **48** (1988) 1782].
- [109] V. N. Baier, V. S. Fadin and V. A. Khoze, Nucl. Phys. B **65** (1973) 381.
- [110] L. Lewin, *Polylogarithms and Associated Functions*, North Holland, 1981.
- [111] F. A. Berends, R. Kleiss, P. de Causmaecker, R. Gastmans, W. Troost and T. T. Wu [CALKUL Collaboration], Nucl. Phys. B **239** (1984) 382; Nucl. Phys. B **239** (1984) 395.
- [112] J. A. Vermaseren, *Symbolic manipulation with FORM*, Computer Algebra Nederland, 1991;
J. A. Vermaseren, *New features of FORM*, arXiv:math-ph/0010025.

- [113] M. Jeřabek, Z. Phys. C **56** (1992) 285.
- [114] M. Przybycień, Acta Phys. Polon. B **24** (1993) 1105 [arXiv:hep-th/9511029].
- [115] M. Skrzypek, Acta Phys. Polon. B **23** (1992) 135.
- [116] A. B. Arbuzov, Phys. Lett. B **470** (1999) 252 [arXiv:hep-ph/9908361].
- [117] S. Jadach and B. F. Ward, Comput. Phys. Commun. **56** (1990) 351.
- [118] S. Jadach, M. Skrzypek and B. F. Ward, Phys. Lett. B **257** (1991) 173.
- [119] M. Skrzypek and S. Jadach, Z. Phys. C **49** (1991) 577.
- [120] A. T. Doyle, Talk given at 29th International Conference on High-Energy Physics (ICHEP 98), Vancouver, Canada, 23-29 Jul 1998. arXiv:hep-ex/9812029.
- [121] G. I. Gakh, M. I. Konchatnij and N. P. Merenkov, J. Exp. Theor. Phys. **92** (2001) 930 [Zh. Eksp. Teor. Fiz. **92** (2001) 1077] [arXiv:hep-ph/0010320].
- [122] D. Müller, D. Robaschik, B. Geyer, F. M. Dittes and J. Hořejši, Fortsch. Phys. **42** (1994) 101 [arXiv:hep-ph/9812448];
X. Ji, Phys. Rev. Lett. **78** (1997) 610 [hep-ph/9603249];
X. Ji, Phys. Rev. **D55** (1997) 7114 [hep-ph/9609381];
A. V. Radyushkin, Phys. Lett. **B380** (1996) 417 [hep-ph/9604317];
A. V. Radyushkin, Phys. Rev. **D56** (1997) 5524 [hep-ph/9704207].
- [123] A. V. Belitsky and D. Müller, arXiv:hep-ph/0111037;
A. V. Belitsky, D. Müller and A. Kirchner, arXiv:hep-ph/0112108.
- [124] A. B. Arbuzov, E. A. Kuraev, N. P. Merenkov and L. Trentadue, JHEP **9812** (1998) 009 [arXiv:hep-ph/9804430];
S. Binner, J. H. Kühn and K. Melnikov, Phys. Lett. B **459** (1999) 279 [arXiv:hep-ph/9902399];
M. I. Konchatnij and N. P. Merenkov, JETP Lett. **69** (1999) 811 [arXiv:hep-ph/9903383];
V. A. Khoze, M. I. Konchatnij, N. P. Merenkov, G. Pancheri, L. Trentadue and O. N. Shekhovzova, Eur. Phys. J. C **18** (2001) 481 [arXiv:hep-ph/0003313];
G. Rodrigo, A. Gehrmann-De Ridder, M. Guillaume and J. H. Kühn, Eur. Phys. J. C **22** (2001) 81 [arXiv:hep-ph/0106132].

- [125] A. Denig *et al.* [KLOE Collaboration], *Measurement of the hadronic cross section at KLOE using the radiative return*, in *Proc. of the e^+e^- Physics at Intermediate Energies Conference* ed. Diego Bettoni, eConf **C010430** (2001) T07 [arXiv:hep-ex/0106100].
- [126] S. Spagnolo, Eur. Phys. J. C **6** (1999) 637.
- [127] Workshop on Monte Carlo Generators for HERA Physics, DESY 1998/1999.
<URL:<http://www.desy.de/~heramc/>>
- [128] A. B. Arbuzov, V. A. Astakhov, E. A. Kuraev, N. P. Merenkov, L. Trentadue and E. V. Zemlyanaya, Nucl. Phys. B **483** (1997) 83 [hep-ph/9610228].